Inter-critical Annealing of a Lean Composition Steel under Controlled Cooling to Produce Multiphase Microstructure

A Dissertation Submitted

In Partial Fulfillment of the Requirements

for the Degree of

Master of Engineering

in

Production Engineering

by

Surinder Singh

Regd. No. 801282026

Under the guidance of

Dr. Tarun Nanda
Assistant Professor,
MED, TU, Patiala

Dr. B. Ravi Kumar
Scientist (E_2)
NML, Jamshedpur

to the

MECHANICAL ENGINEERING DEPARTMENT

THAPAR UNIVERSITY, PATIALA

JULY, 2014

Declaration

I, Surinder Singh hereby declare that the thesis entitled "Inter-critical Annealing of a Lean Composition Steel under Controlled Cooling to Produce Multiphase Microstructure." is an authentic record of thesis work carried out as requirement for the award of degree of ME (Production Engineering) at Thapar University, Patiala under the supervision of Dr. Tarun Nanda, Assistant Professor, MED, Thapar University, Patiala and Dr. B. Ravi Kumar, Scientist E_2, MST Division, National Metallurgical Laboratory (NML), Jamshedpur, during 4th semester, Jan–July 2014.

The matter presented in this report has not been submitted in any other University/Institute for award of Masters of Engineering or any other degree.

(SURINDER SINGH)

Place: Patiala

Date: 15/7/14

Certificate

This is to certify that the thesis entitled, '**Inter-critical Annealing of a Lean Composition Steel under Controlled Cooling to Produce Multiphase Microstructures**', being submitted by Surinder Singh (Regd. No. 801282026), in partial fulfillment of the requirements for the award of degree of Master of Engineering in Production Engineering of Mechanical Engineering Department, Thapar University, Patiala, is a record of candidate's own work carried out by him under our supervision. To the best of our knowledge, the content of this thesis does not form a basis for the award of any previous degree to anyone else.

Dr. Tarun Nanda
Assistant Professor
MED, TU, Patiala

Dr. B. Ravi Kumar
Principle Scientist (E2)
NML, Jamshedpur

Dr. Ajay Batish
Professor and Head
MED, TU, Patiala

(Countersigned by)

Dr. S.K. Mohapatra
Dean of Academics Affairs
TU, Patiala

Acknowledgement

Achievement of one's goal is not a single person's effort but it is the advices, help, suggestions and blessings of many people. So it gives me immense pleasure to express my gratitude, regards and acknowledgment to them.

I would like to express my deep sense of gratitude to **Dr. B. Ravi Kumar**, Scientist (E_2), National Metallurgical Laboratory (NML), Jamshedpur for his invaluable suggestions, excellent supervision, constant encouragement and critical discussion throughout the research work. It is with deep sense of reverence and gratitude that I avail opportunity to thank him.

I express my deep sense of gratitude and a very sincere thanks to my guide **Dr. Tarun Nanda** Assistant Professor, Mechanical engineering department, Thapar University, Patiala for their indefatigable guidance and full support which helped me in the accomplishment of this project. I am highly indebted to them for their painstaking efforts and invaluable suggestions during the period of work.

I acknowledge my heartfelt indebts to Mr. P.N. Rao (high skilled worker), for constant encouragement and valuable support during my dissertation work. I am also grateful to all those who helped me knowingly or unknowingly in various ways in completion of my dissertation work.

The greatest thanks go to my **Parents** for their infinite support. Above all, I express my indebtedness to the "**ALMIGHTY**" for all His blessing and kindness.

Surinder Singh

Abstract

In the past years, there has been growth in the search and use of new advanced materials in the transport industry. So far, conventional steel is the main material for car bodies, but there is a growing demand for other materials to decrease the weight of cars and thereby saving costs, energy and environment. Also, the increasing safety requirements in the automotive industry has forced search for new materials. The different parts need to be as light as possible, but with sufficient strength and ductility. Hereby, multiphase steels like dual phase and TRIP (Transformed Induced Plasticity) steels are important because of their high strength in combination with good formability. Various methods have been used for the production of these steels to get best outcomes. However, extremely limited work has been reported for the production of dual/ multiphase steels with controlled cooling and using a lean chemistry. The present experimental work reports on the methods of production of dual/ multiphase steels (tensile strength range 500–800 MPa; ductility in the range 12–33%) with ferrite/ martensite, ferrite/ bainite/ martensite and ferrite/ martensite/ austenite/ bainite multiphase structures. These structures were obtained in a normalized steel of very lean chemistry (0.11C, 1.8Mn, and 0.325 Si) subjected to inter-critical annealing and soaking followed by controlled cooling in an annealing simulator. Dual phase structures were produced by inter-critical annealing followed by direct cooling to room temperature to achieve high strengths. Multiphase microstructures were produced by holding in the bainitic and martensitic range to get various combinations of strength and ductility (multi-functional). The present work also compares the results for annealing process obtained through experimental investigations and through software predictions. Finally, micro-mechanical modeling has been done for steel with dual phase structure The true stress-strain curves obtained through actual tensile experiments closely matched with the true stress-strain curves predicted by micro-mechanical modelling.

List of Figures

List of Tables

Acronyms

Acronym	Full Name
ACC	Accelerated Cooling
AHSS	Advanced High Strength Steels
ASS	Austenitic Stainless Steels
ASTM	American Society for Testing and Materials
ATMP	Advanced Thermo Mechanical Processing
BH	Bake Hardening
CCT	Continuous Cooling Transformation
CG	Coarse Grained
CP	Complex Phase
DAS	Data Acquisition System
DIFT	Deformation Induced Ferrite Transformation
DP	Dual Phase
DSC	Differential Scanning Calorimetry
FA	Fully Austenized
FEM	Finite Element Method
FG	Fine Grained
HSLA	High Strength Low Alloy
HSM	Hot Strip Mill
HSS	High Strength Steel
ICAT	Inter-Critical Annealing Temperature
LHT	Local Heat Treatment
L-IP	Light Weight with Induced Plasticity
LNQ	Liquid Nitrogen Quenched
M-A	Martensite–Austenite
MART	Martensitic
MP	Multi Phase
MS	Martensitic Steels

MVF	Martensite Volume Fraction
NG	New Generation
PLC	Programmable Logic Controller
Q&P	Quenching and Partitioning
QT	Quench Temperature
RA	Retained Austenite
RP	Resting Pad
SB-TRIP	Super Bainite TRIP
SEM	Scanning Electron Microscope
S-IP	Shear band formation Induced Plasticity
SPD	Severe Plastic Deformation
TM	Tempered Martensite
TMCP	Thermo Mechanical Controlled Processing
TRIP	Transformation Induced Plasticity
TS-EI	Tensile Strength–Elongation
TTA	Temperature Transformation of Austenite
TTT	Time Temperature Transformation
TWIP	Twinning Induced Plasticity
UFC	Ultra-Fast Cooling
UFG	Ultra-Fine Grained
UTS	Ultimate Tensile Strength
VHN	Vickers Hardness Number
VPN	Vickers Pyramid Number
X-AHSS	Extra Advanced High Strength Steels
XRD	X-Ray Diffraction
YS	Yield Strength

Symbols

Symbol	Full Name
σ	Engineering Stress
℃	Degree Celsius
γ	Austenite
r_m	Plastic Strain Ratio
n	Strain Hardening Coefficient
ε	Strain
%	Percentage
S	Second

Table of Contents

Chapter 1

Introduction

1.1 General

The automotive industry aims at the production of vehicles with low weight, fulfilling high requirements concerning safety improvement, reduced fuel consumption and limitation of emission of harmful exhaust gases. In order to meet these demands, improvements in the known materials and searching new materials with high ratio of strength to weight and good suitability for metal forming operations are still being carried out [Meng et al., 2009]. The special groups of interest are steels of multiphase structure. They exhibit superior strength-ductility balance compared to conventional steels and also exhibit the required formability. These are sheets of the ferritic / martensitic structure or ferritic / bainitic structure (Dual Phase-DP), ferritic / bainitic / martensite structure with retained austenite showing TRIP effect (TRIP steels) and complex multiphase structure (Complex Phase-CP). The interest in respect of the suitability for metal forming operations is also connected with high-manganese steels of austenitic structure. To strengthen these steels, mechanical twinning during the technological deformation is used (TWIP effect – Twinning Induced Plasticity). These all steels are called advance high strength steels (AHSS) [Adamczyk and Grajcar, 2006; Bhattacharya, 2006].

1.2 Advanced High Strength Steels

As urban pollution goes on, petroleum consumption increases and the global climate changes year by year, the demand for automobiles with fewer emissions and higher fuel efficiency never stops. Aside from the development of new power generation system which is costly (i.e. hybrid-electric vehicles), technologies that promise improvements in fuel economy include improved aerodynamics, advanced transmission technologies, tires with lower rolling resistance, and reduction of vehicle weight. Among all other technologies, reduction of vehicle weight is believed to be the most promising technology responsible for significant improvement in fuel economy in the future [Hulka, 2005]. For example, 1 percent mass reduction yields up to 0.66 percent improvement in fuel economy. As a result, developing lighter weight vehicles has

become more and more important to the automotive industry over the years. Reduction of vehicle weight can be achieved by technology improvements in many ways, such as materials, structural design, as well as the functional efficiency of vehicle systems or components. These aspects have been fulfilled by AHSS but still there is a need of further developments in these steels [Hao, 2011].

1.2.1 Developments in Advanced High Strength Steels

Early efforts to obtain lighter weight and enhanced crash performance invehicles were aimed at the development of high strength low alloy (HSLA) steel. This kind of conventional high strength steel (HSS) has a tensile strength of 250 to 800 MPa as shown in Fig. 1.1. However, the tradeoff between strength and ductility limited the performance of HSLA. To fulfill the requirements for steel with higher strength while retaining its formability, advanced high strength steels (AHSS) were developed during mid-1990. AHSS, as defined by Bhattacharya, [2006] refer to steels with 500 MPa or more tensile strength and complex microstructures comprising of phases such as bainite, martensite and retained austenite. The strengthening mechanisms involved in AHSS include solid solution strengthening, precipitation strengthening, grain refinement and phase transformation. There are three generations of AHSS based upon the microstructure of steels [Hao, 2011; Matlock et al., 2012].

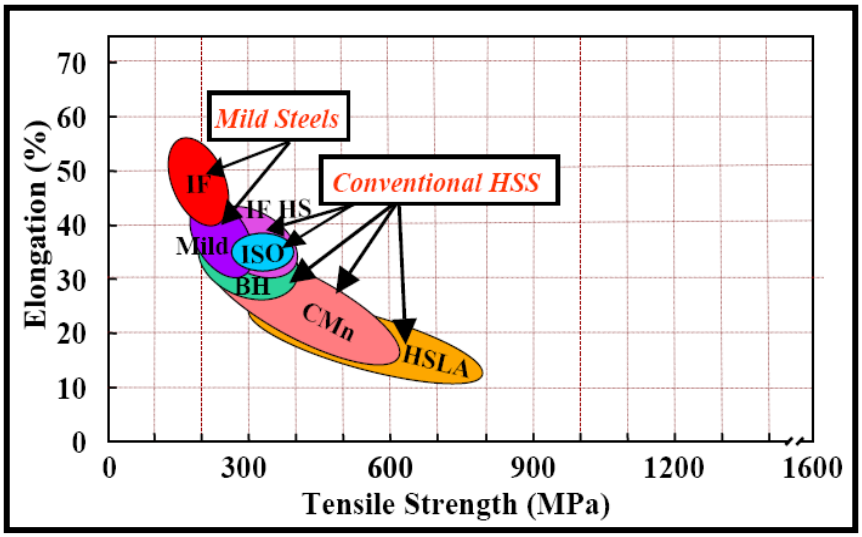

Fig. 1.1: Tensile strength and elongation data for mild steels and conventional HSS [Hao, 2011]

1.2.2 First Generation AHSS

The first generation of AHSS are ferrite based steels, including dual-phase (DP) steels, martensitic steels (MS), complex-phase (CP) steels and transformation induced plasticity (TRIP) steels as shown in Fig. 1.2. Although the strength level for the first generation of AHSS is far beyond that of the conventional HSS, its limited formability and weldability remained a problem [Hao, 2011; Matlock et al., 2012].

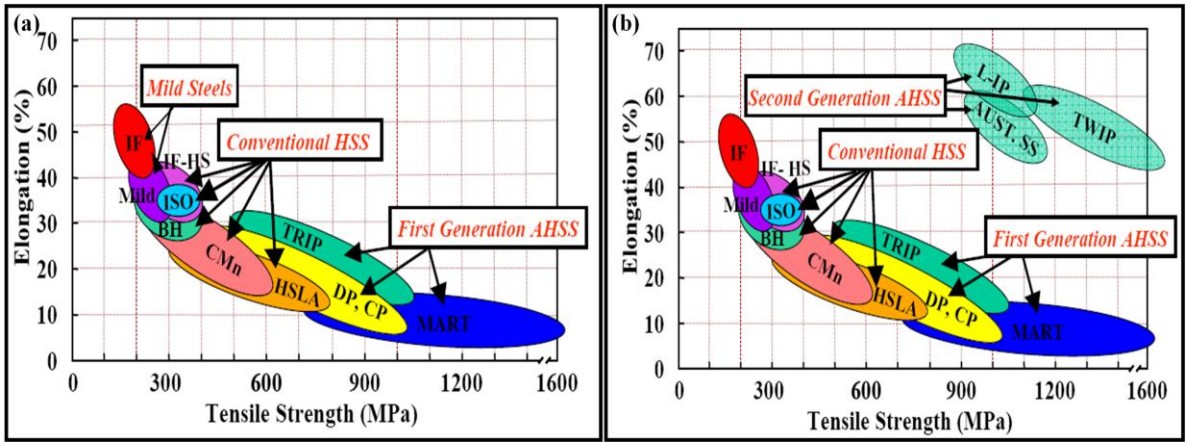

Fig. 1.2: Tensile strength and elongation for (a) mild steel, conventional HSS and 1st Generation AHSS (b) various classes of conventional and AHSS
[Hao, 2011]

1.2.3 Second Generation AHSS

A desire to produce materials with significantly higher strengths has led to the development of a "second generation" of AHSS which are austenitic steels with high manganese contents and are closely related to conventional austenitic stainless steels. During the past few years, a second generation of AHSS has been developed based upon an austenitic microstructure. Twinning-induced plasticity (TWIP) steel, light weight steel with induced plasticity (L-IP) and shear band formation-induced plasticity (S-IP) steel are different grades in this category. A ductile austenite matrix provides better formability to the second generation of AHSS than the first generation. However, the high austenite stabilizer content, such as 20 % manganese and nickel, limits the use of the second generation of AHSS because of its high cost [Hao, 2011]. In addition, industrial processing of these alloys, specifically the TWIP steels with high manganese contents, has shown to be extremely challenging and the TWIP grades have also been shown to be prone to delayed cracking. Figure 1.2 summarizes the tensile strength and total elongation data for

conventional HSS and the 1st and 2nd generation of AHSS [Hao, 2011; Matlock et al., 2012; Kwon et al., 2012].

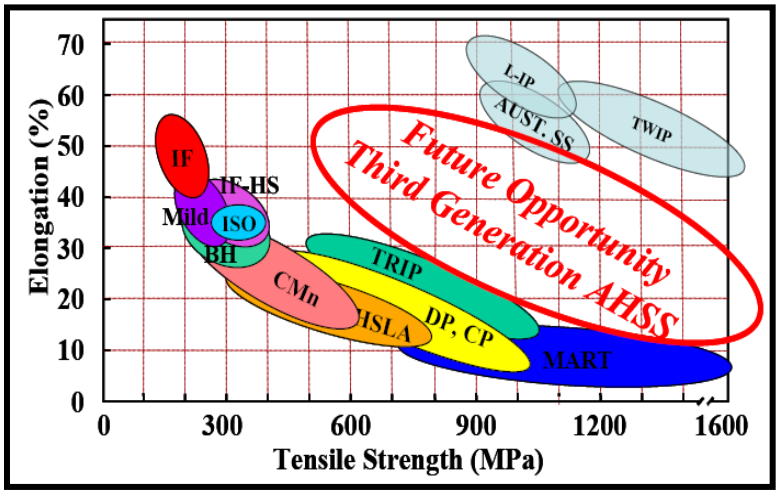

Fig. 1.3: Tensile strength and elongation for various classes of conventional steels and AHSS [Matlock et al., 2012]

1.2.4 Need for Third Generation AHSS

Despite the growing market for AHSS, the trade-off between strength and formability of the AHSS remains the limitation for its application in the automotive industry which requires new vehicle with stylistically and aerodynamically optimized shapes and safety [Bhattacharya, 2006; Hao, 2011; Matlock et al., 2012]. According to Fig. 1.3, the conventional HSS provides steels with total elongation in the range of 10 to 50 %, but the tensile strength of the steels are all below 800 MPa. Most of the first generation of AHSS has tensile strengths greater than the conventional HSS. However, their drops to as low as 10 % when the tensile strength reaches approximately 1000 MPa [Hao, 2011]. Although the second generation of AHSS solves the problem caused by competition between tensile strength and total elongation (Figure 1.3), the high cost for this solution remains the main obstacle for its broad application. Recently, the need to develop AHSS with a range of properties that give engineers more flexibility in selecting an ideal grade of steel for any given application has raised increasing interest in developing a third generation of AHSS [Hao, 2011; Matlock et al., 2012]. The design of the third generation of AHSS is intended to produce steels with a better combination of strength and ductility than the first generation of AHSS and at a lower cost than the second generation AHSS. The mechanical properties of the third generation of AHSS are intended to fall within the gap between the first

and second generation of AHSS (Figure 1.3), e.g. 1000 MPa tensile strength and 30% elongation. In order to reduce the cost, lean alloy steel compositions will need to be used in developing this generation of AHSS. Because microstructure determines the behavior and performance of AHSS steels, the design and control of the microstructure becomes essential for the third generation of AHSS [Hao, 2011; Matlock et al., 2012].

The combination of high strength and ductility that is providing modern AHSS can allow thinner components to be used in the car construction and also to improve the safety due to their high energy absorption capabilities. The better formability of AHSS compared with conventional high strength steels of comparable strength give the automobile designers a high degree of flexibility to optimize the component geometry [Bhattacharya, 2006; Hao, 2011; Matlock et al., 2012].

1.2.5 Third Generation AHSS

From Fig. 1.3 it is clear that a property gap exists between the currently available AHSS grades (first and second generations) and defines a property band for the future "Third Generation" AHSS. Current research is hence focused on filling this property window using modified or novel processing routes where special attention should naturally also be given to industrial feasibility and cost effectiveness. Third generation AHSS are the extension of first generation steels by improving mechanical properties through grain refinement [Bhattacharya, 2006; Hao, 2011; Matlock et al., 2012]. Concurrently with the use of micro-alloyed sheet, steels with a microstructure consisting of at least two different phases can lead to higher strength without deterioration of ductility. These so called multi-phase steels offer attractive combinations of strength and ductility as a result of the different mechanical properties of the microstructural components and their interaction. The ‘‘third-generation’’ AHSS steels should demonstrate the strength–ductility combination significantly better than exhibited by the former (first generation) but need a cost significantly less than required for the latter (second generation). The strategies being pursued for the ‘‘third-generation’’ AHSS steels include processing to enhance properties of DP steels; modifications to traditional TRIP steel processing; development of high-strength steels with ultrafine bainitic microstructures; implementation of new processing routes, including quenching and partitioning (Q&P) and ultra-rapid heating and cooling; and development of high-Mn content TRIP steels [Hulka 2005; Li et al. 2013].

1.3 Microstructure and Properties of Common AHSS Grades

AHSS consist of multi-phase microstructure with a ferrite matrix and /or martensite, bainite and retained austenite. Different types of AHSS show different properties depending upon their microstructure i.e. DP steel (ferrite, martensite/ bainite), TRIP (ferrite, martensite/ bainite, retained austenite), etc. [Kuziak et al., 2008; Matlock et al., 2012].

1.3.1 Transformation-Induced-Plasticity Steel (TRIP)

High-strength transformation-induced-plasticity aided multiphase steels (TRIP steels) have received much attention as these steels have excellent combination of strength and ductility due to the martensitic transformation of retained austenite during plastic deformation. Some authors called it multiphase steel also. This is a much more cost-effective process than the inter-critical annealing process. By heating in inter-critical region and holding in martensitic region by tempering the martensite and stabilize the austenite at room temperature, these steels were produced. In TRIP steels, austenite stabilizers are present (mainly carbon and manganese). During cooling, some austenite transforms to ferrite. The remaining retained austenite transforms to martensite / bainite during plastic deformation [Hulka, 2005; Bhattacharya, 2006; Hao, 2011; Matlock et al., 2012]. Main characteristics of TRIP steel are summarized in Table 1.1 [Kuziak et al., 2008; Hao, 2011].

Table 1.1: Characterstics of TRIP steels

TRIP STEELS	
Microstructure	Ferrite, martensite, bainite, retained austenite
Alloying Elements	High C, Si,Mn and other alloying elements
Formability	Good
Weldability	Carbon should between 0.20–0.25 wt.%
Advantages	High strength, high formability
Performance	High work hardening rate, high energy absorption
Applications	Ancillary parts, Body structure

1.3.2 Dual Phase Steels (DP)

The greatest prospects of the application in the automotive industry have DP-type steels. It 0.05%-0.2%C, 1.2-1.8%Mn, 0.03-0.6%Si and V, Nb and Ti micro additions of total is predicted, that their total share in a car structure can reach over 50%. These steels usually contain concentration up to 0.1%. DP-type sheets can be produced by a classical heat treatment, consisting in their austenitizing at a temperature slightly higher than A_{c1} of the steel with following water quenching or an energy-saving technology of the thermo mechanical treatment, integrating hot-rolling in the austenitic field or $\alpha + \gamma$ region with direct cooling [Adamczyk and Grajcar, 2006; Bhattacharya, 2006; Lorusso et al., 2012; Mohrbacher, 2013].

Microstructure of dual phase steels is composed of soft ferrite matrix and 10–40% of hard mastensite or matrensite-austenite (M–A) particles or bainite as third phase. This type of microstructure allows achieving the ultimate tensile strength in the range of 500–1200 MPa. For some applications, also bainitic constituent may be desirable in the DP steel microstructure. This dual phase type of microstructure can exhibit the following advantageous features over the conventional high strength steels:

- The strength of the DP steel microstructure is controlled by the amount of martensite and ductility by the size and distribution of this phase,
- DP steels do not exhibit yield point elongation,
- DP steels possess low YS/UTS ratio (around 0.5) and high strain hardening characteristics (High *n* value), especially at the beginning of plastic deformation,
- They can be strengthened by static or dynamic strain ageing (BH effect), grades containing low carbon content have been shown to exhibit excellent resistance to fatigue crack propagation.

The microstructure of DP steels do not allow obtaining of high plastic strain ratio value (r_m), which means that these steels are not good candidates for applications that require high drawability. They usually exhibit poor hole expansion ratio values. This drawback, however, can be eliminated by adding Ti with the aim of inducing the precipitation strengthening in ferrite to reduce the differences in hardness between the two phases. Alternatively, M-A constituents may be replaced by bainitic phase. Dual phase steels can be welded with all conventional welding methods currently used in the automotive industry (resistance spot welding, laser welding, arc welding). The most important features influencing mechanical properties of the dual-phase

microstructure comprise shape, size, amount and distribution of ferrite and martensite, the carbon content of martensite, and the volume fraction of retained austenite [Kuziak, et al., 2008].

Very important for the development of dual / multi phase steel is the effect of carbon and alloying elements, which is summarize in Table 1.2.

Table 1.2 Effect and reasons of adding alloying element in Dual/Multi Phase steels [Kuziak, et al., 2008]

Alloying element	Effect and reason of adding
C (0.06–0.15%)	• Austenite stabilizer • Strengthens martensite • Determines the phase distribution
Mn (1.0–2.5%)	• Austenite stabilizer • Solid solution strengtheners of ferrite • Retards ferrite formation
Si (0.005–0.125%)	• Promotes ferritic transformation
Cr, Mo (up to 0.4%)	• Austenite stabilizers • Retards pearlite and bainite formation
V (up to 0.06%)	• Austenite stabilizer • Precipitation strengtheners • Refine microstructure
Nb (up to 0.04%)	• Austenite stabilizer • Reduces M_s temperature • Refine microstructure and promotes ferrite transformation from non-recrystallized austenite

The mechanical properties of Dual Phase steels are controlled by metallurgical factors, such as the volume fractions of the martensitic and ferritic phases, the carbon content of martensitic phase, the grain sizes of the martensite and ferrite and the individual resistances of both martensitic and ferritic phases. The resistance of those phase, is also affected by the chemical composition of steel [Lorusso et al., 2012]. The main characteristics of DP steels are summarized in Table 1.3.

Table 1.3 Characteristics of DP steels [Kuziak et al., 2008; Hao, 2011]

DP STEELS	
Microstructure	Ferrite and martensite/bainite
Alloying Elements	C, Si ,P for strengthening, Mn, Cr, V, Ni For hardenability
Formability	Excellent
Weldability	Good
Advantages	High work hardening rate, excellent elongation, good weldability, high strength
Performance	High UTS, Good manufacturability, good crash resistance
Applications	Body structure, chassis.

1.3.3 Production of Dual/ Multiphase Steels

The development of multiphase steels has become interest in the automobile and truck industries, because of a potential weight reduction by using inexpensive alloying without sacrificing mechanical properties [Saleh and Priestner, 2001]. Multiphase steel mainly consists of two phase viz; ferrite and martensite. But, in addition to martensite, the microstructure may contain small amounts of other phases such as retained austenite, new ferrite, pearlite and bainite, depending on cooling rate and thermo-mechanical process routing [Saleh and Priestner, 2001; Erdogan and Tekeli, 2002].Some of the authors produced multiphase steels by direct quenching from temperature above A_{C1} and inter-critical temperatures. Microstructure produced was ferrite and martensite [Adamczyk and Grajcar, 2006]. Some authors produced multiphase steels by doing slow (air) cooling firstly upto desired ferrite transformation from austenite and then quenching for transforming rest of austenite to martensite (done according to CCT diagram) [Hulka, 2005; Bhattachariya, 2006; Meng et al., 2009]. Few authors produced the steels by a process which includes hot rolling, cold rolling, and continuous annealing in ($\alpha + \gamma$) phase field for the nucleation and growth of austenite into ferrite, quenching for transformation of austenite into martensite, over aging, and air cooling [Saleh and Priestner, 2001; Demir and Erdogan, 2008; Asadi and Palkowski, 2011]. But very few work has been done to produce the bainite/ferrite or martensite/ ferrite microstructure of dual phase steels by controlled cooling (first doing laminar cooling then ultra-fast cooling upto coiling temperature and then by coil cooling to room temperature of hot rolled strip) [Cornet et al., 2003]. Mechanical properties obtained by last

method are better than all other methods due to grain refinement of microstructure and proper volume fraction of phases, which properly fits in the region of third generation AHSS. Also, multi/ dual phase steels of ferrite/ martensite microstructure can be produced by doing ultra-fast cooling directly upto room temperature after slow laminar cooling (3^{rd} generation dual phase steel with refine microstructure). Mechanical properties (strength and toughness) obtained by this method are better than the properties obtained by direct water quenching. However**, c**ertain applications require hot-rolling steel strips that have both high strength and good forming properties. Currently, such a combination of properties is extremely difficult to achieve and moreover is generally obtained only by means of multi/ dual phase steels such as steels with ferrite / bainite of ferrite / martensite microstructure [Cornet et al., 2003].

1.3.4 Properties and Applications of Dual/ Multiphase Steels

The combination of high strength and ductility in modern AHSS can allow thinner components to be used in car construction and also to improve the safety due to their high energy-absorption capabilities. Dual/multi phase steels developed over the past few decades offer impressive mechanical properties, such as continuous yielding behavior and superior strength–ductility combination, high work hardening, in addition to the advantage of reduced cost, better formability, and excellent surface finish [Kumar et al., 2008; Dziedzic and Turczyn, 2010; Sayed and Kheirandish, 2012; Ramazani et al., 2014]. DP steels are strong candidates for structural applications [Kang et al., 2013]. The usage of dual phase steels for automotive applications is increasing because they can meet the formability requirements and other properties such as high tensile strength, fatigue resistance, hole expansion, good drawing and welding properties [Cai et al., 2014].

1.4 Current Trends in the Field of Multiphase Steels

Since the introduction of ultrafast cooling (UFC) technology, multiphase steels have been mostly produced using the combination of laminar cooling and ultrafast cooling and this technology also increases the controllability of the microstructure. The first laminar cooling at low cooling rate allows regulating accurately the intermediate temperature. The ultrafast cooling (UFC) regulates the coiling temperature, and consequently the nature of the second phase [Cai et al., 2014]. In

view of the increasing demands for occupant safety and fuel efficiency, further strengthening of multiphase steels without a loss in ductility is also required. Grain refinement is a promising tool to achieve this aim. In recent years, a variety of new processing routes have been developed to produce ultrafine grained (UFG) low carbon steels with a ferrite grain size of 1μm and below. It is consistently found that yield strength and tensile strength are increased due to grain refinement [Calcagnotto et al., 2010]. Therefore ultrafine grained (UFG) steels with relatively simple chemical compositions have attracted much interest in replacing some conventional high strength alloyed steels.

Methods to obtain UFG multiphase steels can be divided into two categories: (i) advanced thermo mechanical processing (ATMP) routes, which aim at improving conventional processing routes (ii) severe plastic deformation (SPD) techniques. In order to develop new generation steels characterized by friendly environment, low cost and light weight, hot rolled ferrite bainite/ martensite dual phase steels are produced using simple C-Mn-Si chemistry without adding expensive alloys [Tan et al., 2012; Cornet et al., 2003; Demir and Erdogan, 2008; Asadi and Palkowski, 2011]. Thus, it can be said that still development is going on in DP steels, using lean chemistry and different processing routes to manufacture these steels with enhanced mechanical properties.

1.5 Micro-Mechanical Modeling of Dual Phase Steels

Material characterization is an important tool to describe and enhance the mechanical properties of a material by selecting optimum material chemistries and developing suitable microstructures. The usual approach of achieving these objectives through experimental techniques is generally costly and time consuming. To overcome these constraints of experimental approaches, the micro-mechanical modeling approach was developed. This modeling technique helps in predicting the material behavior without extensive experimental investigation. It is based on the microstructural characteristics of the given material [Davies, 1978; Korzekwa et al., 1980; Szewczyk and Gurland, 1982; Alabbasi, 2004; Bouquerel et al., 2006; Reichert and Estrin, 2007; Birgani and Pouranvari, 2008; Bouquerel et al., 2008; Ganguly et al., 2009; Sodjit and Uthaisangsuk, 2011].

1.6 Summary of the Chapter

This chapter includes the introduction and need of Advanced High Strength Steels. It discusses the classification of AHSS based on microstructure and resulting properties. The chapter also discusses the most common types of AHSS in use along with their characteristics. The details of strengthening mechanisms and various issues related to AHSS have been explained. Also, a brief overview of current developments in the area of AHSS has been discussed. Finally, physical mechanical modelling of dual phase steels has been discussed. The next chapter summarizes the research done by various authors in the field of AHSS and gaps in the existing literature.

Chapter 2

Literature Review

2.1 General

This chapter provides literature based background information on the various means adopted by different researchers to produce 3rd generation dual phase steels and to improve upon the properties of 3rd generation Dual Phase Steels.

2.2 Review of the Literature

Patel et al. (2001) studied the effects of micro-alloy addition on a multi-phase hot strip mill (HSM). Author revealed that good toughness could be achieved through grain refinement (the Hall-Petch relationship) and a reduction of second phase micro-constituent. Furthermore, a reduction in the latter also improves the cold formability. Reduction in the sulphur content significantly improves the uniform elongation, and a high uniform elongation equates directly to good cold forming properties. The presence of sulphur will cause the formation of manganese-sulphide (MnS) inclusions, which will elongate during the hot rolling process. The presence of a large number of MnS inclusions (as well as alumina particles - Al_2O_3) will cause cracking or splitting during component forming, especially when the bend axis is parallel to the rolling direction due to the creation of voids at the particle-matrix interface. To retain the original globular shape of the inclusion, additions of elements such as calcium (Ca) can be made, which form sulphides of reduced plasticity at higher temperatures and allow the globular-type inclusions, which are considerably less prone to nucleate voids, to be maintained in the final product.

The relatively low carbon content permits good ductility properties and weldability. The manganese acts as a solid solution strengthener whilst also lowered the austenite-ferrite transformation temperature (Ar_3). However, the manganese content is usually restricted as a solid solution element to levels < 1.80 wt%. Niobium additions up to levels of 0.06-0.07 wt% will generate yield strengths of up to 500MPa. Although, it is noted that at heavier strip gauges (above 6mm), niobium is usually supplemented with additions of vanadium to guarantee the 500MPa yield strength. Nevertheless, the use of niobium as the first choice addition element is

due to its ability to act as a grain refiner, which is well known to increase both strength and toughness. It is caused by the fact, that niobium is far superior to the other micro alloying elements in its ability to raise the temperature at which austenite recrystallization effectively ceases. Furthermore, niobium also provides a further increase in strength via secondary precipitation hardening. For conventional hot strip rolling, niobium mainly acts as a grain refiner, vanadium mainly as a precipitation hardener and titanium's effect can be considered to lie between the two. Hence, niobium has the ability to provide a dual effect in developing high strengths and also improving toughness.

It was also revealed that incomplete dissolution of the micro-alloying elements will mean their exclusion to participate in any grain refinement and/or secondary precipitation hardening. Although a reheating temperature of 1200 ℃ would suffice for the vast bulk of micro-alloyed grades, a reheating temperature of 125 ℃ was commonly applied in modern strip mills, thus guaranteeing an appropriate finish rolling temperature. Temperatures required for complete dissolution of the carbides and carbon-nitrides of niobium that were formed during the cooling of the cast slab. Minimum temperatures required for complete dissolution were determined by the niobium, carbon and nitrogen content and a higher alloy addition will thus require a higher reheating temperature.

Erdogan and Tekeli (2002) investigated the effect of martensite particle size on tensile fracture of surface-carburized steel with dual phase core microstructure. Three specimens were made from surface carburized steel coded as A, B and C. Specimen A corresponded to normalizing and then oil quenching from the inter-critical annealing temperature of 731 ℃ (dual phase with coarse martensite particles in the core). Specimen B was oil quenched from 900 ℃ and then oil quenched from the inter-critical annealing temperature of 731 ℃ (dual phase with fine martensite particles in the core). Specimen C was conventionally heat-treated involving directly oil quenching from 900 ℃ (fully martensitic microstructure in the core). Authors observed that Specimen B exhibited higher tensile and yield strength than specimen A because microstructure of specimen B was finer than specimen A. The martensite particles were almost isolated in the ferrite matrix at 25% MVF in specimen B. The greater tensile and yield strength of specimen B was attributed to different particle size and spacing. Also, finely dispersed, hard second phase in a soft matrix offered more effective barriers to motion of dislocations and provides more effective composite strengthening for a fixed MVF. Total elongation of specimen B was superior

to that of specimen A. Also, tensile strength and initial work hardening rate of specimen B were higher than in specimen A. The ratio of uniform to total elongation was lower for specimen B. Higher ductility of specimen B comparing to specimen A was explained by higher potential of specimen B for the micro-void nucleation sites. There were a greater number of martensite particles per unit volume and therefore more micro void nucleation sites in specimen B. Specimen C with wholly a martensitic structure at the core and surface region exhibited higher yield strength than both specimens A and B but almost the same tensile strength as specimen B. However, specimen C showed no difference between uniform and total elongation. In the coarse microstructure (Specimen A), a martensite particle aligned along a ferrite grain boundary could crack easily. Martensite cracking in the fine microstructure (Specimen B) was less frequent and voids were always smaller, relative to specimen A. The fracture surface of specimen B, which had the finer martensite particle size showed ductile dimples. In specimen B cleavage facets were not observed. In specimen A, predominantly cleavage facets were observed. The specimen C with almost fully martensitic structure in the core showed completely cleavage type fracture.

Seong et al. (2004) studied the effect of retained austenite and solute carbon amount on the mechanical properties of TRIP steels. Two cold-rolled strips namely CS1 of composition (C-.077, Si-1.00, Mn-1.50, P-0.0084, and Sol. Al-0.036) and CS2 of composition (C-0.079, Si-1.51, Mn-1.50, P-0.0095 and Sol. Al-0.033) with thickness of 1.3 mm were processed for heat treatment. Heat treatment process consisted of austenizing at 830 ℃ for 50 s, rapid quenching to the bainitic transformation temperature 360 ℃–460 ℃, and an isothermal holding (austempering) for 5 min. High-resolution powder diffractometer was used to measure the diffraction pattern. Data was collected between 10^{o} and 155^{o} in 2θ sample rotation with intervals of 0.05^{o}. Tensile properties were measured by ASTM A370 tensile specimens. It was observed that retained austenite content decreased with increase in austempering temperature in CS1 steel specimens. This was because higher austempering temperature led to cementite precipitations causing faster decrease of carbon content in retained austenite so that nucleation of new bainitic ferrite plates became easier. The CS15 sample with more silicon caused suppression of carbide formation during bainite transformation and thus enriched the retained austenite with carbon. Authors concluded that the increase in austempering temperature caused decrease in retained austenite and carbon content. Also, the amount of retained austenite was proportional to the carbon content in austenite and elongation increased with increase in retained austenite and carbon content.

Hulka (2005) investigated the effect on properties of Multi Phase (MP/TRIP) steels by addition of niobium. In production of MP steel, first heat treatment was carried out at slightly higher temperature in two phase region (50% ferrite and 50% austenite by wt). Quenching was done to avoid any major ferrite formation. Final transformation was carried out isothermally in bainite region (second heat treatment). During the bainite formation, the carbon diffused into remaining austenite islands, which got finally enriched to a level of more than 1% carbon. Austenite with high carbon was stable at room temperature also.

Austenite can also be stabled at room temperature by addition of niobium in multiphase steels. Addition of niobium affects the microstructure and mechanical properties viz: addition of Nb reduces annealing time which resulted in greater retained austenite at room temperature due to carbon enrichment of austenite; formation of NbC precipitates which hamper the grain growth resulted in fine grained austenite. Nb also retards recrystallization of austenite during hot strip rolling. Thus, prepared more nuclei for the austenite to ferrite transformation resulted in a finer grain size of the hot band. So above factors increased the strength (due to grain refinement and NbC precipitation) and elongation (due to stability of austenite at room temperature and also by nucleation of ferrite at austenite-ferrite inter-phase during cooling). It was revealed that Nb alloyed MP/TRIP steel hardness was about 20 % higher than niobium free steel (due to finer grain size). MP/TRIP steel with 0.03 % to 0.04 % Nb has greater strength than MP/TRIP steel without Nb. Also observed that increase in yield strength and tensile strength was around 15 MPa per 0.01 % of niobium.

Adamczyk and Grajcar (2006) investigated the effect of heat treatment conditions on the structure and mechanical properties of Dual Phase (DP) type steel. For the experimentation steel (C:0.09; Mn:1.5; Si:0.26; Ni:0.07; P:0.014; S:0.009; B:0.003; Al:0.029; N:0.012: Fe: balance; all in wt %) was melted and continuous casting of 100x100mm slabs were done. After solidification the slabs were hot-rolled and forged in order to obtain the rods with a section of 24x24mm. The specimens for structure and mechanical properties investigations were prepared after the heat treatment. The heat treatment of the specimens was realized according to three routes. In the routes I and II, the steel was heated to a temperature of 910 ℃ ($\alpha + \gamma$ region), hold at this temperature for 30min. In route I specimen air cooled to room temp then again heated to 750 ℃ and water quenched. In route II specimen was water quenched from both temperatures viz: 910 ℃ and 750 ℃. The route III consists in austenitizing of steel at a temperature of 910 ℃ and

air cooling for 45 s to a temperature of 750 ℃ in order to realize the partial α to γ transformation, followed by water quenching. The steel heat-treated according to the route I has the ferrite structure with an irregular envelope of martensite on grain boundaries. In route II during heating the steel to an under hardening temperature, the nucleation of austenite mainly occurs on the boundaries of martensite laths formed after primary quenching from a temperature of 910 ℃. The predominated martensite fraction occurs mainly as thin fibers located in surroundings of grain boundaries. Moreover, in surroundings of martensite, especially at a boundary zone of large grains of the alpha phase, small grains of the recrystallized ferrite can be identified. In route III Martensite was located on grain boundaries of the alpha phase. The optimum fraction of martensite averaging 20% occurs after air cooling of the specimens for 45s.The used conditions of the heat treatment led in obtaining the DP-type steels of comparable fractions of ferrite and martensite. The optimum fraction of the martensite was from 21% to 24%, and a grain size of α phase equals from 7 μm to 10 μm. The diversified morphology of martensite had the influence on various mechanical properties of the steel and its deformability. The optimum strength and ductile properties had the route II steel. The yield point of this steel was about 520 MPa, tensile strength about 800 MPa, total elongation 20%, and uniform elongation about 16%.

Ahmad et al. (2007) studied the effect of thermo-mechanical processing on the hardenability and tensile fracture behaviour of dual-phase (DP) steels. Thermo-mechanical processing with various rolling reductions (0-50%) was applied in the inte-rcritical temperature range of 725–830 ℃ on low alloy hot rolled steel (0.09 C, 1.2 Mn, 0.78 Cr, 0.26 Si, 0.15 Ni, 0.2 Cu, 0.04 Mo and balance Fe, % wt) followed by quenching in the iced brine solution Metallographic examination of the as-received steel showed a microstructure comprising of ferrite and pearlite phases. Samples were inter-critically heat treated in an argon atmosphere in the range 725–830 ℃ for 20 min and then quenched in brine solution. Due to very fast cooling rate, the austenite phase almost fully transformed to martensite. Point counting method was used to determine the volume fraction of austenite. It was observed that at a temperature of 790 ℃, about 50% of austenite got formed; at this temperature, samples were rolled and cross section reductions in the range 0–50% (0, 20, 30 and 50 % reduction respectively) in lateral and longitudinal direction were achieved. All the specimens were quenched in iced brine solution, offering a cooling rate of about 500 ℃ /s After grinding and polishing, specimens were etched with 5% picral followed by 2% nital

solution and then immersed in a boiling alkaline chromate solution (8g CrO_3 + 40 g NaOH + 72 ml H_2O). It was observed that with rolling at a temperature of 790 ℃ for 0 to 50% thickness reduction, about 6% of ferrite increased in rolled specimens even after quenching but not in the un-rolled condition which reflected that rolling in the inter-critical region decreased the hardenability. The increase in the rolling reduction resulted in more strain and martensite particles became more fibrous. In longitudinal direction, the martensite fibers were lengthened and got reduced in thickness by rolling. In the transverse direction, they did not lengthen but thinned in the direction normal to the rolling plane. Thus, the aspect ratio of the martensite fibers was more in the longitudinal than in the transverse direction, and this affected the tensile properties to a great extent. For 30% reduction, maximum true stress in longitudinal and transverse direction were 1023 MPa and 902 MPa respectively; similarly for 50%, values were 1021 MPa and 939 MPa respectively. The UTS almost remained equal in both directions. Total elongation was also significantly affected for 50% rolling in transverse and longitudinal directions with total elongation of 12% and 18% respectively. Hot rolling in the Inter-critical region increased the strength of the steel without an appreciable loss in ductility. Rolling also increased the aspect ratio of the martensite more in the longitudinal direction than in the transverse directions, which developed the tensile properties.

Kuziak et al. (2008) presented some basic concepts of Advanced High Strength Steels (AHSS) for use in the automobile industry, which included their chemical composition design, microstructure analysis, and mechanical properties development during thermo-mechanical processing, production technology characterization, potential applications and performance in service. The authors reported that AHSS are characterized by improved formability and crash worthiness compared to the conventional steel grades. The category of AHSS covers the following generic types: dual phase (DP), transformation induced plasticity (TRIP), complex phase (CP) and martensitic steels (MART). As opposed to the conventional high strength steels in which ductility decreases with strength, modern AHSS steels combine high strength and formability/ductility.

Microstructure of dual phase steels is composed of soft ferrite matrix and 10–40% of hard martensite or martensite-austenite (M–A) particles which allows achieving the ultimate tensile strength in the range of 500–1200 MPa. The strength of the DP steel is controlled by the amount

of martensite and ductility by the size and distribution of this phase. DP steels possess low YS/UTS ratio (around 0.5) and high strain hardening characteristics (high *n* value).

Transformation-induced plasticity (TRIP) steels are based on the principle that the strain or stress induced transformation of retained austenite present in the microstructure in a sufficient amount can substantially harden the steel during deformation. The mechanical properties of TRIP steels are derived from their dispersed multi-phase microstructure which is composed of ferrite (0.50–0.55), bainite (0.30–0.35), retained austenite (0.07–0.15), and possibly martensite (0.01–0.05). To obtain the best mechanical properties in a product, carbon should be distributed to austenite and should enrich this phase as much as possible to preserve the M_s below the room temperature (generally 15−25 ℃ below room temperature).

Complex phase (CP) steels belong to a group of steels with very high ultimate tensile strength of 800 MPa or even greater. The chemical composition of CP steels contains some quantities of Nb, Ti and or V to cause the precipitation strengthening effect. CP steels have no retained austenite in the microstructure, but contain more hard phases like martensite and bainite. Their mechanical properties are characterized by continuous yielding and high uniform elongation. Martensitic (MART) steels provide the highest ultimate strength in final products, up to 1500 MPa. Microstructure of martensitic steels is mainly composed of lath martensite, which is developed by the transformation of austenite during quenching after hot rolling or annealing.

AHSS are produced in complex processes involving thermo-mechanical processing followed controlled cooling. For producing DP steels, the cooling process after rolling starts with slow cooling stage (on the run out table) after rolling in which the desirable amount of ferrite is obtained as a result of the austenite transformation. The ferrite transformation allows the carbon content enrichment in the remaining austenite, which increases its hardenability and reduces Ms Temperature. The optimal combination of strength and ductility of TRIP steels is achieved by grain refinement and obtaining a uniform distribution of fine second phase particles. The cooling stage in the strip rolling process of TRIP steels is more complicated than that for DP strips. After producing 50–60% of ferrite in the microstructure, accelerated cooling with cooling rate greater than 20 ℃/s to the coiling temperature which lies in the bainitic transformation temperature range, is realized. During coil cooling, bainitic transformation proceeds, further increase the carbon content in remaining austenite to around 1.2%. A part of this austenite, in the amount of 10–15%, remains untransformed accounting for the TRIP effect. The concept of CP steels is

essentially similar to those of TRIP steels, however less stringent cooling practice is imposed on the hot band during the last stage of processing as no presence of retained austenite is required in their microstructure. Martensitic steels are produced by applying rapid quenching from the austenitic phase to produce the laths martensite microstructure. Finally from the discussion it was concluded that a substantial progress has been achieved during the last same years in the development of AHSS.

Calcagnotto et al. (2010) studied the effect of grain refinement on the strength and toughness of dual phase steels. Large strain warm deformation at different temperatures and subsequent inter-critical annealing had been applied to obtain fine grained (2.4 μm) and ultrafine grained (1.2 μm) ferrite/martensite dual-phase (DP) steels. The mechanical properties of the produced steels were tested under tensile and impact conditions and were compared to a hot deformed coarse grained (12.4 μm) reference material. The chemical composition of the steel used was (in wt. %) 0.17 C, 1.49 Mn, 0.22 Si, 0.033 Al, 0.0033 N, 0.0017 P and 0.0031 S. To obtain the final ferrite/martensite dual-phase microstructure, the specimens were subjected to inter-critical annealing in a salt bath furnace. The temperature was held constant at 730 ^{o}C. The samples were annealed for 3 min in the salt bath, before they were quenched in water to obtain a ferrite/martensite DP structure. The martensite volume fraction and grain size were determined using the scanning electron microscope (SEM). The coarse grained (CG) steel had a grain size of 12.4 μm and contained 31.3% martensite in ferrite matrix. Fine grained (FG) steel had grain size of 2.4 μm and comprised of 30.1% martensite while the ultrafine grained (UFG) steel had grain size of 1.2 μm with 29.8% martensite. Cylindrical tensile test specimens with a diameter of 4 mm and a gauge length of 20 mm were machined and tensile tests were conducted at room temperature. Impact tests were also carried out in the temperature range of -40℃ to 200℃. Results showed that with decrease in the grain size, ultimate tensile strength and yield strength increased remarkably while uniform elongation and total elongation were affected marginally. The ductile to brittle transition temperature was decreased from 127 ℃ to 100 ℃ for fine grained steels and for ultrafine grained steels it was decreased to 90 ℃ which showed the improvement in the impact toughness. The formation of the cracks and cleavage fracture was also suppressed in the fine grained and ultrafine grained steels. Therefore, it was concluded that the grain refinement affects the properties of dual phase steels and ultrafine grained dual phase steels provide better properties as compared to fine grained and coarse grained dual phase steels.

Dziedzicand and Turczyn (2010) investigated the influence of cooling rate on phase volume fraction and some mechanical properties of hot rolled DP strips. The round ingot of diameter 210/190 mm and length 400 mm was cast in laboratory condition. After head and tail cropping it was preliminary hot deformed to the flat specimens of dimensions 12.4 × 26.8 × 120 mm. These specimens were used in experimental hot rolling and cooling, which schedule presented in following Table.

Series	Heating Temp (°C)	Roll End Temp (°C)	Number of Passes	Reduction in Passes, %	Cooling Way	Phase Content
2P –A	1250	909	2	2×60	water	F–30.4; M–69.6
2P –B	1250	880	2	2×60	air	F–66; P–34
3P –C	1250	787	3	2×60 + 1×35	water	F–34.4; M–65.6
3P –D	1250	747	3	2×60 + 1×35	Water spray	F–59.3; B–40.7
3P –E	1250	735	3	2×60 + 1×35	air	F–79; P–21
3P –F	1250	768	3	2×60 + 1×35	Water + holding in ferrite region	F–69.4; M–19.1; B–11.5

The increase of cooling rate after hot rolling above the critical cooling rate results in increased martensite volume fraction in steel, and thus higher strength and lower formability of investigated strip samples. The cooling rates for different coolants (water, water sprinkle, air) were computed after some tests. Martensitic phase prevails (from 66 to 70%) when using water cooling (rate about 100 ºC/s) and thus very high strength (*Re*, *Rm*, and HV) and low formability of steel strips were obtained. In case of water spray cooling (rate about 15 ºC/s), the bainitic phase (41%) was formed. Thus, lower but enough high strength and better formability of strip samples were obtained. When air was used as a coolant (rate about 4 ºC/s), only ferritic-pearlitic microstructures were observed. However, the best results were obtained when water cooling with holding inside ferrite region (about 7 s) was applied. In this case hot rolled strips had microstructure containing much lower of martensite (19.1 %) and some quantities of bainite (11.5 %). The obtained microstructure results in adequately low yield stress (*Re* = 479 MPa) and high ultimate strength (*Rm* = 786 MPa), allowing for obtaining sufficiently good *Re*/*Rm* ratio (equal 0.61) and acceptable level of cold formability (15%). By combining a number of different microstructures a wide range of mechanical properties of DP steel strips are possible for

obtaining. This shows that rolling mills can adjust processing of DP strips to meet the applications requirements demanded by the automotive industry.

Kwon et al. (2010) discussed the new trends in development of Advanced High Strength Steels and elaborated on the salient characteristics of the next generation AHSS having enhanced performance.

The conventional AHSS are high strength steels having tensile strength – elongation (TS-EI) product lower than 25,000 MPa. %. The typical steels in this group are DP, TRIP and martensite-based complex microstructure steels. The microstructure of these steels contains phase transformation products like retained austenite, martensite and bainite. In addition, various thermal cycles are generated to obtain the desired microstructure. These steels have their own advantages and disadvantages as compared to each other (e.g. a primary advantage of DP steels compared to TRIP steels is better weldability. However ductility of TRIP steels is more than DP steels). AHSS with higher hole expansion ratio value have been developed to enhance stretch flangeability and bendability. A few authors are focusing on the development of TRIP steels having TS-EI product greater than 25,000 MPa%. This group of steels are categorized as the so called X-AHSS (e.g. M-TRIP (martensite based TRIP) steel is defined as the TRIP steel with martensitic matrix). M-TRIP steel is produced by Q&P process in which austenite is formed at high temperature either by full austenitization or by inter-critical heat treatment, which is followed by rapid cooling to a temperature between M_s and M_f to control the fraction of martensite and retained austenite. The typical TS-El product value is slightly greater than 25,000 when conventional TRIP steels with lean alloying elements are Q&P processed and the microstructure consists of uniformly distributed annealed martensite matrix and retained austenite. In SB-TRIP (Super Bainite TRIP) steel, nano-sized bainitic microstructure is embedded with retained austenite. This steel has a tensile strength of 1187 MPa and an elongation of 39%. In order to enhance the ductility of AHSS, it is desired to have austenite as the matrix phase. For improved ductility, it is also important to utilize transformation hardening phenomenon and to control the mechanical stability of austenite phase properly. The typical TS-El product for ultra-AHSS is greater than 50,000 MPa·%. These steels have superior strength and ductility combination. TWIP (Twinning Induced Plasticity) is a potential mechanism to obtain the superior balance of tensile strength and elongation, and is extensively utilized to develop steels of the Ultra-AHSS class. The typical value of TS-El product for TWIP steels is about

65,000 MPa·%, more than three times greater than those of conventional AHSS. This superior mechanical performance has been obtained by gradual twinning during deformation. The formation of twins partitions austenite grains and induces the continuous strain hardening, resulting in improved ductility.

Matlock and Speer (2010) studied the processing opportunities for new advanced high-strength sheet steels. In this paper author represent the three categories of AHSS and argued that complex microstructure will be required to obtain good combination of strength and ductility. Authors represent the conventional cold-rolled processing of DP and TRIP steel. After that author represents some new techniques to process DP and TRIP steels. For processing of DP steel a new technique in which a sample of 0.17C-0.74Mn steel was processed in 5 steps to produce ultrafine grained DP steel. In first step sample was quenched in ice-brine bath from a temperature of 1000 ℃ after 30 min soaking and result in fully martensite microstructure that was tempered in second step. In third step sample was cold rolled up to 80%. In fourth step sample was annealed to a temperature 550 ℃ and soaked for 75 min and then water quenched to form an ultra fine aggregate of ferrite and carbide. In step five a system was heated rapidly at 300 ℃ /s to a temperature between A_{c1} and A_{c2} soaked for 5–10 sec to minimize the ferrite grain growth and promote carbide dissolution and austenite formation. An ultrafine structure was developed with a martensite volume fraction of approximately 0.42 having a uniform distribution of 2 um martensite islands on water quenching. For processing TRIP steel author recommended the nitrogen as an austenite stabilizer to provide improved mechanical properties, because of limited nitrogen solubility, 200 ppm N_2 was recommended for conventional steelmaking practice. Because of high nitrogen content lead to high amount of retained austenite stabilization. Author recommended the use of Q&P heat treatment for better result of all kind of AHSS steels. At the end author concluded that steels with good properties will contain significant amounts of a austenite and high strength constituents, including martensite, bainite, ultrafine grained ferrite. The significant opportunities for the production of new AHSS products have been identified, although most require higher heating and/or cooling rates, and advance techniques are required to implement these processing routes.

Asadi and Palkowski (2011) investigated the effect of the local influence and developed processes which were able to induce a locally restricted strengthening effect for multipurpose steels. Two different methods were investigated to achieve local strengthening.

For the first method the sheet is deformed partially and afterwards heated globally. The sheets were deformed locally with the specific deformations and then subsequently aged at different temperatures (100 ℃, 170 ℃ and 240 ℃) for a holding time of 20 min.

A second method was to deform the sheet globally with defined degrees of deformation. Consequently, the deformed sheet was heat treated locally by laser. To understand the dependencies, samples of size 500 × 80 × 2.0 mm had been strengthened homogeneously by cold rolling with different thickness reductions (e = 2%, 5% or 10%) before the local heat treatment (LHT).

In first type of samples the hardness values were determined both in locally deformed region and as well as in the basic sheet. It was revealed that heat treating at 100 ℃ produces no change in the hardness values compared to the initial state. At 170 ℃, an increase in hardness of about 15 HV0.1 in locally deformed region was obtained. In addition to this, there was also an increase of hardness in the basic metal at this temperature. A further increase in the aging temperature up to 240 ℃ did not show a change in hardness value as compared to that at 170 ℃. the yield and tensile strength values rose steeply as the pre-strain increased, while the total elongation decreased with increasing pre-strain for all aging temperatures. Total elongation decreased with increasing the aging temperature.

In second type the hardness distribution of steel followed a global deformation by cold rolling to 5% and laser treatment with different laser powers at constant laser speed was done. It was revealed that after cold rolling to 5% the measured hardness was 235 ± 8HV0.5. For a laser power of 0.6 kW and 1.4 kW a minor increase in hardness could be observed. For a laser power of 2.2 kW, the highest hardness increase of 135 ± 9 HV0.5 and, consequently, local strengthening was measured. For 2.8 kW, a significant hardness increase of 120 ± 11 HV0.5 could be observed. Compared to 2.2 kW the hardness distribution decreased in the middle of laser treated region. This was due to an overheating effect. The reason for the enhancement of the hardness values of samples, which were treated with lower laser powers, compared to the non-laser treated condition, could be contributed to the bake hardening effect. The significantly higher hardness values at higher powers were due to affecting of microstructure. The higher heat

treating temperatures lead to the formation of a large number of martensite and bainite with local plastic zones, having a high dislocation density, in polygonal ferrite and local strengthening due to phase transformation. Similar hardness distributions could be measured for DP steels with 2% and 10% deformation. In tension test local laser treatment leads to strengthening of steel and therewith reduced deformation in these areas, where necking occurs in the non-treated areas. The treated areas show a strong reduced deformation compared to the non-treated areas. The partial heat treatment with the laser leads to a reduced deformation in the tensile test and can be used for local reinforcement.

Thomas et al. (2011) produced dual phase, Quenched and Partitioning (Q&P), TRIP and ferrite-pearlite microstructure in a single steel alloy by thermal processing of hot-strip mill cooling practices through varying the coiling temperature.

Commercially cold rolled TRIP sheet steel (C: 0.19; Mn: 1.59; Si: 1.63; Fe: balance; all in wt %) was taken. Thermal processing was conducted on sheet specimens with dimensions of 127 mm×25.4 mm×1.2 mm. The samples were heated to the temperature 1173 K (Fully austenized) and 1093 K (inter-critical temperature) and held for 180 seconds. After that samples were helium quenched (run out table water cooling). Fully austenized (FA) samples were quenched upto 473–573 K and inter-critically annealed samples were quenched upto 373–773 K temperature (with 25 K step in each). Then all samples were coil cooled to room temperature. For IC samples the coiling temperature range from ~448 K to 523 K, microstructures were observed that had primarily Q&P-like character. The mechanical properties of the Q&P microstructures transition between those of dual-phase microstructures (high tensile strength with lower elongation) and the TRIP microstructures (lower tensile strength with higher elongation) in this range of coiling temperatures. The TRIP microstructures contained significant fractions of retained austenite stabilized via the formation of bainitic ferrite. The fraction of bainitic ferrite increased with increasing coiling temperature (up to the Ms). The samples coiled between 548 K and 698 K exhibited significantly higher uniform elongations, while the UTS remained relatively unchanged. This range of coiling temperatures included some samples that were classified primarily as Q&P microstructures and some that were classified as TRIP microstructures, with mixed microstructures at intermediate temperatures within this regime. These samples exhibited work hardening characteristics involving a constant or increasing instantaneous strain hardening exponent with true strain, often associated with TRIP behavior. The transformation from retained

austenite to martensite increases uniform elongation by virtue of the volume expansion associated with the transformation, thus delaying the geometric instability condition, while maintaining high UTS due to the formation of a harder phase (martensite), the generation of additional dislocations, and the resulting work hardening effect. The steels exhibiting the dual-phase microstructures (i.e., the lower coiling temperatures) exhibited the lowest yield strengths with the highest tensile strengths. That was due to high density of mobile dislocations and the internal stresses caused by the shear and volume expansion associated with martensite formation from austenite. The unpinned dislocations around the martensite allow the steel to yield continuously. With increased coiling temperature, the extent of aging of the ferrite around the martensite presumably increased (i.e., some dislocations become pinned by solute atoms and others were recovered). Thus, the yield strength increases slightly with increasing temperature. Mechanical properties of steel samples were insensitive to coiling temperature in range of 273 to 498 K. In coiling temperature range 498 to 623 K both strength and elongation varied coiling temperature. In coiling temperature range 623 to 773 K uniform elongations were significantly affected with variation in coiling temperature.

FA samples were showed high tensile strength (1100-1400 MPa) with uniform elongation between 4 and 7 pct, due to the formation of martensite and some retained austenite (2 to 4% wt) and few ferrites.

Wang et al. (2011) presented the experimental results for the development of Ti-micro-alloyed bainite-ferrite multiphase steel with perfect comprehensive properties by Ti-micro-alloying which had relative lower cost comparing with niobium and vanadium alloying. The experimental steel (C: 0.04–0.06; Si: 0.25–0.45; Mn: 1.4–1.6; Al: 0.02–0.04; Ti: 0.06–0.12; N: 0.003–0.005; Fe: balance; all in wt %age) was firstly melted in a vacuum induction furnace and casted into a 50 kg billet, this was then heated in reheating furnace to 1373 K. After that steel was rolled to a 5.5 mm-thick plate. Rolling finish temperature of plate was 1153-1103 K. Then steel was cooled to finish cooling temperature range of 903-863 K with cooling rate of 13-40 K/s and then quenched to room temperature. Authors revealed that microstructure obtained was composed mainly of lath bainite and some ferrites. Matrix of experimental steel was refined bainite laths, which showed 3–6 mm sheaves with interrupted or film type retained austenite between the laths. There was irregular granular bainite or acicular ferrite between the sheaves. These refined matrix structures had high strength and toughness. In addition, there were different volumes

fractions of polygonal ferrite distributed at original austenitic grain boundary or in the grain interior. With the increase of cooling rate after rolling (13–40 K/s), volume fraction of ferrite reduced gradually and the ferrite morphology turned from approximately polygonal to acicular which increased strength. In addition to this, Nano-sized cubic shape TiN and approximate spherical TiC precipitates existed in the experimental steel, which provided the strengthening effect by grain refinement, strengthening and precipitation hardening so as to increase the strength and toughness. The increase of cooling speed prevented or delayed the premature precipitation of titanium carbide during cooling, which was ready for formation of more dispersed precipitates, further improving strength and toughness of the steel. Through rational chemical composition design, control over rolling and rapid cooling, making full use of titanium precipitation hardening and grain refinement strengthening, Ti micro-alloyed bainite-ferrite multiphase steel was successfully developed with good comprehensive properties and relatively low cost. Experimental steel had tensile strength up to 875 MPa, impact energy of 27 J at 253 K, showing a good balance of strength and toughness.

Matlock et al (2012) studied recent advanced high strength steels developments and also unique strength and ductility combinations for these steels were discussed.

Ongoing AHSS research is focused on increasing strength and/or ductility to higher level than exhibited by the first generation AHSS without significantly enriching the alloy compositions, or is aimed at reducing the alloying levels in second generation AHSS grades. These strategies for making third generation steel (AHSS) include: processing to enhance properties of DP steels; development of high strength steels with ultrafine bainitic microstructures; implementation of new processing routes including quenching and partitioning (Q&P); and development of high Mn content TRIP steels.

An increase in strength of Dual Phase steels can be readily obtained by increasing the martensite volume fraction by altering carbon content and/or inter-critical annealing temperature. A strength increase has also been obtained by microstructural refinement resulting from special hot deformation practices, one of which is referred to as Deformation Induced Ferrite Transformation (DIFT).

Recent work has been conducted to create ultrafine bainitic microstructures. The microstructure was obtained after a 15 day heat treatment, a time which may be too long for industrial purposes

and thus further work has been done on increasing bainite kinetics, reducing heat treatment to hours rather than days by alloying with Al and/or Co.

Quenching & Partitioning (Q&P) has been proposed recently as a new way of producing martensitic steels containing enhanced levels of retained austenite. The process consists of a two-step thermal treatment where the steel is quenched to a predetermined temperature (quench temperature, QT) in the Ms-Mf range to produce a partially martensitic, partially austenitic microstructure. The second, so-called partitioning step, aims at carbon enrichment of the austenite by (partial) carbon depletion of the martensite and carbon transport to the austenite. Thus, carbon stabilized austenite is retained in the microstructure after final quenching to room temperature. The addition of molybdenum retards bainite transformation kinetics and increase the retained austenite volume fraction whereas aluminum substitution for silicon has been found to accelerate the bainite reaction, and reduce the retained austenite fractions. High retained austenite fractions are believed to result in improved strength and ductility.

An alternative process to produce fine grained or ultra-fine grained duplex ferrite-austenite microstructures based on "medium" manganese (5–7 wt %), low carbon (0.1 wt %) compositions is manganese enrichment of austenite during inter-critical annealing applied to a cold rolled 0.1-C, 7.1-Mn (wt %) steel to produce a range of microstructures with varying austenite fraction and stability. Based on equilibrium thermodynamic predictions samples of the steel were annealed for 168 h at temperatures between 575℃ and 675 ℃. The long annealing times were employed to facilitate Mn partitioning. The resulting microstructures included between 2 and 43 pct retained austenite in a fine grained ferrite matrix (between 0.9 and 1.5 μm). It is important to note that alloy designs have been based primarily on low carbon steels due to welding considerations. Modifications to weld designs or joining processes may allow the use of higher carbon equivalent grades in the future, enabling new process/product concepts that are considered infeasible at present. With the extensive current research activities leading to new AHSS products, the challenges to researchers, steel producers, and designers are to identify and optimize promising alloys and processing routes to minimize the time required for economic implementation of new AHSS products in vehicles of the future.

Mohapatra et al. (2012) investigated the different cooling processes for getting ultra-fast cooling rate for a hot static plain carbon steel plate. Additionally, process controlling parameters for UFC have been investigated.

Air assisted spray and conventional water spray experiments were conducted on 12 mm thick plate, which was heated in a muffle furnace to 1100 ℃ having K-type thermocouple inserted within plate. The steel plate to be analyzed was prepared with the proper number of holes for thermocouples. After inserting the thermocouples, the strip was put inside the Muffle furnace. The thermocouple extensions were connected to the data acquisition system (DAS). After attaining the desired temperature in the muffle furnace, the pump (CP) and compressor (C) were switched on to make the spray system ready. The hot steel plate was brought out from the muffle furnace and put on the resting pad (RP); simultaneously, the temperature was recorded continuously in real time and saved in a file for further analysis. The flow rate of water was controlled by valves. The flow rate of air and water were set at a particular value by rotameters. The air pressure was controlled by valve (V1) and monitored by pressure gauge (G1). The data collected was analyzed for the heat flux study.

From the experimental investigation, it was found that atomized spray can produce UFC cooling rates for both the early and late varieties for a hot steel plate. The maximum rate obtained by early UFC was 134 ℃/s, whereas that of late UFC was 155 ℃ /s for 12mm thick plate. In addition to the above, the effect of water impingement density, air pressure and plate thickness on rate of cooling were also investigated. It was revealed that, on increasing the water impingement density, the cooling rate increased; also, on increasing air pressure, the cooling rate increased. On increasing plate thickness, the cooling rate decreases.

Yong et al. (2012) investigated the industrial applications of ultrafast cooling (UFC also known as NG-TMCP) and compared with the conventional thermo mechanical controlled processes (TMCP also ACC-accelerated cooling) for X70 pipeline. The authors revealed that the typical microstructure of X70 pipeline steel consisted of acicular ferrite and quasi polygonal ferrite. Ultra-fast cooling of plates immediately after the last finishing rolling pass led to ferrite grain refinement and finer precipitation of Nb (C, N). The nucleation rate increased with increasing cooling rate, which refined the acicular ferrite. Mechanical properties were improved by finer gain size and refined precipitates. It was also important for hot rolled steel to keep enough shape accuracy. The passing rate of shape of 17.2 mm X70 pipeline steel without UFC was only qualified by 10%. Also, severe plate warping occurred when conventional laminar cooling (ACC) was conducted. On the contrary, the passing rate of shape of the same X70 pipeline steel as described above with UFC was qualified by 95%. It was very difficult to find plate warping

phenomena for X70 pipeline steel after UFC. The control accuracy of red back temperature at UFC mode was much higher than that at ACC mode. The temperature uniformity in the longitudinal direction of X70 pipeline steel was improved significantly due to the UFC control systems, and this undoubtedly reduced cutting quantity of head and tail of the plate. The total cutting of head and tail got reduced from 900 mm (ACC) to 600 mm (UFC). Therefore, the UFC control system offered advantages of low cost and good performance, and they were suitable for X70 pipeline steel on production line.

Li et al. (2013) investigated a Transformation Induced Plasticity (TRIP) steel (based on dynamic transformation of under cooled austenite) treated by thermo-mechanical processes to combine the effect of microstructure refinement and solution strengthening of alloying elements. The steel (C: 0.2; Mn: 2.0; Si: 2.0; Fe: balance; all in wt %) blanks were hot forged at temperature of 1373–1223 K and air cooled, then machined into the special compression samples. After austenization at 1273 K for 5 minutes, the samples were cooled at 5 k/s to 1023 k and deformed at 1/sec to various strains (S1-0.36; S2-0.69; S3-0.92; S4-1.20), then cooled to 673 K at 30 K/s and held for 3 minutes and finally cooled to room temperature by water.

Microstructure of steel after holding 3 m at 673 K temperature was consisted of bainite, martensite, austenite and ferrite. Austenite remained in two types viz: deformed grain austenite (A), blocking islands of austenite between ferrite grains. It was revealed that with increase in strain, ferrite increased, bainite decreased, austenite A decreased and blocky austenite increased. But, grain size of ferrite decreased according to Hall-Petch relationship so yield strength decreased. Yield strength also decreased due to decrease in bainite. Another reason for decrease in yield strength was formation of blocky M/A islands between ferrite grains by generation of new mobile dislocations in surrounding ferrite grains.

Ultimate tensile strength first increased and then decreased. At the same time, the uniform elongation and the total elongation first increased then decreased. Variation in ultimate tensile strength was due to two reasons viz: decrease in yield strength or increase in flow stress from S1 to S4, due to carbon content in retained austenite which, firstly increased and then decreased.

For the used steel treated by the thermo-mechanical process, product of tensile strength and total elongation can be upto 2500 MPa pct.

Mohrbacher (2013) discussed microstructural optimization for multiphase steels with improved formability and damage resistance. Author revealed that Multiphase steels typically available in the tensile strength range of 450–980 MPa are widely used in today's car body manufacturing. Their characteristics of high n-value and good elongation (A80) are connoted with good press formability. However, practical experience has shown unexpected failure in forming operations where tight bending, stretch flanging or hole expansion were predominant due to the hardness difference between phases. The inhomogeneous microstructure of soft ferrite and hard phase constituents in combination with local straining was inherent to these problems. However this forming behavior can be much improved by microstructural refinement and homogenization of the phases as well as modification of hardness contrasts. Although this effect is principally unavoidable, measures can be taken to reduce the criticality of this phenomenon. Microstructural refinement in combination with homogenization of the individual phases is the key approach in this respect. A small addition of Nb and optimized hot–rolling are the most effective in achieving such optimized microstructure. This is reflected in a clearly improved hole expansion ratio and bending angle. Grain refinement also leads to better elongation and n-value. Low-carbon DP steel offers improved weldability and improved hole expansion ratio. Processing of low-carbon DP grades is challenging especially in a hot-dip galvanizing line. Mo alloying is the most efficient means of making low-carbon DP robust for processing under such conditions. It can be concluded that the combination of microstructural refinement and reduced carbon content provides the best spectrum of application properties for dual phase steel.

Wu et al. (2013) studied the thermal stability of retained austenite in Q&P steel during tempering at elevated temperature by use of differential scanning calorimetry (DSC). Steel with composition (C-0.20; Si-1.42; Mn-1.87; Al-0.0405; P- 0.012; S-0.0006) was selected for testing. In Q&P process, steel was heated to a temperature of 900 ℃ soaked for 5 min followed by quenching in a salt bath at 320 ℃ for 60 s (i.e. named as Q&P 320-60) and then water quenched to room temperature. Another specimen was quenched into liquid nitrogen from 900℃ after soaking for 5 min to produce a fully martensite structure and was named as (liquid nitrogen quenched) LNQ. Zwick (T1-FR020TN A50) tensile testing machine was used to measure the mechanical properties at a strain rate of 10^{-3} s at room temperature. Nikon (EPIPHOT 300) optical microscope was used for microstructure examination after Nital etching. Austenite volume fraction at room temperature was determined by X-ray diffraction by using a (D/max-

2550) X-ray diffractometer. Kinetics of austenite decomposition was studied by differential scanning calorimetry (DSC) for which specimens of size1.3mm (in height), 3.5 mm (in diameter) were heated from 25 ℃ to 500 ℃ at heating rates of 5, 10, 15, 20 K/min in DSC chamber, and then cooled to 25 ℃ at a rate of 40 K/min. Kissinger method was used to determine activation energy (E). Q&P based specimen resulted in high amount of retained austenite (10.6%) than LNQ (1.5%) specimen. Also Q&P based steel resulted in a good combination of tensile strength (1311 MPa) and elongation (13.6%) with large n value (0.085) compared to LNQ (0.033). These results indicated that the Q&P steels had more potential to show a better TRIP effect than LNQ. Also, the activation energy of austenite decomposition was determined to be 221.3 KJ/mol with thermal decomposition temperature of retained austenite in range of 400 ℃ to 500 ℃ which was also an indicative of good TRIP effect. At the end the authors concluded that the Q&P steel was superior to LNQ steels with better combination of strength (1311 MPa) and elongation (13.6%) and with high thermal stability.

Meng et al. (2014) studied the effect of fast-heating annealing of a cold-rolled dual-phase steel on the mechanical properties. For experiments, an industrial Dual Phase (DP590) steel (Fe, 0.07 C, 1.7 Mn, 0.429 Si, % weight) was taken. The Ac1 and Ac3 temperatures for pearlite to austenite transformation were taken as 1023 K and 1193 K. A heating rate of 500 K/s was performed on the specimen of dimension 300×260×1.5 mm3 and was rapidly heated to 1133 K, on the self designed fast-heating test bench, soaked for 2s and then cooled down to 323 K at a cooling rate of 100 K/s. The same DP590 steel commercially manufactured through continuous inter-critical annealing at a cooling rate of (3 to 5 K/s) was also studied for comparison. Two tensile samples were cut parallel to the rolling direction each for annealing routine and tensile testing. Quantitative phase measurements were conducted using a point counting method. Two typical tensile engineering stress–strain curves were obtained from the DP steel subjected to different annealing routines. Both curves showed clear discontinuous yielding characters of DP steel. It was found that the average yield strength of fast-heating samples increased from 277 MPa to 372 MPa (34.3% higher) and ultimate tensile strength improved from 625 MPa to 666 MPa (6.6% higher), total elongation was improved from 23.3% to 26.6% (14.1% higher). Cold rolled DP590 steel contained elongated ferrite grains and pearlite colonies, the average ferrite grain sizes in the fast-heating sample refined remarkably from about 11.2 to 4.3 μm, and the secondary phase changed from coarse lath-like martensite to fine fiber-like martensite. The

improvement of strength was thus related to the ferrite grain refinement. It was also noticed by quantitative measurement that the content of martensite increased slightly from 23 % (volume fraction) to 27 %, which also played a positive role on the strength in the fast-heating samples in addition to the grain refinement effect. In continuous annealing, ferrite matrix and the grain boundary dislocations were free and martensite had a coarse lath like structure. In the fast heating process, there was lesser time spent by steel above the Ac1 temperature (only 3.3 s); so full austenite formation did not take place and a fine fibrous morphology of martensite was obtained. This improved the strength (some bainite may also be formed due to lack of carbon). During the conventional continuous annealing with slow heating rates, the ferrite recrystallization would have fully completed when heated to the inter-critical zone and then the austenite would have nucleated at the recrystallized ferrite grain boundaries and grew along them. However, under the fast-heating conditions, the recrystallization stage was strongly suppressed, during the heating stage; the austenite formation and its distribution were strongly influenced by the overlapping of the processes of recrystallization and austenization. The microstructure characterization was done by optical microscope which showed that the steel composed of the complex phases mainly of refined soft ferrite, hard martensite and bainite etc. This unique distribution of soft and hard microstructure was correlated with the improved strength and ductility, which implied that the simplified high-efficiency fast-heating process could be a promising alternative over the conventional continuous annealing process.

Cai et al. (2014) studied the process design and evaluated the mechanical properties of dual phase (DP) steels with pre-positional ultra fast cooling. The authors investigated the three-stage cooling process for DP steels with pre-positional ultra fast cooling (UFC) equipment, which was different from the normal DP production line. DP steel strips (0.085 C, 0.62 Si, 0.92 Mn, 0.013 P, 0.008 S, 0.39 Cr, 0.08 Cu, 0.02 Nb, 0.02 Ti and balance Fe % weight) of dimensions 110×83×70 mm3 were taken. Trials were conducted under both laboratory as well as industrial conditions. Laboratory samples were hot rolled on a two-high hot mill with provision for pre-positional UFC and laminar cooling. The mill was equipped with multi-functional cooling system (such as laminar cooling, water curtain, ultra fast cooling, and spray cooling) and could realize a wide range cooling paths and cooling rates. The slab was reduced from 70 mm to 4 mm thickness. The cooling process involved air cooling, UFC, air cooling followed by laminar cooling. The cooling began at a temperature of 1050–1100 ℃ intermediate cooling temperature

was kept between 740℃–700 ℃ with a holding time of 6 s. The cooling rate of UFC was 120 ℃/s and that for laminar cooling was 40 ℃/s. The industrial trials were carried out at the same conditions with the exception that the intermediate temperature was kept at 710 ℃ with a holding time of 5 s. For analysis purpose, a two-dimensional finite difference method (FEM) was employed to estimate temperature distribution across the cross-section and the CCT diagrams were prepared (for both conditions). The temperature field was simulated for various cross sections.

It was found that a higher cooling rate was achieved at the corners because of which there was more martensite in the final product. The biggest temperature difference across the cross-section was 7 ℃, 14 ℃, 22 ℃ and 45 ℃ for thickness of 2 mm, 3 mm, 4 mm, and 5 mm respectively. It was found that ferrite grain size was related to prior austenite grain size; the grain size distribution across the cross-section was obtained by coupling the temperature distribution and the grain size under different cooling routes. The microstructure varied a little from surface to centre (internal ferrite grain size was 5.2–5.4 μm but at the corner it was 4.5–5.2 μm). The stress–strain plot of each phase (ferrite and martensite respectively) was simulated and plotted. The laboratorial trial results were: 365–375 MPa (YS), 590–640 MPa (TS), and 0.57–0.78 (YR). The industrial trial results were: 400–476 MPa (YS), 575–670 MPa (TS) and 0.57–0.79 (YR), which was a little better than laboratorial trial. In pre-positional UFC, the austenite transformation was inhibited (and there was suppression of pearlite and bainite formation), and the residual austenite transformed to martensite. The coil box was used for good temperature homogeneity. The finishing temperature was controlled precisely; UFC was mainly used to refine the grains. If the martensite fraction was to be increased then accordingly, the holding time should also be increased to obtain adequate austenite. The DP steels made by prepositional UFC had tensile strength and yield strength in excess of 590 MPa and 400 MPa respectively, the yield ratio was in the range 0.60–0.78 and the elongation was greater than 22%. Also by the combination of temperature field and phase field, the cooling process of DP steels could be simulated, and ferrite grain size and tensile behavior could be predicted with reasonable accuracy. This simulation method, however, did not take into account precipitation effect of Nb, Ti and their compound.

2.3 Summary of the Given Literature

1. Several authors worked on the first generation AHSS and successfully achieved high strengths as compared to conventional steels but could not achieve good formability. Several authors worked to overcome this problem and substantially improved the ductility and strength by forming second generation AHSS. The mechanical properties of second generation depend upon expensive alloy additions which made them expensive for use. Authors became successful in achieving good strength and ductility but because of alloying, the weldability suffered. Finally, a few authors have reported their work on third generation AHSS, where first generation steels have been modified through a suitable alloy additions, improved processing routes to improve formability, strength and toughness. DP steels were not good candidates for applications that require high drawability. They were usually exhibit poor hole expansion ratio values. That drawback eliminated by adding Ti with the aim of inducing the precipitation strengthening in ferrite to reduce the differences in hardness between the two phases [Bhattacharya, 2006; Kuziak et al., 2008; Matlock and Speer, 2010; Matlock et al., 2012].
2. Some researchers have studied the effect of inter-critical annealing and water quenching parameters on the microstructure and mechanical properties of DP steels. Water quenching is one of the most economical and high powerful rapid cooling methods. Also, the authors have reported that multiphase microstructure consisting of significant amount of retained austenite and high strength constituents, including martensite, bainite, ultrafine grained ferrite is required to obtain good combination of strength and ductility [Bhattacharya, 2006; Kwon et al., 2010; Matlock and Speer, 2010].
3. Some of the authors have reported that TRIP steels, based on the Transformation Induced Plasticity effect, offer the highest combination of strength and elongation, which is a measure of high level of energy absorption and has great potential to act as a third generation AHSS [Bhattacharya, 2006; Kuziak et al., 2008; Kwon et al., 2010; Matlock and Speer, 2010; Matlock et al., 2012].

2.4 Gaps in the Existing Literature

The following gaps have been identified after the review of literature:

1. Though several authors have used the water quenching route for producing dual phase microstructure in steels, but have not been able to produce refined microstructure. Investigations need to be carried out to produce dual phase ferrite-martensite structures with martensite phase finely dispersed in the ferrite matrix. For this, this structure needs to be produced through controlled cooling which has not been adequately reported in literature.
2. Very limited literature has been reported on the fabrication of TRIP steels through the quenching and partitioning (Q&P) route which can provide better TRIP effect and hence properties that are obtained through the conventional processing routes.
3. Several authors have reported their work on production of dual/multi-phase microstructures in steels containing titanium, vanadium, niobium etc. as the alloying elements. The results are encouraging but the presence of such elements in the steel makes it very costly. Very few authors have worked with steels of lean chemistry to produce AHSS. TRIP effect obtained in AHSS has largely been exploited in the presence of heavy alloy additions (austenite stabilizers). Limited attempts have been made to generate TRIP effect in AHSS with steels of lean composition.

Chapter 3

Design of the Study

3.1 Introduction

This chapter presents the overall design of the study. It describes the objective of the present research, methodology, experimental procedure adopted, and provides details of machines, equipment and commercial software used for carrying out the research work.

3.2 Establishment of the Objective Function

The review of literature for the present work revealed that extensive work has been reported with regards to production of dual phase steels of the third generation. Most of the reported work has shown utilization of conventional cooling (i.e. direct quenching either from austenization temperature or from inter-critical temperature range) for producing DP steels. Very few authors have reported on production of these steels using the concept of controlled cooling. Further, in these limited writings also (on controlled cooling), the reported work has involved steels of rich chemistry (high alloy additions) to obtain desired properties. Because of the high alloy additions in such steels (Ti, V, Nb, B, etc.), the objective of cost effectiveness is not met. Thus, there was a scope of work to produce third generation dual phase steels with leaner chemistry providing equivalent or better mechanical properties. Also, work had been reported with regards to production of DP steels through conventional cooling methods to obtain different strengths by taking different compositions. Very few authors reported on the production of multi-functional multi/dual phase steels by using a single chemistry through controlled cooling. Thus, the *overall objective of the present study is to produce a multi-functional multi/dual phase steel through controlled cooling of a steel with lean chemistry.*

The present research work is an effort to address the following:

- To study the formation and stabilization of austenite phase during inter-critical (isothermal) annealing of normalized steel under fast heating rates (up-quenching).
- To establish the process routes for the annealing cycle in order to produce the required multi/ dual phase microstructures.

The overall objective of the present work consisted of several sub-problems/ issues. The key issues taken up during the present research work are as follows:

- To investigate the microstructure of the as-received material using optical microscopy and to perform its tensile testing for determining the mechanical properties.
- To obtain the inter-critical annealing parameters (annealing temperature, holding time, cooling rates etc.) for the given alloy chemistry using available literature and JMat-Pro/ Thermo-Calc software. To utilize this temperature range for conducting annealing experiments in the muffle furnace and annealing simulator.
- To provide isothermal annealing (through water quenching) to the samples in the inter-critical range 750–850 ℃ for 3 min for observing formation of austenite phase. Also, to quantify the austenite volume fraction through optical microscopy.
- To subject the samples to inter-critical annealing process at the selected annealing parameters under controlled cooling using an annealing simulator. To develop annealing process routes for producing multi/dual phase steel.
- To conduct microstructure characterization of the annealed specimens using optical microscopy and hardness measurements. Also, to determine the volume fraction of constituent phases viz. ferrite and martensite etc. using Image Analyzer software 'Image J'.
- To conduct tensile testing of the annealed samples treated under various annealing conditions for determining the ultimate tensile strength and percentage total elongation. Also, to make theoretical predictions of the flow curve behavior of dual phase microstructure.

3.3 Experimental Procedure

The details of experimental procedure followed in the present research work have been described as follows:

3.3.1 Characterization of the as-received material

The starting material was a normalised steel sheet of 1.0 mm thickness having a chemical composition as shown in Table 3.1.

Table 3.1: Chemical composition of the as-received steel

Element	C	Mn	Si	S	P	Al	N	Fe
% wt.	0.11	1.8	0.325	0.006	0.016	0.052	0.0056	Balance

Specimens of the as-received steel were prepared for microstructural examination using standard metallographic techniques like mounting, planar grinding, rough polishing, final polishing, etching etc. Nital, a solution of HNO_3 (3%) in ethanol was used as the etchant to etch the surface of the specimens. Micrographs were recorded with an optical microscope for different resolutions (100X, 200X, 500X, and 1000X).

3.3.2 Phase Transformation Studies using Commercial Software

After microstructure analysis of the as-received material, the next step was to determine the annealing process parameters which could result in desired microstructure in the heat treated steel. Thus, this phase of research was to work on the details of annealing temperature range (lower and upper critical temperature of steel), soaking time spans, cooling rates etc. to be followed for the steel during its annealing. These details were worked out using commercial software viz. JMat-Pro and Thermo-Calc. The software packages were used to determine the CCT, TTT, equilibrium diagram, and phase fraction diagrams of the steel under investigation.

3.3.3 Heat Treatment and Microstructural Analysis

Next, annealing experiments were conducted with process parameter values calculated by Thermo-Calc and JMat-Pro software. For annealing, two types of samples were taken. Samples to be heat treated in muffle furnace were of 10 X 10 X 1 mm^3 size and samples to be treated in the annealing simulator were prepared as tensile specimens in the standard dog-bone shape with 35 mm gauge length. Annealing experiments were conducted in muffle furnace (heating in furnace followed by water quenching), just to note the amount of austenite that forms in the given steel under specific time-temperature conditions during annealing. Annealing experiments performed in annealing simulator were subjected to different cooling routes. The alternate cooling routes were obtained in the simulator through a mixture of hydrogen and nitrogen gases taken in different concentrations and injected in the simulator at different pressures.

Samples were subjected to isothermal annealing in the temperature range, Ac_1–Ac_3 at different inter-critical temperatures and held for 3 minutes followed by cooling. Holding periods as reported by Thomas et al. [2011] were used in the present work. For muffle furnace samples, cooling mode was water quenching. For samples to be treated in the annealing simulator, cooling was done in a controlled manner according to the CCT diagram. Controlled cooling with different cooling routes (marked as A, B, C in Figure 3.1) resulted in different microstructures. Samples of type A were directly cooled (at a rate more than critical cooling rate) to room temperature from the heat treatment temperature and showed martensite/ ferrite microstructure. Samples of type B were cooled rapidly and were held in the bainitic region for 1 minute to obtain ferrite-bainite-martensite multi-phase microstructure. Samples of type C were rapidly cooled to a temperature in the M_S–M_F range and held for 1 minute in the martensitic region to temper the martensite. Heating chamber of the annealing simulator was charged with the mixture of hydrogen and nitrogen gases even before loading the samples to also provide protection against oxidation of samples through a reducing environment.

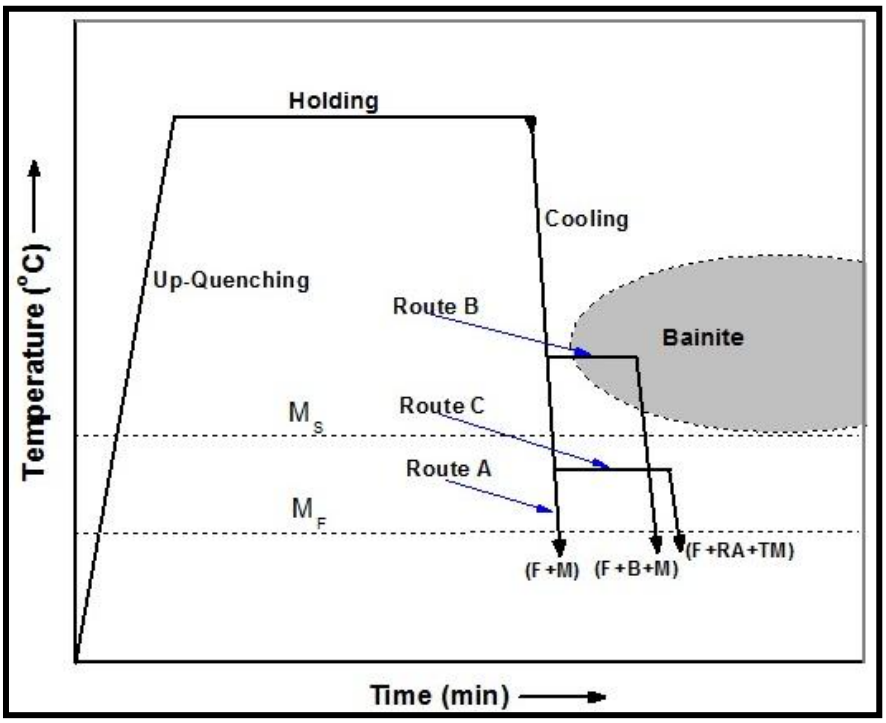

Fig. 3.1: Schematic of different heat treatment routes

After heat treatment under various temperature-time conditions, microstructure of samples was investigated by optical microscopy and even SEM analysis for a few samples. Phase fraction of

constituent phases was calculated using the software 'Image-J'. In this manner, the overall objective of producing a multi-functional multi/dual phase steel through controlled cooling of a steel with lean chemistry is to be achieved. Also, the experimental results obtained were compared with those calculated from Thermo-Calc and JMat-Pro.

3.4 Machines and Equipment

This section describes the detail of various machines, equipment, commercial software etc. used for the present experimental work. A brief outline and description of the characteristic features of these is described as below:

3.4.1 Precision Cutter

The precision cutter (Make: Mecatome T 255/300, Metal Power Analytical (I) Pvt. Ltd, Andheri, India.) is a compact, multi-purpose cutter for cutting a variety of materials. The sheet of the given steel was mounted between the two clamping vices. The sheet was positioned in any starting position relative to the cutting wheel and then the arm was gently lowered until the cutting wheel had cut the sample from the steel sheet. Figure 3.2 shows the precision cutter used in the present work.

Fig. 3.2: Low Speed Precision Cutter (Courtesy: NML, Jamshedpur)

3.4.2 Muffle Furnace

Muffle furnace is a front loading box type oven or kiln for high temperature applications such as for fusing glass, creating enamels coatings, ceramics soldering and brazing of articles. The inner

chamber is made of stainless steel and heaters are clamped to its outside and operated at low heat. Glass wool insulation is used between the two walls. Temperature control is provided by a capillary thermostat which possesses excellent durability and accuracy. Heaters are made of 80/20 nichrome wire, uniformly wound on the muffle. The safety fuse limits the temperature from exceeding the value of the set temperature. A control box is fitted at the bottom of the furnace and consists of indicating lamps, On/Off switch, digital temperature controller along with Cr/Al thermocouple sensor. The furnace is electrically operated at 230 volts (AC), single phase, and 50 Hz supply. The muffle furnace used in the present work is shown in Fig. 3.3.

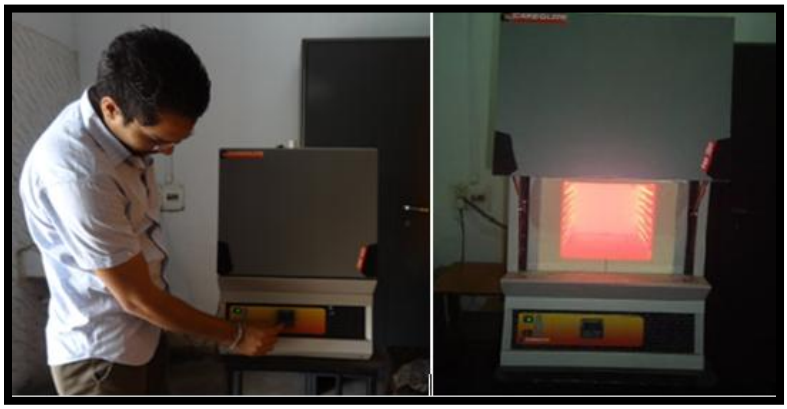

Fig. 3.3: Muffle Furnace (Courtesy: NML, Jamshedpur)

3.4.3 Tensile Testing Machine

The primary use of the tensile testing machine is to create the stress-strain diagram. After the diagram is generated, a computer algorithm calculates the yield strength, tensile strength and total elongation of the tested specimen.

Fig. 3.4: Tensile Testing Machine (Courtesy: NML, Jamshedpur)

Figure 3.4 shows the set-up of tensile testing machine used in the present work. Tensile tests were conducted at room temperature using a tensile testing machine (Make: Instron 8501 System, *Instron Engineering Corporation*, Norwood, USA) of 100 kN capacity in the region of uniform elongation. Elongation was measured by an extensometer of 25 mm range. In the present study, a flat dog-bone shaped specimen of 35 mm gauge length as per the ASTM standard E-8M was tested at a strain rate of 1×10^{-3} s^{-1}.

3.4.4 Hardness Testing Machine

Vickers hardness tester is a key piece of equipment that is vital to metallographic research. In Vickers micro-hardness test procedure, indentation is made with a range of loads using a diamond indenter which is then measured and converted to a hardness value. For this purpose, test samples are carefully and properly prepared by grinding and polishing. Two types of indenters are generally used for Vickers test family; a square base pyramid shaped diamond indenter for Vickers hardness testing and a narrow rhombus shaped indenter for Knoop hardness testing. The Vickers hardness test method requires a pyramidal diamond with square base having an angle of 136° between the opposite faces. Upon completion of indentation, the two diagonals are measured and the average value is considered.

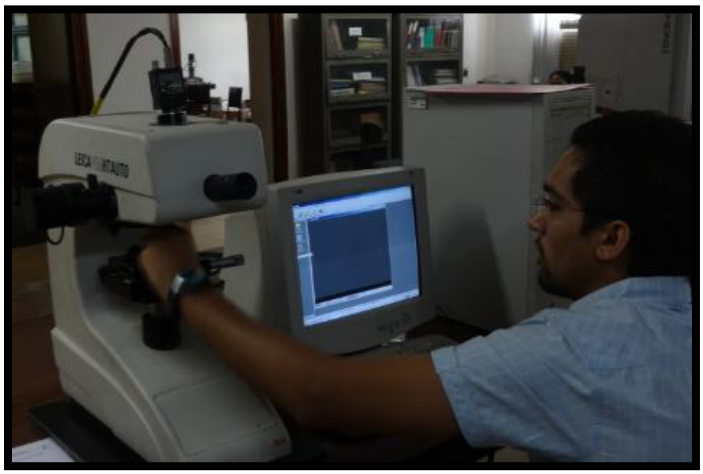

Fig. 3.5: Vickers Micro-hardness Tester (Courtesy: NML, Jamshedpur)

Vickers Hardness Number (VHN/ VPN) is obtained by dividing the applied load in kilogram-force by surface area of indentation. Figure 3.5 shows the hardness tester used in the present work (Make: Leica Q550MW VMHT Auto, *Leica Microsystems*, Wetzlar, Germany**).** In the

present study, the micro-hardness tester was operated at a low load of 50 g-force for a dwell time of 15 s and with an indenter speed of 30 μm/s.

3.4.5 Annealing Simulator

Annealing simulator is specialized equipment for annealing of steel samples in a controlled environment. In this simulator, the samples to be annealed can be heated in a controlled environment and can be cooled under controlled cooling rates. The simulator has been designed and developed jointly by CSIR-NML and Tata Steels, Jamshedpur. The following is a description of the annealing simulator.

A. Heating System: The simulator is based on a unique high speed heating method which makes it capable of typically running the thermal tests at rates 7–10 times faster than the conventional furnace equipped devices. The heating system can be manipulated by the specimen's loading technique to achieve heating rates of upto 100 ℃/min and higher. Also, the simulator can maintain and hold the specimens at steady-state equilibrium temperatures. The thermocouples fitted in the chamber provide signals for accurate feedback control of specimen temperatures.

B. Cooling System: Cooling of the specimens is achieved by purging a gas mixture of hydrogen and nitrogen at very high pressures. Different cooling rates can be achieved by either changing the percentage of hydrogen gas in the gas mixture or the purging pressure or both.

C. PLC based Digital Control System: The heart of the system is the PLC based Digital Control System. It provides all the signals necessary to control the annealing simulator variables simultaneously through a digital closed-loop system. The system can be operated in several modes (totally manual control, combination of computer and manual control etc.) to provide maximum versatility in the annealing simulations.

D. Process Simulation of Annealing Simulator Simulation of metallurgical processes requires controlled process environment, high temperatures and controlled heating and cooling rates over a wide range. Annealing simulator enables controlled process environment and controlled heating and cooling rates.

Heating Mode: Heating mode is by radiation. A maximum operating temperature of 1050 ℃ is achievable at a controlled heating rate of > 25 ℃/s or slower.

Process Environment: Gas mixing system can produce a H_2-N_2 gas mixture of 5–30% H_2 for adjusting the dew point, which is desired for bright annealing of steels. Pure H_2 gas medium can also be used in the system.

Cooling Medium: Controlled cooling rates (>100 ℃/s) of specimens is achieved by using high pressure gas jet. Multiple options for cooling medium are available; such as hydrogen, nitrogen, or mixture of these, atomized water, air humidification etc. Specific heat capacity studies of various gases indicate that cooling efficiency of H_2 is several times higher than that of others.

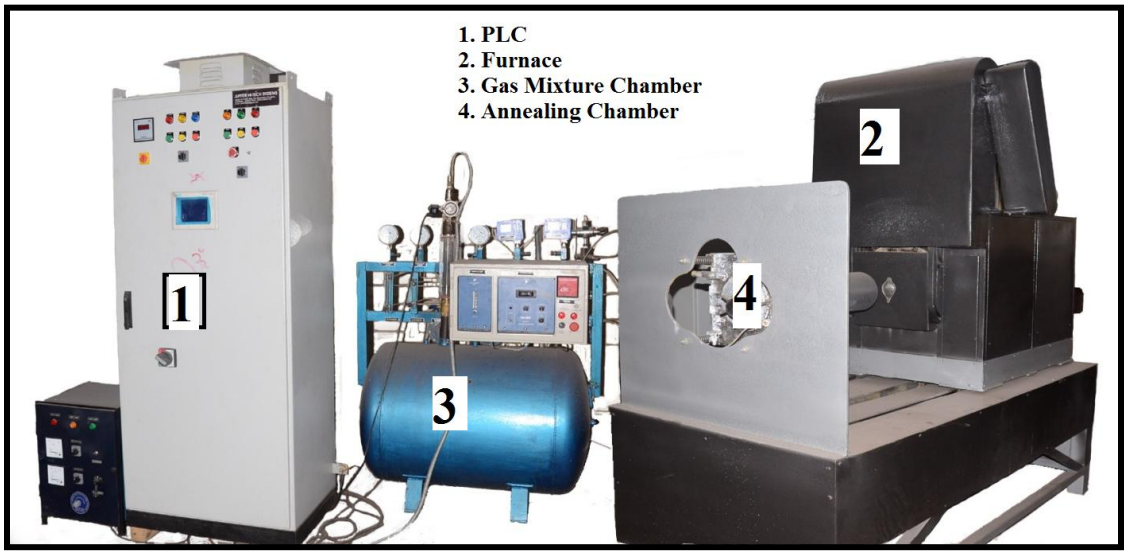

Fig. 3.6 Annealing Simulator (Courtesy: NML, Jamshedpur)

3.4.6 Commercial Software

Two main commercial software viz. Thermo-Calc and JMat-Pro were used in the present study. The details regarding use of these software packages in the present research are as follows:

A) Thermo-Calc

To investigate the critical temperatures of the given steel and to determine the phase fractions at various inter-critical temperatures (during heating), Thermo-Calc software (*Thermo-Calc 3.0*; developed by *Thermo-Calc Software AB*, Stockholm, Sweden) was used to obtain the phase fraction diagram and equilibrium diagram. Equilibrium diagram provides data both on critical temperatures (Ac_1 and Ac_3) as well on phase fractions of ferrite and austenite at the inter-critical temperatures. Phase fraction diagram presents the volume fraction of constituent phases at a

given inter-critical temperature. Figure 3.7 shows some screen shots to demonstrate the working of Thermo-Calc software.

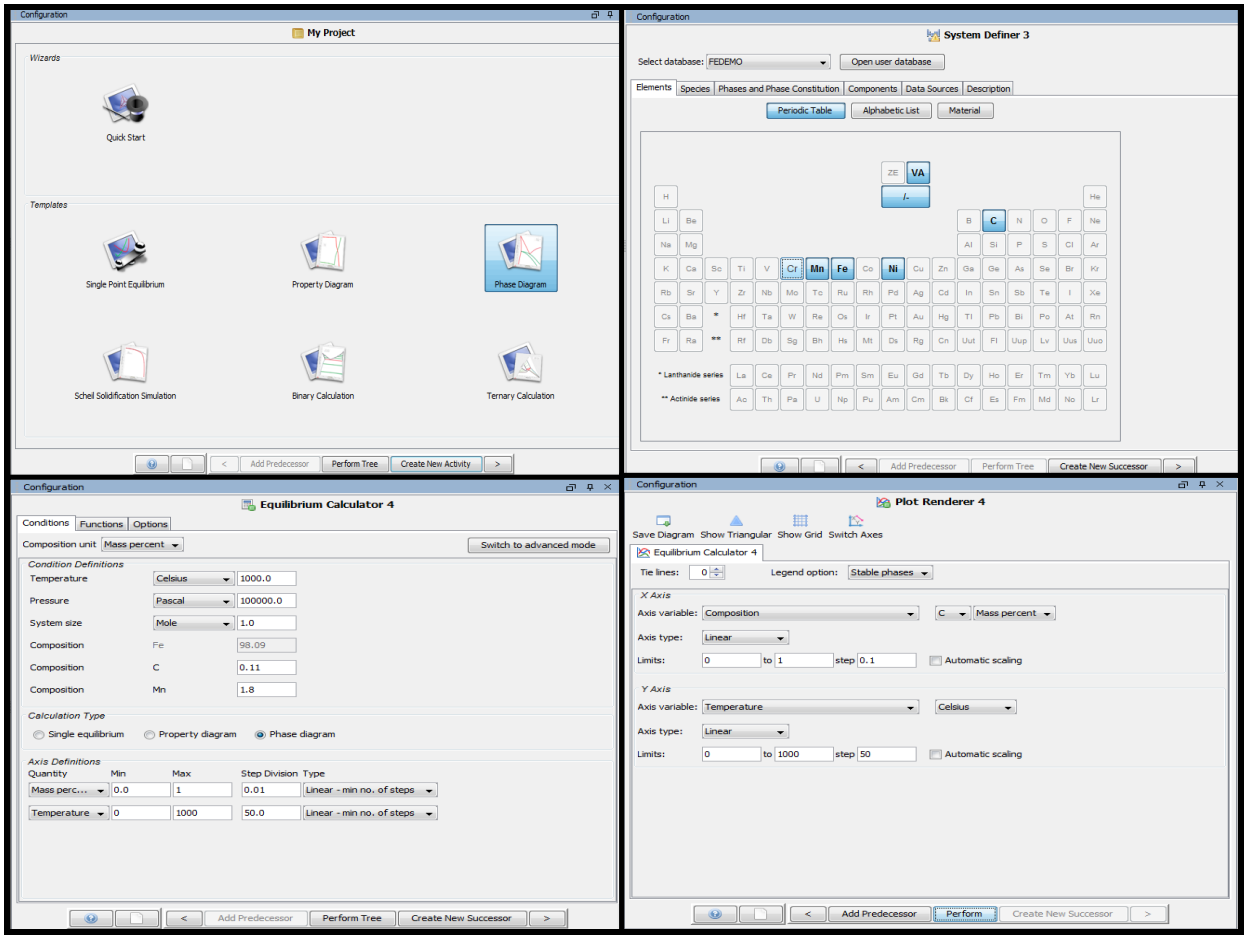

Fig. 3.7: Screenshots of input window of Thermo-Calc Software

B) JMat-Pro

To investigate the effect of heating rates on austenite formation (TTA diagram) and to construct the CCT, TTT, and phase fraction diagram, (*JMat-Pro 6.1*; developed by *Sente Software Limited*, Guildford, United Kingdom) was used. CCT diagram explains the effect of different cooling rates on the microstructure and hardness of samples, TTT diagram provides information on isothermal transformation of austenite phase, and phase fraction diagram presents the volume fraction of constituent phases at a given inter-critical temperature. Figure 3.8 shows some screen shots to demonstrate the working of JMat-Pro software.

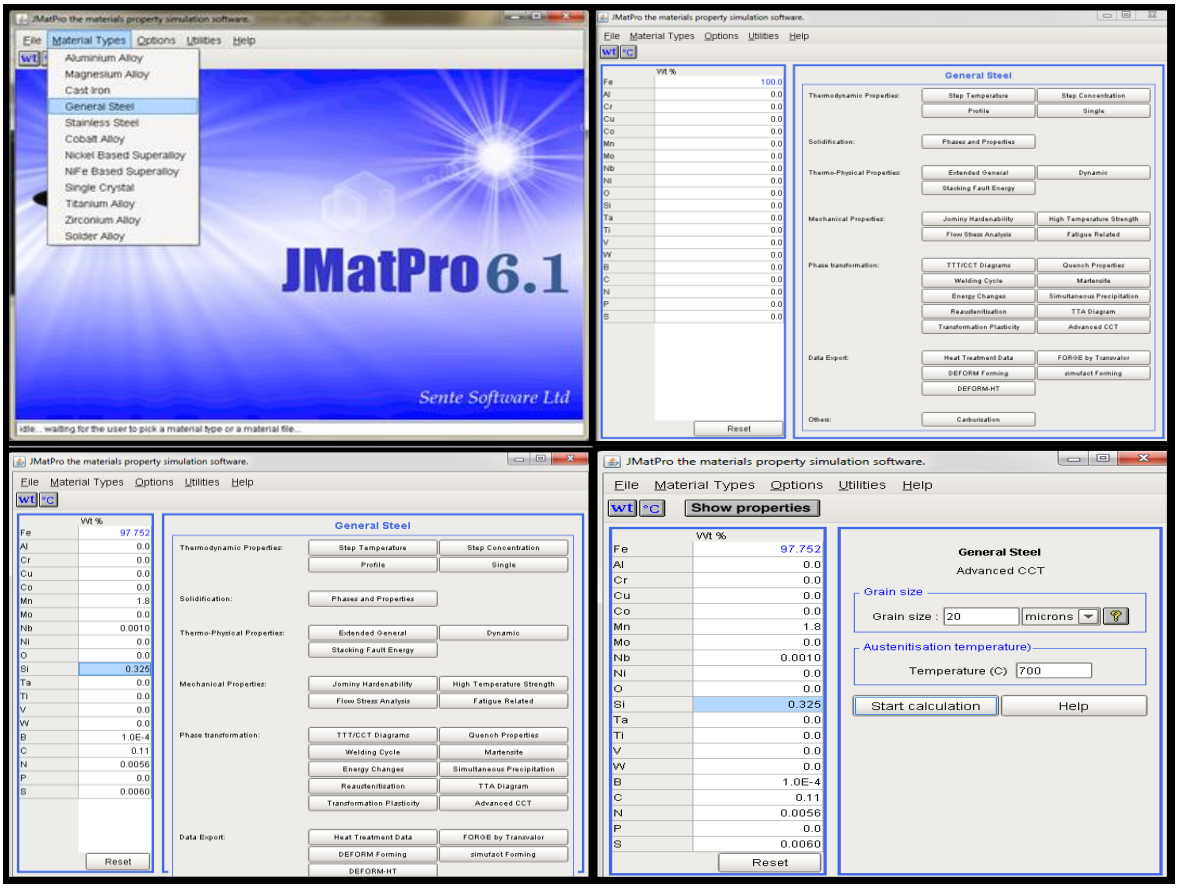

Fig: 3.8. Screenshots of input window of JMat-Pro Software

3.5 Sample Preparation for Metallography

After the heat treatment, all samples were prepared for metallographic examination. In order to prepare samples for material characterization, some basic steps need to be followed carefully. These include mounting, planar grinding, rough polishing, final polishing, etching, and microscopic analysis.

3.5.1 Preparation of Samples

The steps for preparation of samples for metallographic examination are discussed in brief as follows:

A) Mounting

Mounting of samples is usually done in order to facilitate their easy handling. Mounting is done with either copper or bakelite. In the present work, specimens were hot mounted at a temperature

of 160 ℃ by following the procedure similar to powder metallurgy. The edges of the mounted samples were rounded to minimize the damage to grinding/polishing discs. The mounting press (Make: BAINMOUNT METCO, *Chennai Metco Pvt. Ltd.*, Chennai, India) is shown in Fig. 3.9.

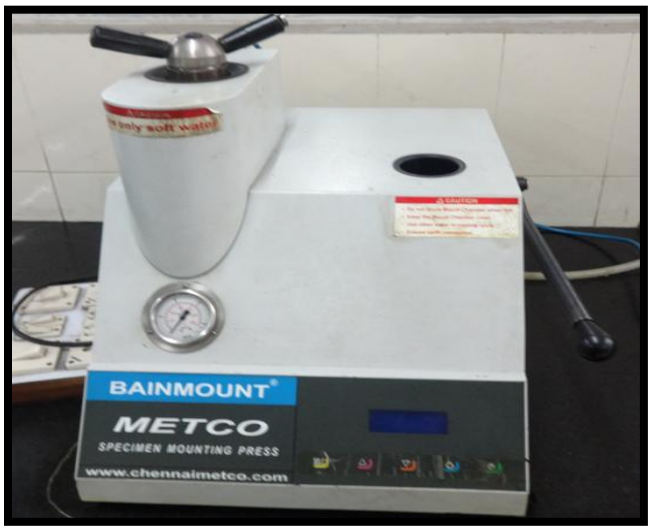

Fig. 3.9: Mounting Press (Courtesy: NML, Jamshedpur)

B) Grinding

Grinding is required to planarize the specimens. The surface to be examined by microscope is polished with abrasive papers of successive finer grades such as 80, 120, 220, 320, 400, 600, 800, 1000, 1200, 1500, and 2000 mesh abrasive paper (shown in Figure 3.10). Each time the sample is rubbed on SiC paper, it produces scratch marks and therefore polishing is continued till the scratches from earlier stages (SiC paper) have been obtained in uniform one direction.

Fig. 3.10: Abrasive Papers (Courtesy: NML, Jamshedpur)

Then, the direction of scratching or rubbing is switched perpendicular to previous scratches on the next paper with finer grade. Again, this is repeated until all scratches get oriented uniformly in one direction. The over-heating of samples is avoided as it may cause modification in the microstructure. Further, the pressure needs to be adjusted wisely as high pressure applied can lead to introduction of deep scratches and low pressure applied can result in elongated time consumption. Starting from the coarse grade paper (80 grit size), the procedure was carried up to fine grade paper (2000 grit size).

C) Polishing

The next step in preparation of sample is polishing on a horizontal rotating wheel. Polishing wheels are covered with a soft cloth (velvet, canvas, suede or selvet etc.) which needs to be impregnated with polishing medium (alumina or colloidal). The polishing medium is spread on to the rotating disc and specimen is held on the rotating disc in order to obtain a scratch free surface with mirror like polishing. Precautionary measures such as washing the specimen and also polishing the cloth thoroughly with water prior to initiating polishing should be done. This would divert any chances of introduction of contaminant or abrasive particles (from abrasive paper during grinding) which may lead to scratches. Polishing medium is spread on to a well washed cloth and as soon as the specimen starts to stick or friction starts to act between the specimen and cloth, water is poured on to the rotating wheel. Polishing machine (Make: BANIPOL METCO, Model No: PMV018, *Chennai Metco Pvt. Ltd.,* Chennai, India) of 0.37 kW capacity was used in the present work. Polishing machine is shown in Fig. 3.11.

D) Etching

Etching is done in order to reveal the microstructure of the metal/alloy system through selective chemical attack as the constituents mostly show similar reflectivity, causing difficulty in distinguishing them. Etching occurs by electrolytic action at structural variations on the sample surface. Chemical etchants produce either a metallographic contrast as grains etch at different rates because of variation in their crystallographic orientation which produces steps at grain boundaries and reflectivity difference or by grain/ phase-boundary etching, which produces grooves. The sample must be thoroughly cleaned before etching. A satisfactory etchant must be selected and prepared, and etchant may be applied using a cotton bud wiped over the surface for

a few seconds, about 15 s (necessary precautions must be taken while etching, as there is only a hair line difference between etching and over-etching). Nital (a solution of 3% nitric acid in ethanol) was used as etchant in the present work. The specimens were immediately washed with ethanol after applying the etchant and were dried with an electric drier.

Fig. 3.11: Polishing Machine (Courtesy: NML, Jamshedpur)

E) Leveling

Ideally, the surface to be examined optically should be perfectly flat and leveled. If not, then as the viewing area is moved across the surface it will pass in and out of focus. In addition, it will make it difficult to have the whole of field of view in focus—while the centre is focused, the sides will be out of focus. By using a specimen leveling press (shown in Figure 3.12) this problem can be avoided, as it presses the mounted specimen into clay on a microscope slide, making it leveled. A small piece of paper or cloth covers the surface of the specimen to avoid scratching.

3.5.2 Microstructural Evaluation

Since the most important technological properties are strongly influenced by microstructure, this understanding is important for development of metallic materials. In the present work, optical microscopy and scanning electron microscopy (SEM) were used for microstructural evaluation of the given steel.

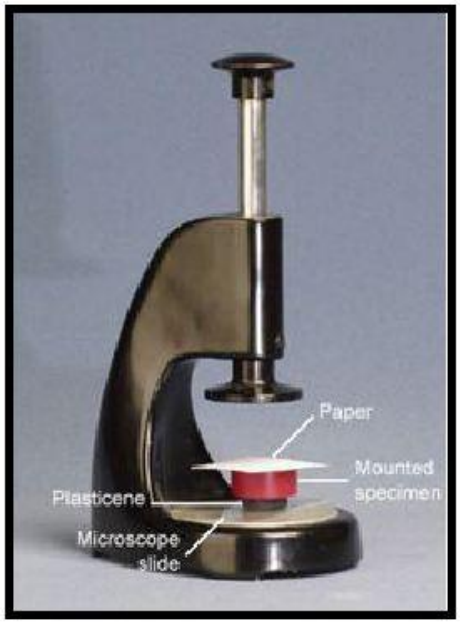

Fig. 3.12: Leveling Machine (Courtesy: NML, Jamshedpur)

A) Optical Microscopy

Optical microscope is used for the purpose of magnifying small samples by using visible light and a system of lenses. The image from an optical microscope can be captured by normal light sensitive cameras to generate micrographs. Metallic materials are usually opaque and therefore investigations of plane cross-sections by incident light prevail in metallography. While amplitude objects become visible owing to differences in light absorption and thus appear in different grey shades or even colors, phase objects only differ in the refractive indices which cannot be recognized without additional provision. Starting from the cross-section preparation, to etching of the specimen, and setting up of microscope, all steps should be carefully performed in order to get maximum information from a microscopic study. The optical microscope (Make: Leica DM2500 M; *Lieca Microsystems*, Wetzlar, Germany) used in the study is shown in Fig. 3.13

B) Scanning Electron Microscopy

A scanning electron microscope (SEM) is a type of electron microscope that images a sample by scanning it with a high-energy beam of electrons in a raster scan pattern. The electrons interact with the atoms that make up the sample and produce signals that contain information about the sample's surface topography, composition, and other properties such as electrical conductivity etc. SEM can produce very high-resolution images of a sample surface, revealing details less

than 1 nm in size. Due to the very narrow electron beam, SEM micrographs have a large depth of field yielding a characteristic three-dimensional appearance useful for understanding the surface structure of a sample. Figure 3.14 shows the scanning electron microscope (Make: Nova Nano SEM 430; *Field Emission Inc.*, Hillsboro, USA) that was used in the study.

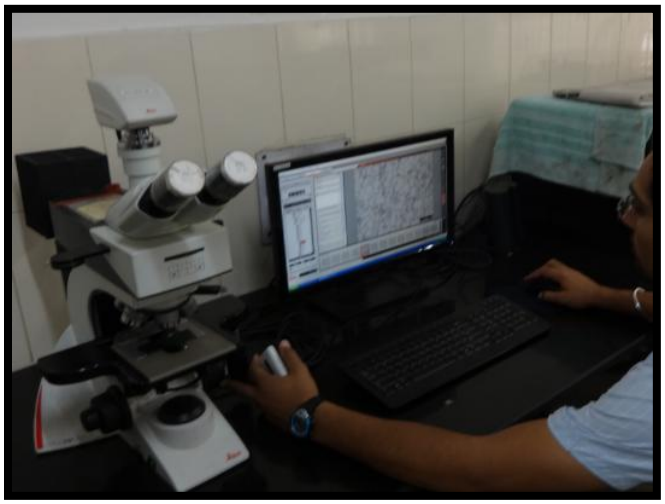

Fig. 3.13: Optical Microscope (Courtesy: NML, Jamshedpur)

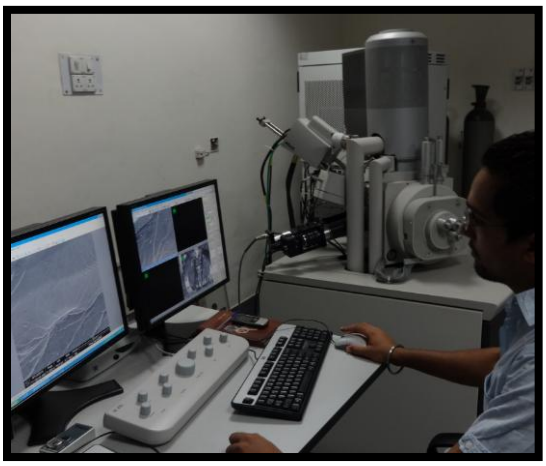

Fig. 3.14: Scanning Electron Microscope (Courtesy: NML, Jamshedpur)

3.6 Property Evaluation

The mechanical properties evaluated in the present study include hardness, yield strength, ultimate tensile strength, and percentage total elongation. The measurement procedure for these properties is discussed as follows:

3.6.1 Tensile Property Evaluation

Flat dog-bone shaped specimen of 35 mm gauge length as per the ASTM standard E-8M were machined from the normalised steel sheet and were annealed in the selected range. After heat treatment, full tensile tests were conducted for all samples at room temperature under displacement control at a strain rate of 1×10^{-3} s^{-1} using a tensile testing machine (Make: Instron 8862 System, Instron Engineering Corporation, Norwood, USA) of 100 kN capacity in the region of uniform elongation. Elongation was measured by an extensometer of 25mm gauge length.

3.6.2 Hardness Measurements

Micro-hardness measurements on Vickers Hardness (HV) scale were taken for all annealed samples in order to validate the phases observed through optical microscopy. Hardness measurements were made under a force of 50 g with a dwell time of 15 s. The presence of each phase was validated by comparing the experimental hardness values with the standard hardness values of phases.

3.7 Summary of the Chapter

This chapter puts forward the design of the present study. In this chapter of the report, the objective function with key issues has been discussed. An overview of the methodology, experimental procedure to be followed and machines and equipment has been provided. Finally the chapter describes the procedure for sample preparation for metallography, microstructural analysis and mechanical properties evaluation.

Chapter 4

Results and Discussion

4.1 Introduction

This chapter deals with the results obtained by Thermo-Calc and JMat-Pro predictions on phase diagram, CCT curves etc. under different annealing conditions. The simulations carried out by the annealing simulator based on inputs provided by software predictions are also included in this chapter. The chapter brings forth the detailed results of microstructural analysis for various temperature-time conditions during the inter-critical isothermal annealing process performed on the steel under investigation. The results of mechanical properties (mainly tensile properties) obtained through various proposed annealing routes have also been discussed.

4.2 Characterization of the As-received Material

The initial microstructure of the as-received alloy typically comprised of ferrite and pearlite structure as shown in Fig. 4.1. Linear intercept method calculated the grain size as 20 μm. The volume fractions of pro-eutectoid ferrite and pearlite were calculated as 88% and 12% respectively using 'Image J' software.

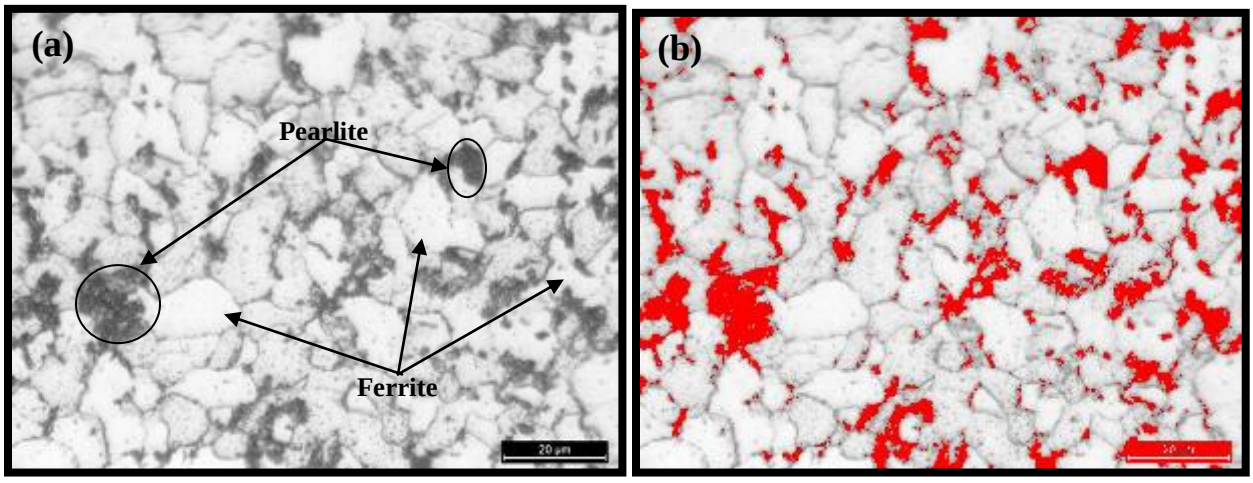

Fig. 4.1: Optical micrographs of the as-received material (a) optical microscope (b) Image J

4.2.1 Tensile Properties of the As-received Material

The as-received sample showed an ultimate tensile strength of 475 MPa, yield strength of 350 MPa and 33 % elongation as shown in the Fig. 4.2.

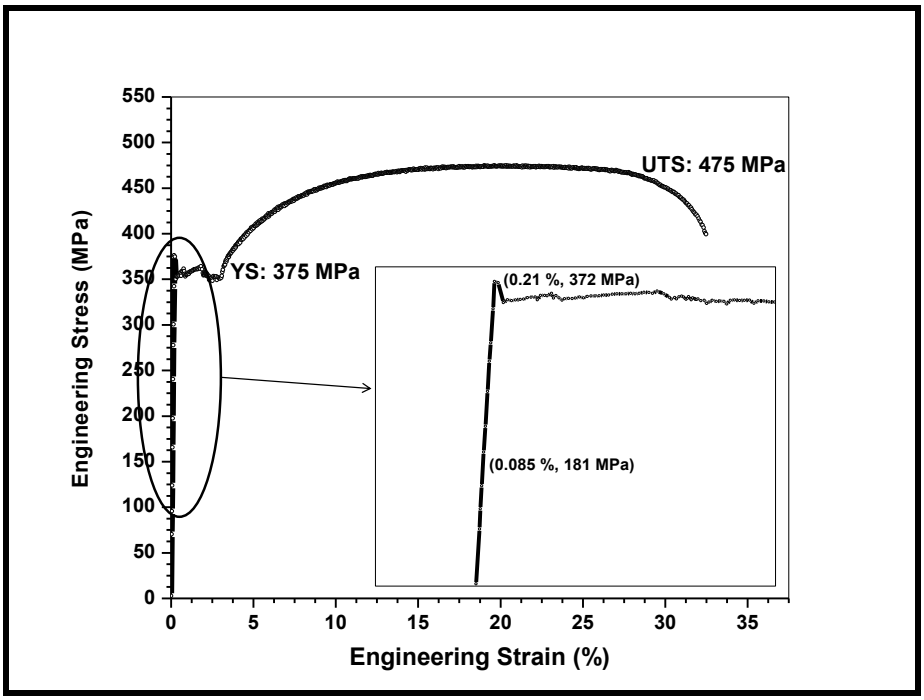

Fig. 4.2: Stress-strain curve for the as-received steel sample

4.3 Phase Transformation Studies using Commercial Software

The next step was to determine the annealing process parameters which could result in desired microstructure in the heat treated steel. The annealing temperature range (lower and upper critical temperatures), soaking periods, cooling rates etc. to be followed during annealing were worked out using commercial software viz. JMat-Pro 6.1 and Thermo-Calc 3.0.

4.3.1 Process Parameter Predictions using Thermo-Calc

Thermo-Calc 3.0 software was used to construct the equilibrium diagram and the phase fraction diagram (Figure 4.3) for the as-received normalized steel. The diagrams predicted the lower (Ac_1) and upper (Ac_3) critical temperatures of the steel as 684 ℃ and 834 ℃ respectively. The

volume fraction of austenite phase in the steel during equilibrium heating was also predicted from the phase fraction diagram at different annealing temperatures as shown in Table 4.1.

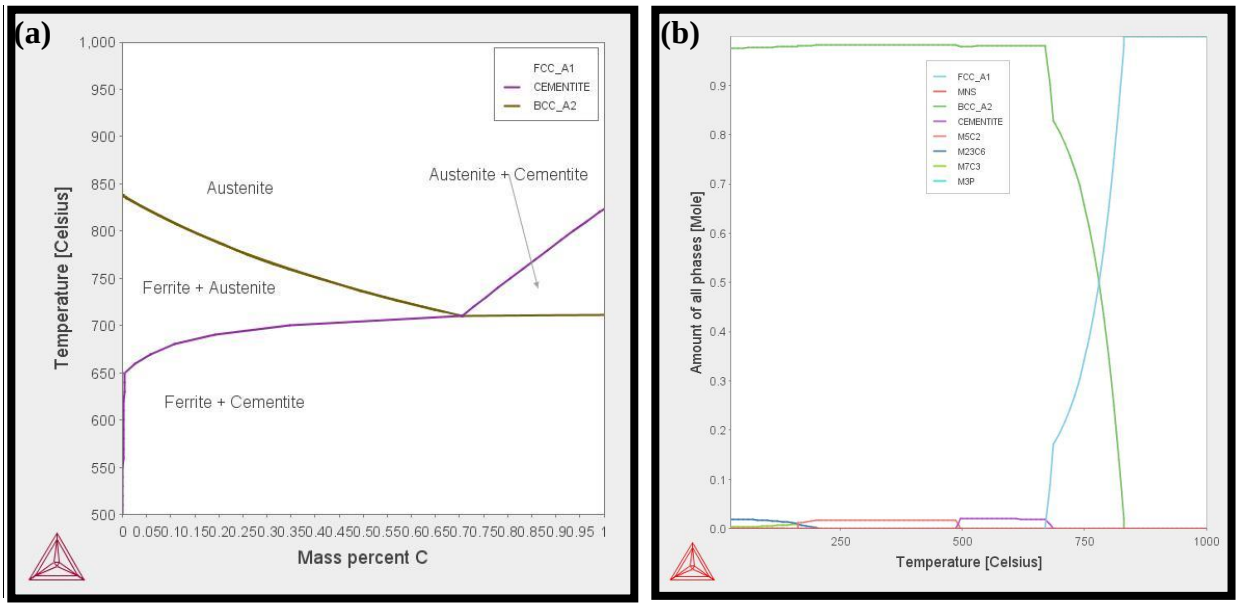

Fig: 4.3 Result window of Thermo-Calc for a) Equilibrium phase diagram b) Phase fraction diagram for the as-received material

Table: 4.1 Phase fractions at different austenization temperatures from JMat-Pro

Temperature (℃)	Austenite (wt. %)	Ferrite (wt. %)
700	20	80
750	34	66
800	70	30
825	90	10
850	100	0

4.3.2 Process Parameter Predictions using JMat-Pro

JMat-Pro 6.1 software was used to construct the phase fraction diagram, TTT, TTA and CCT diagrams. For each annealing temperature, a separate CCT diagram was constructed.

The phase fraction diagrams (Figure 4.3b and 4.4d) constructed by JMat-Pro and Thermo-Calc matched exactly.

The CCT diagrams (e.g. Figure 4.4b) obtained for the given steel at different annealing temperatures gave results as shown in Table 4.2. The summary of results is as follows:

- with increase in cooling rate at a specific annealing temperature, the volume fraction of martensite increases.
- with increase in austenization temperature, for same amount of martensite formation, relatively higher cooling rates are required.
- with increase in austenization temperature, the start and finish temperatures for both martensite and bainite increase.

Table 4.2 Transformation products of austenite with different cooling rates as per CCT diagram

Austenization Temperature (℃)	Cooling Rate (℃/ s)	Fraction of austenite available at the austenization temperature which converts to		
		Ferrite (wt. %)	Bainite (wt. %)	Martensite (wt. %)
700	10	0	0	90
	20	0	0	92
	30	0	0	92
750	10	0	37	61
	20	0	7	93
	30	0	2	98
	35	0	1	99
800	10	10	74	16
	20	4	34	62
	30	2	12	86
	40	1	6	93
850	20	16	41	43
	30	11	32	57
	40	7	16	77
	50	5	9	86
	60	3	6	91
• If the total of any row is not 100%, it signifies the presence of retained austenite phase in the microstructure				

TTA diagram (Figure 4.2c) showed that with increase in heating rate, the lower and upper critical temperatures also increase. For the Ac_1 temperature, it was observed that with increase in heating rate, the critical temperature starts increasing exponentially. However, for the Ac_3 temperature, initial increases in the heating rate upto 8 ℃/ s did not affect the critical temperature. But for heating rates in the range 8–60 ℃/ s, for any increase in the heating rate, the critical temperature increased linearly.

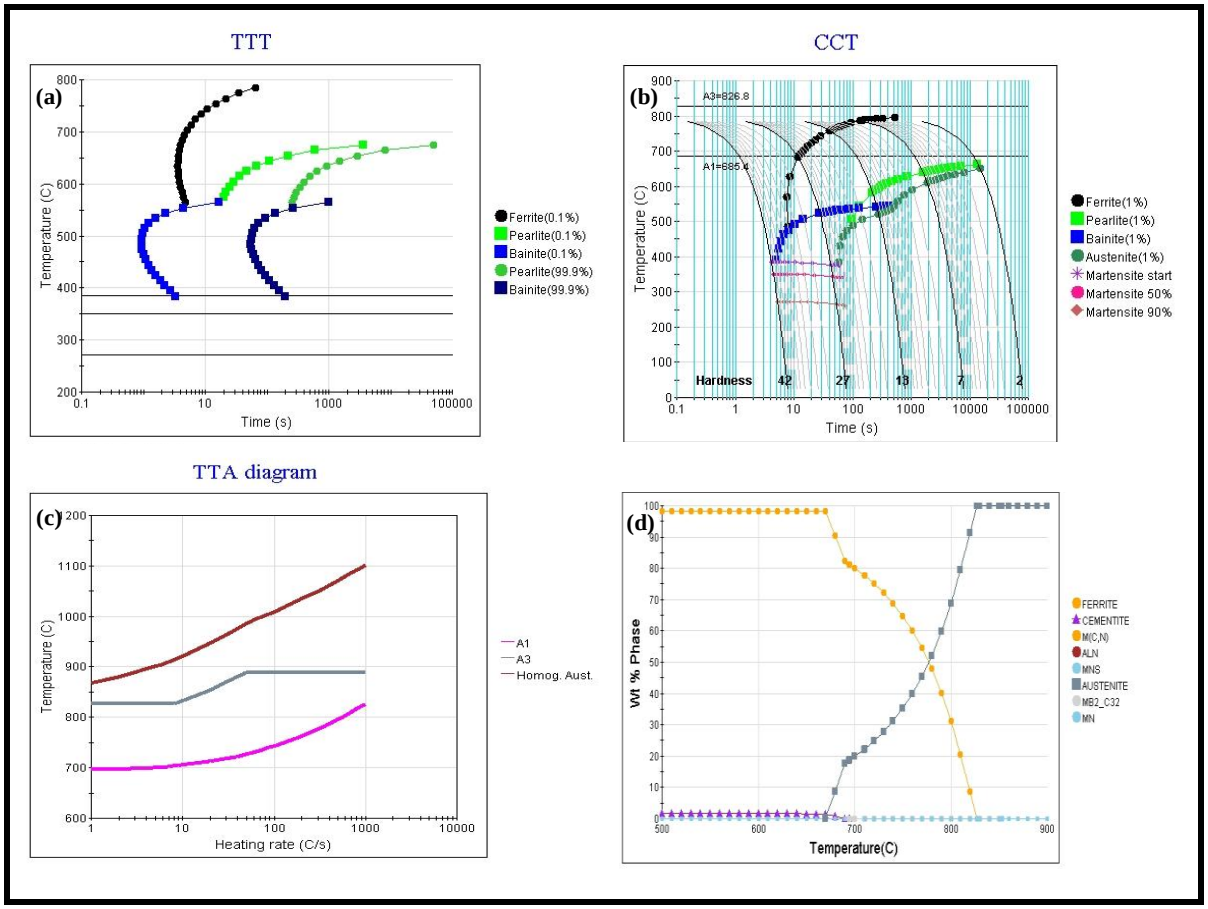

Fig. 4.4 Result window of JMat-Pro (a) TTT diagram at 800 ℃ (b) CCT diagram at 800 ℃ (c) TTA diagram (d) Phase Fraction diagram, for equilibrium heating conditions

4.4 Heat Treatment in Muffle Furnace

Annealing experiments were now conducted with process parameter values calculated by Thermo-Calc and JMat-Pro software. Initially, samples of size $(10 \times 10 \times 1)$ mm^3 were heat treated in the muffle furnace. The steps involved were up-quenching, soaking for 3 min and finally water quenching. Annealing experiments were conducted in the muffle furnace just to note the amount of austenite that forms in the given steel under specific time-temperature conditions during annealing. These experimental results on austenite formation were used to compare with the results obtained by JMat-Pro/ Thermo-Calc software packages. A main objective of conducting annealing in muffle furnace was to identify the temperature range over which austenite formation actually occurs, so that annealing in the simulator is conducted in that temperature range only. Samples were subjected to isothermal annealing at inter-critical

temperatures of 750, 800, 825 and 850 ℃ respectively with 3 min soaking followed by water quenching.

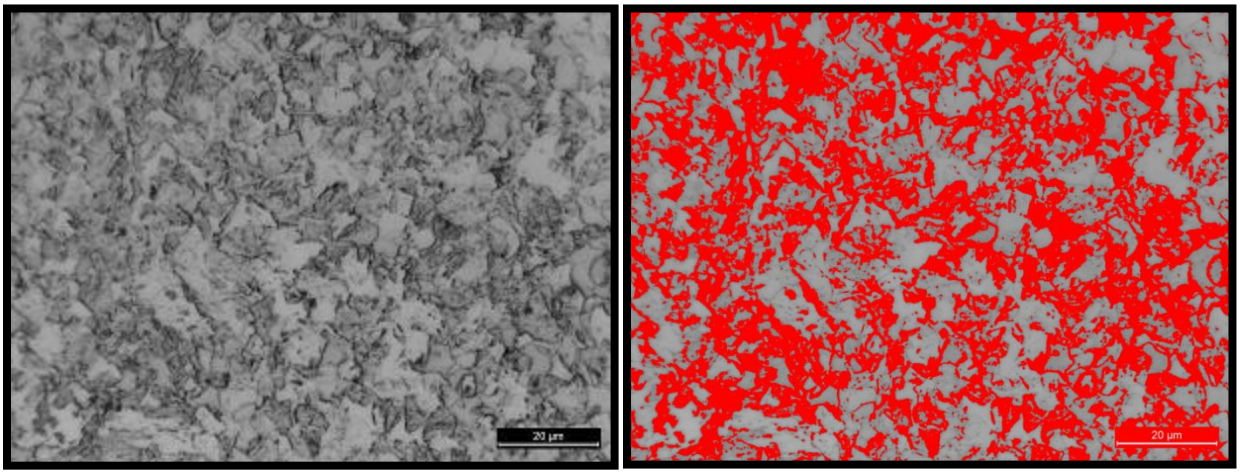

Fig. 4.5 Optical micrograph of annealed sample and its corresponding image from 'Image J' software

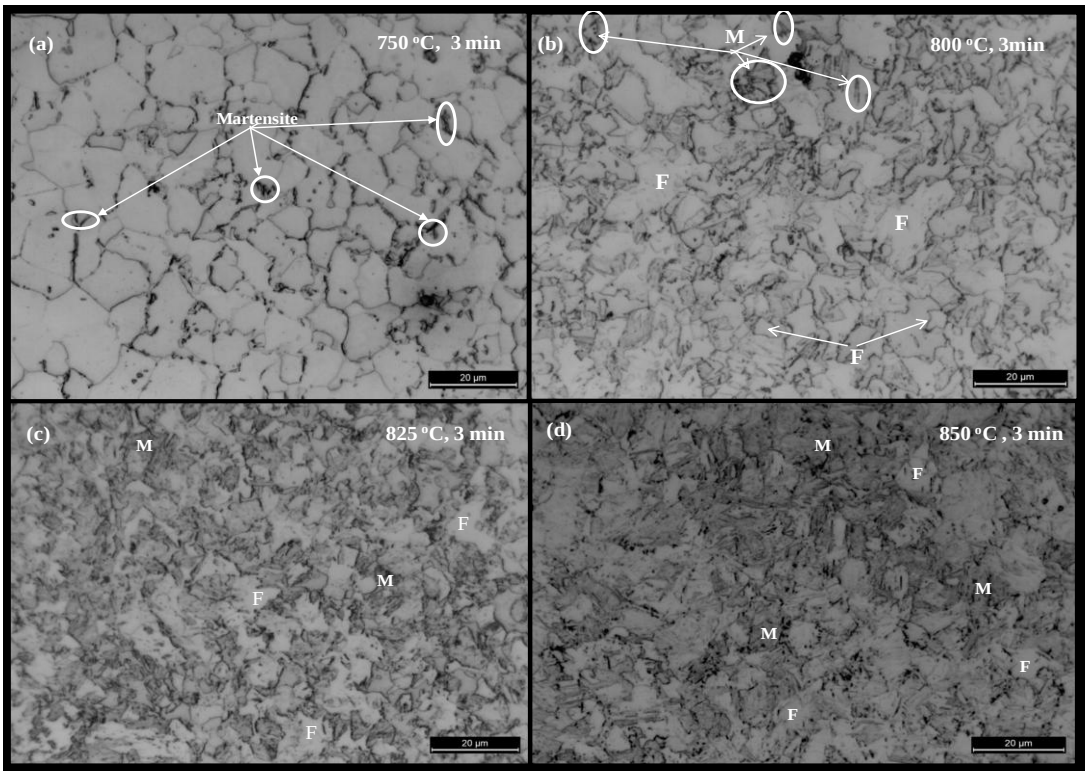

Fig. 4.6: Optical micrographs of samples annealed in muffle furnace at various temperature-time conditions. M = Martensite and F = Ferrite

After heat treatment under various temperature-time conditions, microstructure of samples contained different volume fraction of martensite/ ferrite phases. Phase fraction of constituent

phases under various annealing temperatures is shown in Table 4.3. Phase fraction of phases was calculated using 'Image J' software (e.g. Figure 4.5 shows the optical micrograph for annealing conditions (825 ℃, 3 min) and the corresponding image obtained from 'Image J' for phase fraction calculation). Figure 4.6 shows the optical micrographs for samples annealed under various temperature-time conditions. Microstructural analysis of annealed samples revealed that with increase in austenization temperature, the volume fraction of austenite (observed as martensite in the quenched samples) also increases (6, 30, 45, 63 wt. % respectively at different annealing temperatures).

Table 4.3 and Fig. 4.7 compare the results of JMat-Pro software and actual annealing experiments regarding the austenite volume fraction obtained under various annealing conditions. The results show that austenite fraction predicted by the software (i.e. for equilibrium heating conditions) is considerably different from the fraction obtained in the muffle furnace (i.e. under up-quenching). For the same temperature-time annealing conditions, JMat-Pro predicted higher amount of austenite to be present than was observed in the samples during actual experiments. However, with increase in annealing temperature, the percentage difference in the austenite fraction being observed under the two cases continuously decreased. The observed variations in the austenite fraction were due to difference in heating rates. Higher heating rates followed during actual experimentation led to increase in critical temperatures to higher values (than the equilibrium values of 684 and 834 ℃ respectively).

Table 4.3: Comparison of JMat-Pro and experimental results regarding austenite fraction

Temperature (℃)	**Austenite Fraction (wt. %) from**		**Percentage Difference**
	JMat-Pro	**Actual Experiments**	
750	34	6	82
800	70	30	57
825	90	45	50
850	100	63	37

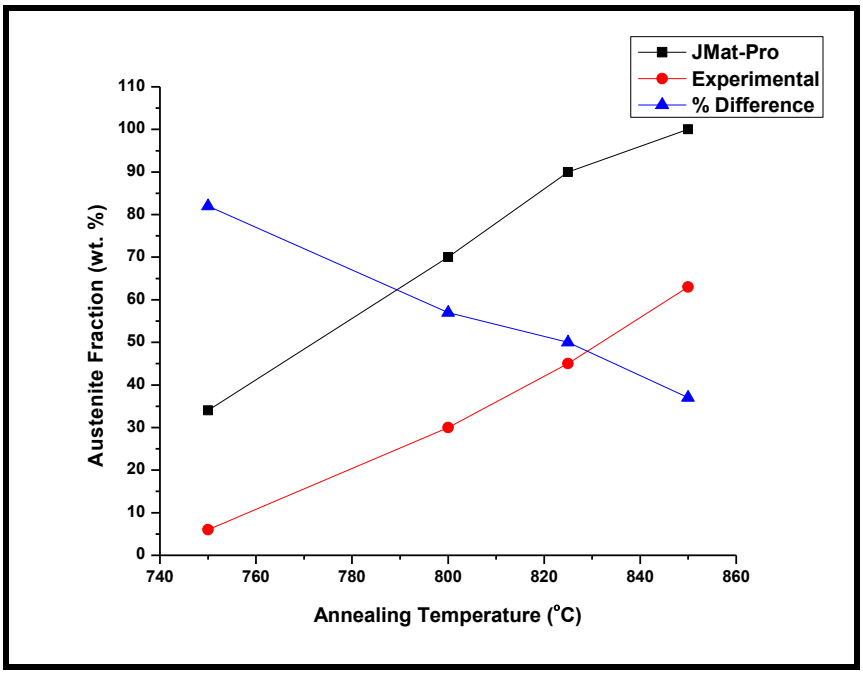

Fig. 4.7: Difference in JMat-Pro and experimental results regarding austenite fraction

4.5 Heat Treatment for Producing Dual/ Multiphase Steel

This section describes the details of annealing process conducted in the annealing simulator to meet the overall objective of producing a multi-functional multi/dual phase steel through controlled cooling of a steel with lean chemistry.

In this simulator, tensile samples (dog bone shaped samples of 35 mm gauge length as per ASTM standard E8M) were heated in a controlled environment and were cooled under controlled cooling rates. Annealing experiments were performed in the annealing simulator by following different cooling routes. The alternate cooling routes were obtained in the simulator through a mixture of hydrogen and nitrogen gases taken in different concentrations and injected in the simulator at different pressures. Samples were subjected to isothermal annealing at inter-critical temperatures of 750, 800, 825 and 850 ℃ with 3 min soaking at each temperature. This was followed by controlled cooling according to the CCT diagram. Controlled cooling with different cooling routes (marked as A, B, C in Figure 3.1) resulted in different microstructures. After heat treatment under various temperature-time conditions, microstructure of samples was investigated by optical microscopy and even SEM analysis for a few samples. Phase fraction of constituent phases was calculated using the software 'Image-J'. In this manner, the investigated

steel of lean chemistry was developed as multifunctional steel with multi/dual phase microstructure. Finally, the experimental results obtained with controlled cooling were compared with those calculated from Thermo-Calc and JMat-Pro.

4.5.1 Annealing Simulator

The detail of process environment and other conditions within the annealing simulator is as follows:

Heating Mode: The specimens were heated in the heating chamber by up-quenching at heating rates of the order of 50 ℃/s or faster.

***Process Environment*:** A gas mixture of almost 5% hydrogen in nitrogen was filled in the mixing system, which resulted in desired bright annealing of steels.

***Cooling Medium*:** The samples during cooling were subjected to controlled cooling rates. Cooling rates as suggested by JMat-Pro software predictions through constructed CCT diagrams were followed (Table 4.4). Multiple options of controlled cooling were achieved through high pressure jet of gas mixture, with variations of mixture constitution, mixture pressure, use of atomized water, etc.

***Cooling Data Logs*:** The thermocouples fitted in the annealing chamber gave the temperature-time logs for successive time periods (one reading in 1 s) in the excel format. This data was imported to 'Origin' software package (*OriginPro 8*) to plot the cooling curves corresponding to the cooling logs.

4.5.2 Heat Treatment of Samples in Simulator at 700 ℃

This section describes the heat treatment of tensile specimens subjected to inter-critical isothermal annealing at a temperature of 700 ℃. The samples were heated to 700 ℃ in the simulator and were soaked there for 3 min. Gas mixture etc. settings for this annealing temperature were adjusted to provide relatively slow cooling rates in the range of 20–30 ℃/ s.

For annealing of samples with 700 ℃ as the austenization temperature, two different samples following different cooling routes (A and B) were annealed (route C was not followed for this annealing temperature because it did not form martensite in significant quantity in the annealed samples). The cooling curves for routes A and B were obtained from the data logs of

thermocouple (Appendix I) of the annealing chamber and were superimposed on the CCT diagram (Figure 4.8a) for the steel. The CCT diagram for this austenization temperature (700 ℃) was constructed using JMat-Pro with main inputs as alloy chemistry and annealing temperature.

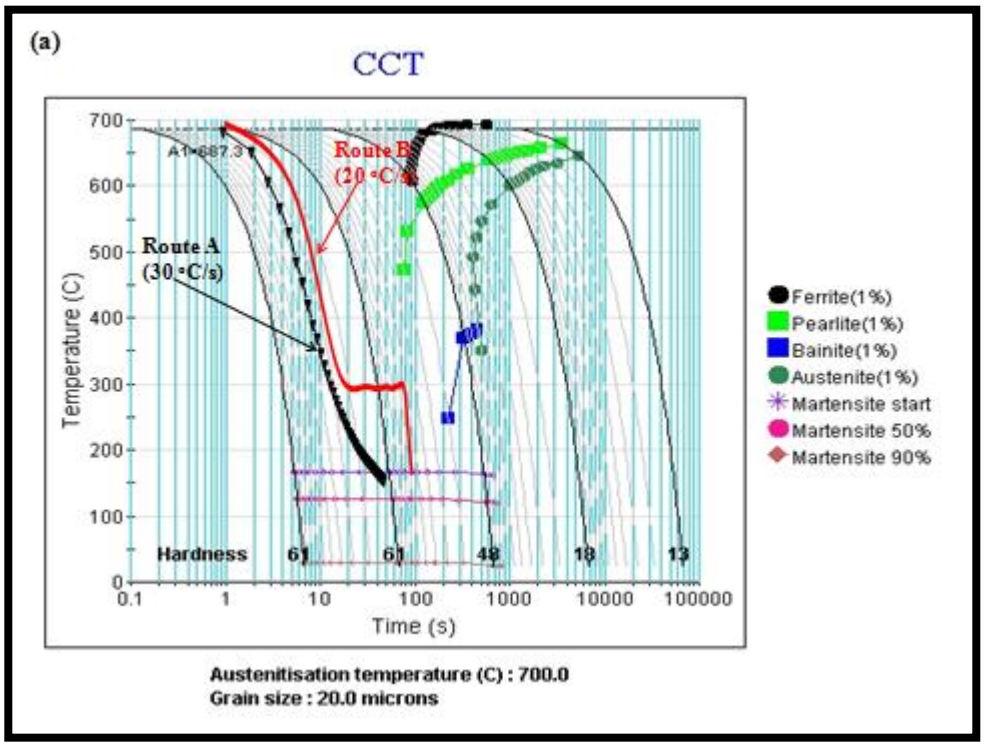

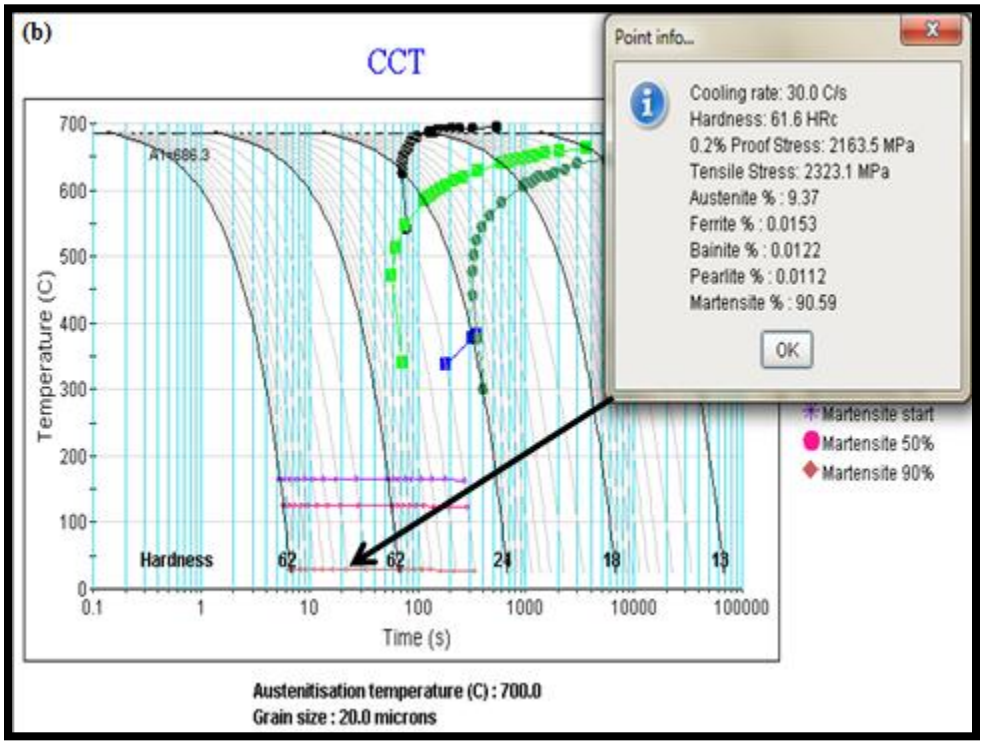

Fig. 4.8 CCT diagram at 700 ℃ a) cooling curves superimposed on the CCT diagram b) screen shot from JMat-Pro window

4.5.2.1 Microstructural Analysis

Samples annealed at 700 ℃ were first cooled along cooling route A. For this, from the austenization temperature of 700 ℃, after 3 min of stipulated soaking, the sample was directly cooled to room temperature at a cooling rate of 30 ℃ /s. On investigating the microstructure of this annealed sample (initially by optical microscopy), only ferrite phase was observed as shown in Fig. 4.9a. Also, 'Image J' did not detect any fraction of martensite phase. To deeply investigate the microstructure further, SEM analysis of the annealed sample was done which showed presence of negligible amount of martensite (shown in Figure 4.10a) along with ferrite, thus validating the optical micrographs. This means during the heating and holding steps of annealing at 700 ℃, pearlite phase mixture converted to ferrite with small amount of austenite. During subsequent cooling along route A, the bulk ferrite phase remains unchanged whereas austenite transforms to traces of martensite. Thus, annealing at 700 ℃ with cooling route A did obtain a dual phase microstructure but with very limited fraction of martensite (due to unavailability of austenite in a significant amount).

Next, the samples annealed at 700 ℃ were cooled along the cooling route B. For this, from the austenization temperature of 700 ℃, after 3 min of stipulated soaking, the sample was cooled upto 350 ℃ (bainitic region, identified from the CCT diagram, Figure 4.8a) at a cooling rate of 20 ℃ /s. After holding for 1 min in the bainitic region, the sample was again cooled at the same cooling rate (20 ℃ /s) to room temperature. On investigating the microstructure of this annealed sample (initially by optical microscopy), again only ferrite phase was observed as shown in Fig. 4.9b. Also, 'Image J' did not detect any fraction of martensite phase. Again, to deeply investigate the microstructure further, SEM analysis of the annealed sample was done which showed presence of ferrite and very small amount carbides (shown in Figure 4.10b). The reason behind formation of this microstructure is explained as follows. During the heating and holding steps of annealing at 700 ℃, pearlite phase mixture converted to ferrite with small amount of austenite. During subsequent cooling along route B, the bulk ferrite phase remained unchanged, but during soaking, redistribution of carbon started in austenite which led to varying carbon content in different regions in austenite. As reported by Rajan et al. [2011], some regions in austenite become carbon enriched whereas others become depleted in carbon. The low carbon austenite transforms to martensite/ ferrite (during soaking only) due to shifting of M_s in the

bainitic region. A portion of the carbon enriched austenite forms carbides (MnC, SiC etc.) during cooling whereas the remaining high carbon austenite (becomes stable due to high carbon) is seen as retained austenite in the room temperature microstructure (Rajan et al., 2011). Thus, route B should have resulted in a microstructure comprising of ferrite, martensite, carbides, and a small amount of retained austenite. However, because of the very limited austenite fraction at the heat treatment temperature of 700 ℃, phases other than ferrite were not properly identified by optical microscopy and even SEM analysis (a few regions containing carbides were detected by SEM).

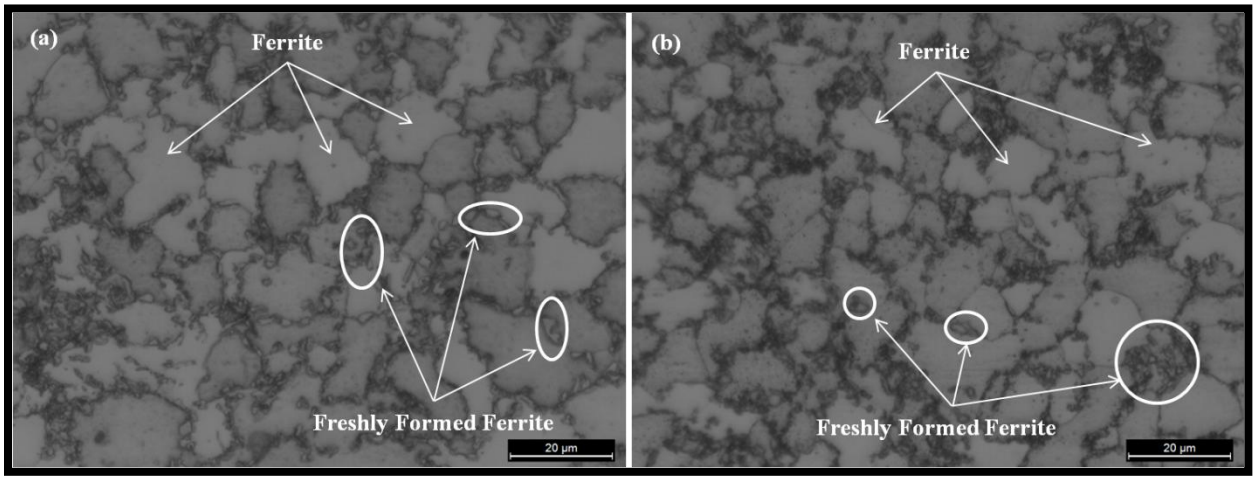

Fig. 4.9: Optical micrographs of samples annealed at 700 ℃ for (a) cooling route A (b) cooling route B

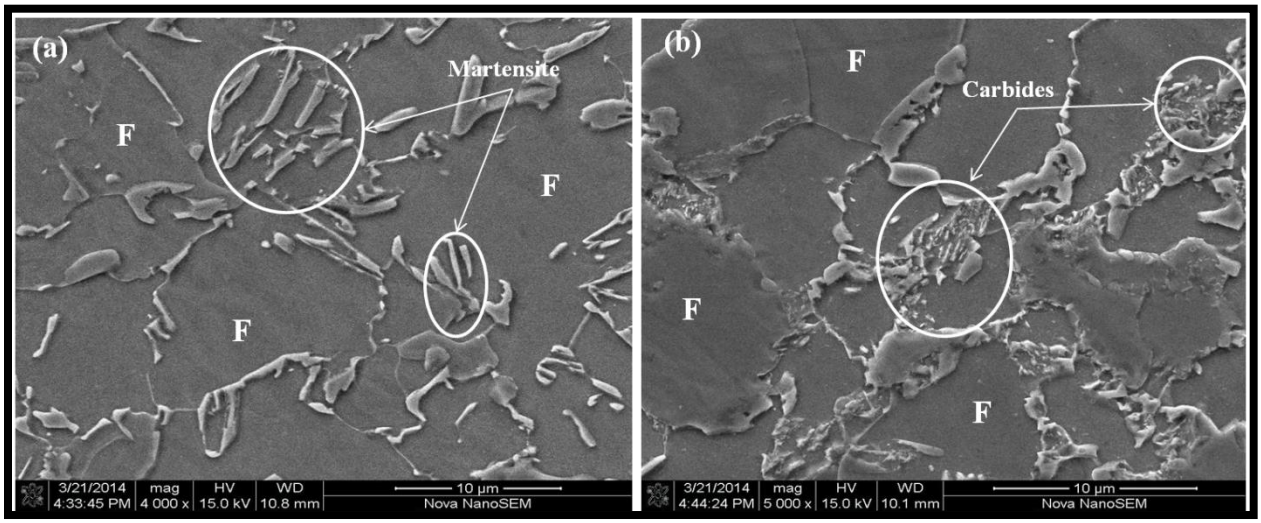

Fig. 4.10: SEM images of samples annealed at 700 ℃ for (a) cooling route A (b) cooling route B. F= Ferrite

Thus, annealing at 700 ℃ with cooling route B did obtain a multi-phase microstructure but with very limited fraction of non-ferritic phases (due to unavailability of austenite in a significant amount).

4.5.2.2 Tensile Property Evaluation

After the heat treatment, full tensile tests were conducted for both the samples (samples formed by routes A and B respectively) annealed at 700 ℃ under displacement control at a strain rate of 1 x 10^{-3} s^{-1} using a tensile testing machine. The results from the machine were obtained in the form of data logs of load versus strain. Load was converted into engineering stress (Appendix II) (by dividing it with cross-sectional area of the annealed specimen). Finally, the stress-strain curve was generated (using 'Origin' software package, *OriginPro 8*) as shown in Fig. 4.11.

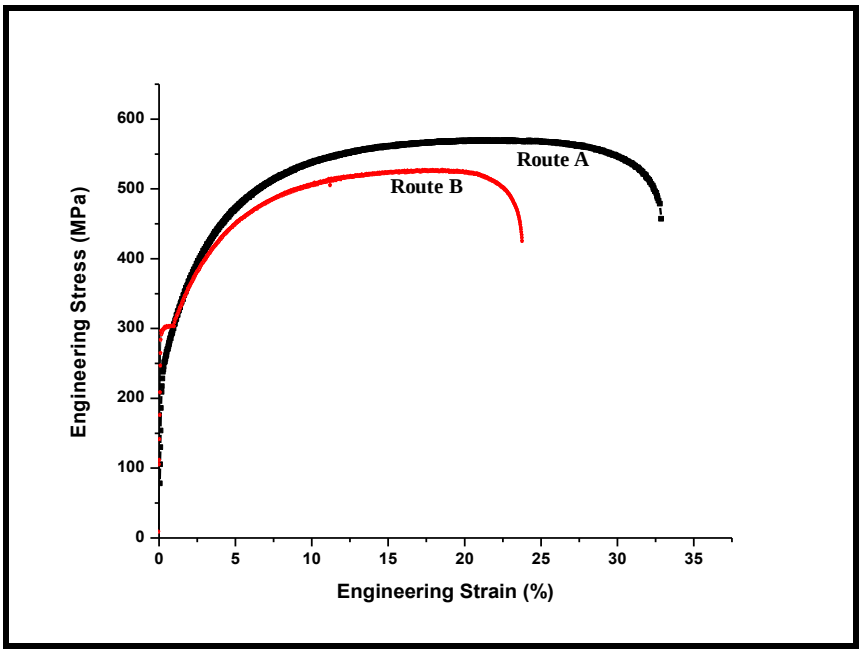

Fig. 4.11: Stress-strain curves for steel samples annealed at 700 ℃

For the sample annealed at 700 ℃ through cooling route A, the yield stress (YS), ultimate tensile strength (UTS), and percent total elongation were calculated as 250 MPa, 550 MPa and 33 % respectively from tensile curve. A decrease in yield strength (from 375 to 250 MPa) as compared to as-received steel was observed. This was attributed to the presence of the brittle martensite phase in the heat treated steel (presence of martensite decreased the elastic range). Further, the ultimate tensile strength improved (from 475 to 550 MPa) both due to the presence martensite

and freshly formed fine grained ferrite obtained during the annealing process. No yield point elongation was observed in the tensile curve. The steel showed continuous yielding which was attributed to mobile dislocations introduced during cooling from the inter-critical annealing temperature (ICAT). As reported in literature, many dislocation sources come into action at low strain and plastic flow begins simultaneously throughout the specimen, thereby suppressing discontinuous yielding [Erdogan and Tekeli, 2002]. The mobile dislocations introduced due to the formation of martensite phase facilitate the beginning of plastic deformation and prevent from the occurrence of discontinuities at the physical yield point [Dziedzic and Turczyn, 2010]. Further, it can be noted that the annealed sample (route A) led to improvement in ultimate tensile strength while retaining the ductility (due to more fraction of ferrite in the microstructure achieved).

For the sample annealed at 700 ℃ through cooling route B, the yield stress (YS), ultimate tensile strength (UTS), and percent total elongation were calculated as 290 MPa, 527 MPa and 24 % respectively from tensile curve. The formation of carbides and martensite (in the annealed sample decreased both the yield strength (by decreasing the elastic range) and the total percentage elongation. However, their presence contributed to increase in ultimate tensile stress. The UTS also increased because of the presence of freshly formed fine grained ferrite during the annealing process.

4.5.2.3 Comparison of Experimental and Software based Results

This section compares the results regarding martensite fraction observed in the actual microstructure after the annealing experiments with the martensite fraction predicted by the JMat-Pro software. A comparison of results from the two sources is presented in Table 4.4.

For annealing experiments at 700 ℃, martensite was only formed during cooling route A (cooling rate: 30 ℃/ s) in a very small quantity (martensite fraction: < 5%). However, JMat-Pro predictions at 30 ℃/ s calculated the martensite fraction to be 18.4 %. This amount of martensite (18.4 %) was calculated as follows. For austenization temperature of 700 ℃, the software had calculated [Table 4.1] austenite fraction as 20 % assuming equilibrium heating. For cooling rate of 30 ℃/ s, the software predicted [Table 4.2] that 92% of the available austenite converts to martensite. Therefore, martensite fraction according to software was 92 % of 20 i.e. 18.4 %.

Table 4.4 Comparison of martensite fraction from annealing experiments with JMat-Pro predictions

Annealing Temperature (℃)	Martensite Fraction (wt. %) from	
	JMat-Pro Predictions	Annealing Experiments in Simulator
700	18.40	< 5
750	33.32	15
800	63.00	20
850	91.00	37

The martensite fraction predicted by the software did not match with the actual experimental outcome. This difference was due to the higher heating rates during up-quenching of samples in the annealing simulator.

4.5.3 Heat Treatment of Samples in Simulator at 750 ℃

This section describes the heat treatment of tensile specimens subjected to inter-critical isothermal annealing at a temperature of 750 ℃. The samples were heated to 750 ℃ in the simulator and were soaked there for 3 min. Gas mixture etc. settings for this annealing temperature were adjusted to provide relatively slow cooling rates in the range of 20–40 ℃/ s. For annealing of samples with 750 ℃ as the austenization temperature, three different samples following different cooling routes (A, B, and C) were annealed. The cooling curves for routes A, B and C respectively were obtained from the data logs of thermocouple of the annealing chamber and were superimposed on the CCT diagram (Figure 4.12) for the steel. The CCT diagram for this austenization temperature (750 ℃) was constructed using JMat-Pro with main inputs as alloy chemistry and annealing temperature.

4.5.3.1 Microstructural Analysis

Samples annealed at 750 ℃ were first cooled along cooling route A. For this, from the austenization temperature of 750 ℃, after 3 min of stipulated soaking, the sample was directly cooled to room temperature at a cooling rate of 30 ℃ /s. On investigating the microstructure of

this annealed sample by optical microscopy, ferrite and martensite dual phase structure was observed as shown in Fig. 4.13a. The 'Image J' software detected volume fraction of martensite phase to be 15 %. This showed that during the heating and holding steps of annealing at 750 ℃, pearlite phase mixture converted to austenite. Also, some existing ferrite transformed into fine grained austenite. During subsequent cooling along route A, the ferrite phase remain unchanged whereas austenite transformed to fine grained martensite. Thus, annealing at 750 ℃ with cooling route A obtained a true dual phase microstructure due to availability of austenite in a significant amount (15 %).

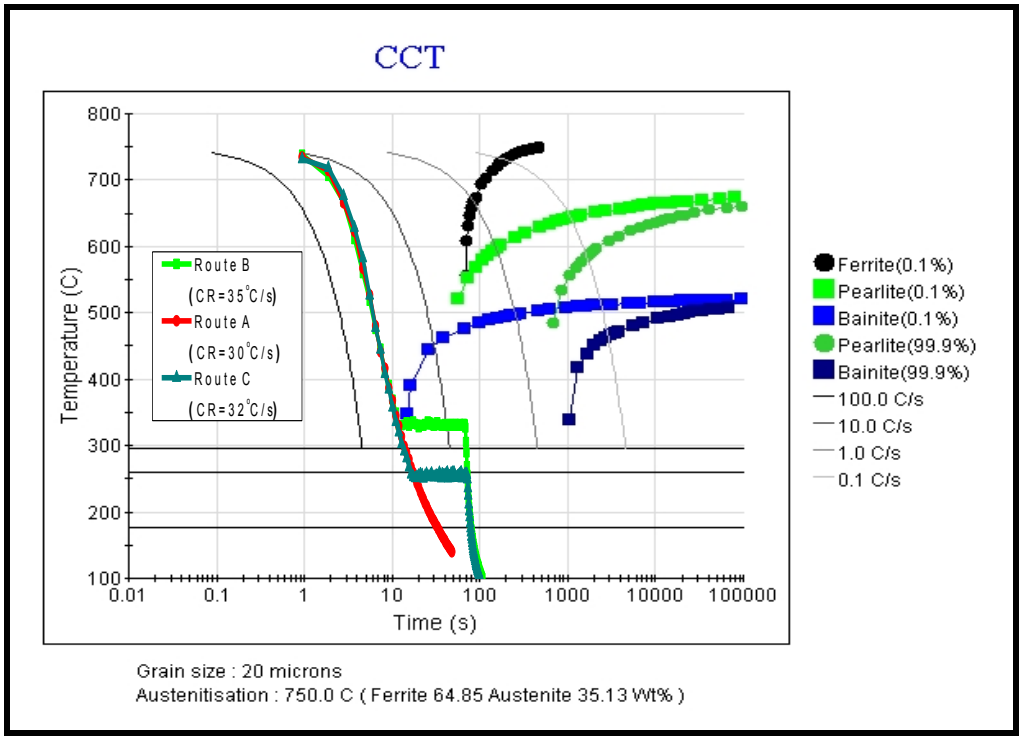

Fig. 4.12: Cooling curves superimposed on CCT diagram at 750 ℃

Next, the samples annealed at 750 ℃ were cooled along the cooling route B. For this, from the austenization temperature of 750 ℃, after 3 min of stipulated soaking, the sample was cooled upto 350 ℃ (bainitic region, identified from the CCT diagram) at a cooling rate of 35 ℃ /s. After holding for 1 min in the bainitic region, the samples were cooled at a cooling rate of 20 ℃ /s to room temperature. On investigating the microstructure of this annealed sample by optical microscopy, multi-phase microstructure comprising of ferrite, fine bainite, martensite, and retained austenite was observed as shown in Fig. 4.13b. This means during the heating and

holding steps of annealing at 750 ℃, pearlite phase mixture converted to austenite. Also, some amount of existing ferrite converted to austenite. During initial cooling and subsequent holding in the bainitic region, redistribution of carbon occurred in austenite which led to varying carbon concentration in austenite. Low carbon austenite partially transformed to martensite due to shifting of M_s in the bainitic region. The remaining low carbon austenite transformed to supersaturated ferrite (called bainitic ferrite) which ultimately led to formation of bainite phase mixture. Further, during the second cooling, the carbon enriched austenite partially converted to carbides like MnC, SiC etc. The remaining high carbon austenite remained stable and was observed as retained austenite in the microstructure [Rajan et al., 2011]. Thus, annealing at 750 ℃ with cooling route B developed a multi-phase microstructure in the given steel.

Next, the samples annealed at 750 ℃ were cooled along the cooling route C. For this, from the austenization temperature of 750 ℃, after 3 min of stipulated soaking, the sample was cooled upto 250 ℃ (martensitic region, identified from the CCT diagram) at a cooling rate of 32 ℃ /s. After holding for 1 min in the martensitic region, the samples were again cooled at a cooling rate of 20 ℃ /s to room temperature. On investigating the microstructure of this annealed sample by optical microscopy, again a multi-phase microstructure was observed comprising of tempered and conventional martensite, ferrite, a small amount of bainite and retained austenite as shown in Fig. 4.13c. During the heating and holding steps of annealing at 750 ℃, pearlite phase mixture converted to austenite. Also, some amount of existing ferrite converted into austenite. During initial cooling along route C, some amount of austenite transformed to conventional martensite; on holding in the martensitic region, the newly formed martensite liberated some fraction of its carbon, thus becoming tempered martensite. This liberated carbon was picked up by the untransformed austenite by which it became carbon enriched and got stabilized.

However, on subsequent cooling along route C, some fraction of the untransformed austenite converted to conventional martensite and the remaining carbon enriched untransformed austenite was seen as retained austenite in the room temperature microstructure. Bainite was formed due to the transformation of super saturated solution of carbon in ferrite (as discussed in this section for route B) during the soaking period. The carbides were formed from the high carbon austenite during second cooling. Thus, annealing at 750 ℃ with cooling route C produced a multi-phase microstructure.

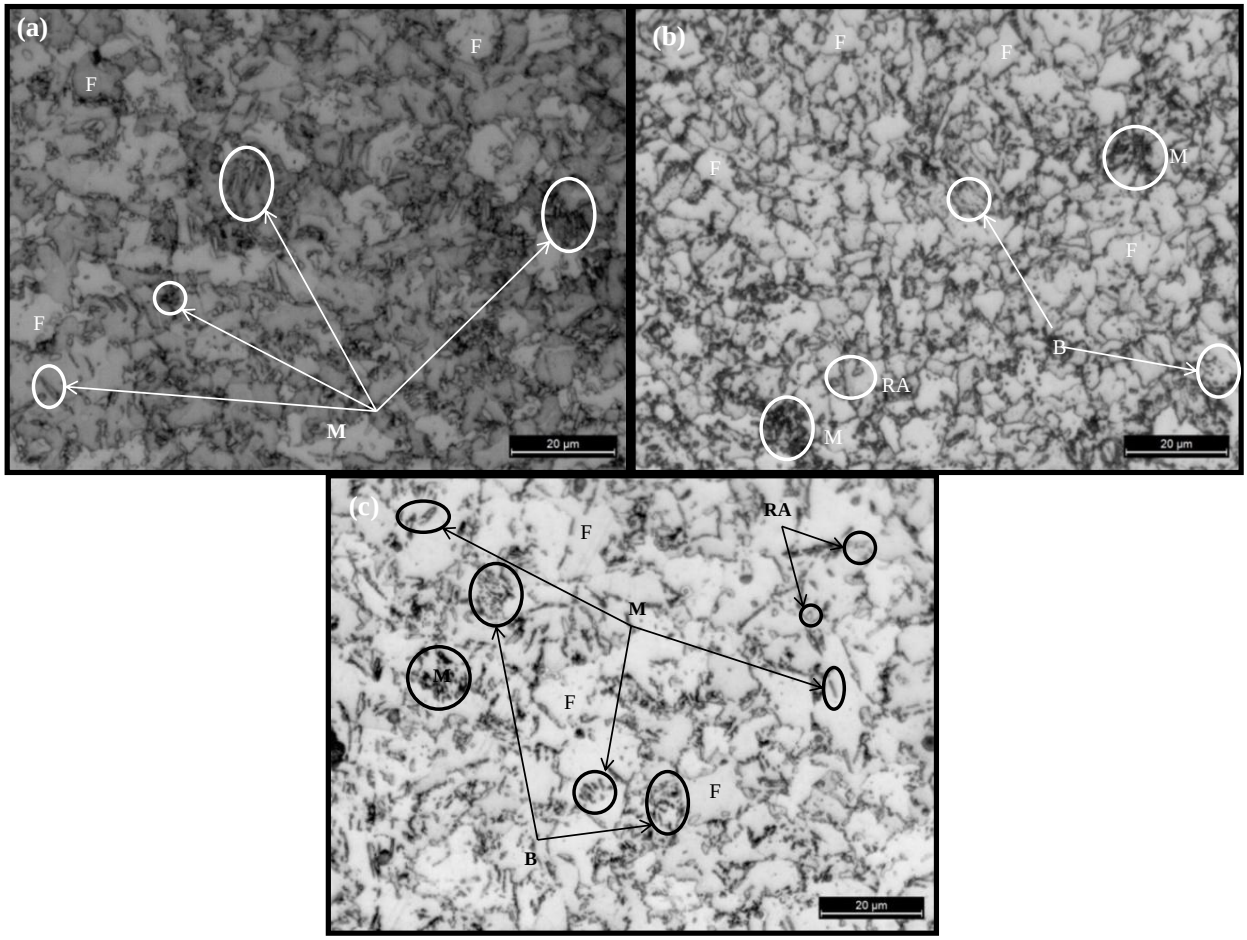

Fig. 4.13: Optical micrographs of samples annealed at 750 ℃ for (a) cooling route A (b) cooling route B (c) cooling rate C. F = Ferrite, B= Bainite, M = Martensite, RA = Retained Austenite

4.5.3.2 Tensile Property Evaluation

After the heat treatment, full tensile tests were conducted for all the three samples (formed by routes A, B, and C respectively) annealed at 750 ℃. The results of the tensile tests are presented in Fig. 4.14.

For the sample annealed at 750 ℃ through cooling route A, the yield stress (YS), ultimate tensile strength (UTS), and percent total elongation were calculated as 260 MPa, 570 MPa and 30 % respectively from tensile curve. No yield point elongation was observed in the tensile curve. The annealed sample showed a low YS/ UTS ratio (0.46 as compared to 0.79 for the as-received steel sample), which is a characteristic of DP steels.

For the sample annealed at 750 ℃ through cooling route B, the yield stress (YS), ultimate tensile strength (UTS), and percent total elongation were calculated as 320 MPa, 514 MPa and 29 % respectively from tensile curve.

For the sample annealed at 750 ℃ through cooling route C, the yield stress (YS), ultimate tensile strength (UTS), and percent total elongation were calculated as 286 MPa, 521 MPa and 29 % respectively from tensile curve.

The reasons for change in properties of the annealed samples as compared to as-received sample are the same as discussed in section 4.6.2.2.

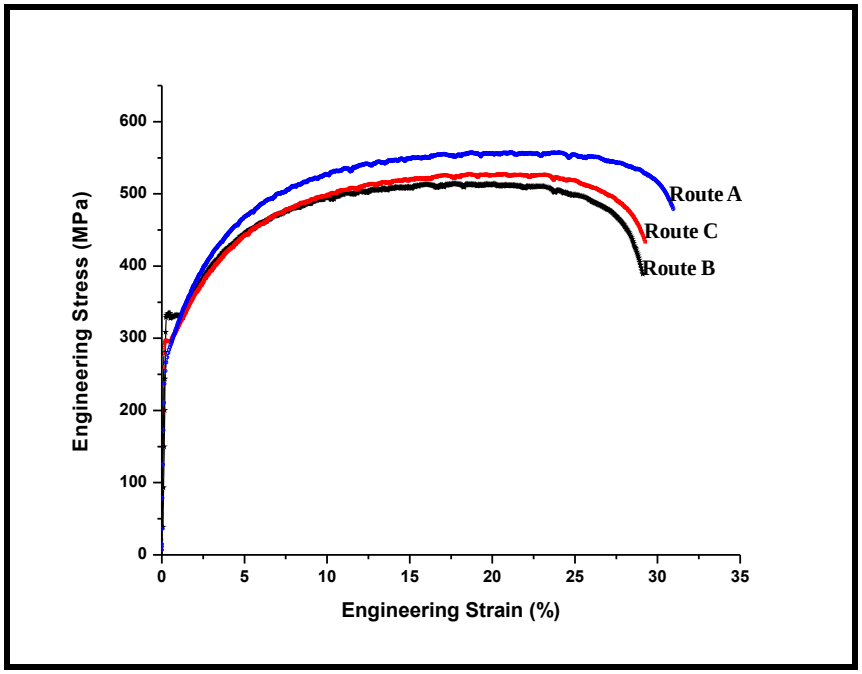

Fig 4.14: Stress-strain curves for steel samples annealed at 750 ℃

4.5.3.3 Comparison of Experimental and Software based Results

This section compares the results regarding martensite fraction observed in the actual microstructure after the annealing experiments with the martensite fraction predicted by the JMat-Pro software. For annealing experiments at 750 ℃, martensite was formed during cooling route A (cooling rate: 32 ℃/ s) with a volume fraction of 15 % (using Image J). However, JMat-Pro predictions at 32 ℃/ s calculated the martensite fraction to be 33.32 %. This amount of martensite (33.32 %) was calculated as follows. For austenization temperature of 750 ℃, the software had calculated [Table 4.1] austenite fraction as 34 % assuming equilibrium heating. For

cooling rate of 32 ℃/ s, the software predicted [Table 4.2] that 98% of the available austenite converts to martensite. Therefore, martensite fraction according to software was 98 % of 34 i.e. 33.32 %. The martensite fraction predicted by the software did not match with the actual experimental outcome. This difference was due to the higher heating rates during up-quenching of samples in the annealing simulator.

4.5.4 Heat Treatment of Samples in Simulator at 800 ℃

This section describes the heat treatment of tensile specimens subjected to inter-critical isothermal annealing at a temperature of 800 ℃. The samples were heated to 800 ℃ in the simulator and were soaked there for 3 min. Gas mixture etc. settings for this annealing temperature were adjusted to provide relatively slow cooling rates in the range of 20–40 ℃/ s. For annealing of samples with 800 ℃ as the austenization temperature, three different samples following different cooling routes (A, B, and C) were annealed. The cooling curves for routes A, B, and C respectively were obtained from the data logs of thermocouple of the annealing chamber and were superimposed on the CCT diagram (Figure 4.15) for the steel. The CCT diagram for this austenization temperature (800 ℃) was constructed using JMat-Pro with main inputs as alloy chemistry and annealing temperature.

4.5.4.1 Microstructural Analysis

Samples annealed at 800 ℃ were first cooled along cooling route A. For this, from the austenization temperature of 800 ℃, after 3 min of stipulated soaking, the sample was directly cooled to room temperature at a cooling rate of 40 ℃ /s. On investigating the microstructure of this annealed sample by optical microscopy, ferrite and martensite dual phase structure was observed as shown in Fig. 4.16a. The ‘Image J’ software detected volume fraction of martensite phase to be 20 %. This showed that during the heating and holding steps of annealing at 800 ℃, pearlite phase mixture converted to austenite. Also, some existing ferrite transformed into fine grained austenite. During subsequent cooling along route A, the ferrite phase remain unchanged whereas austenite transformed to fine grained martensite. Thus, annealing at 800 ℃ with cooling route A obtained a dual phase microstructure due to availability of austenite in a significant amount (20 %).

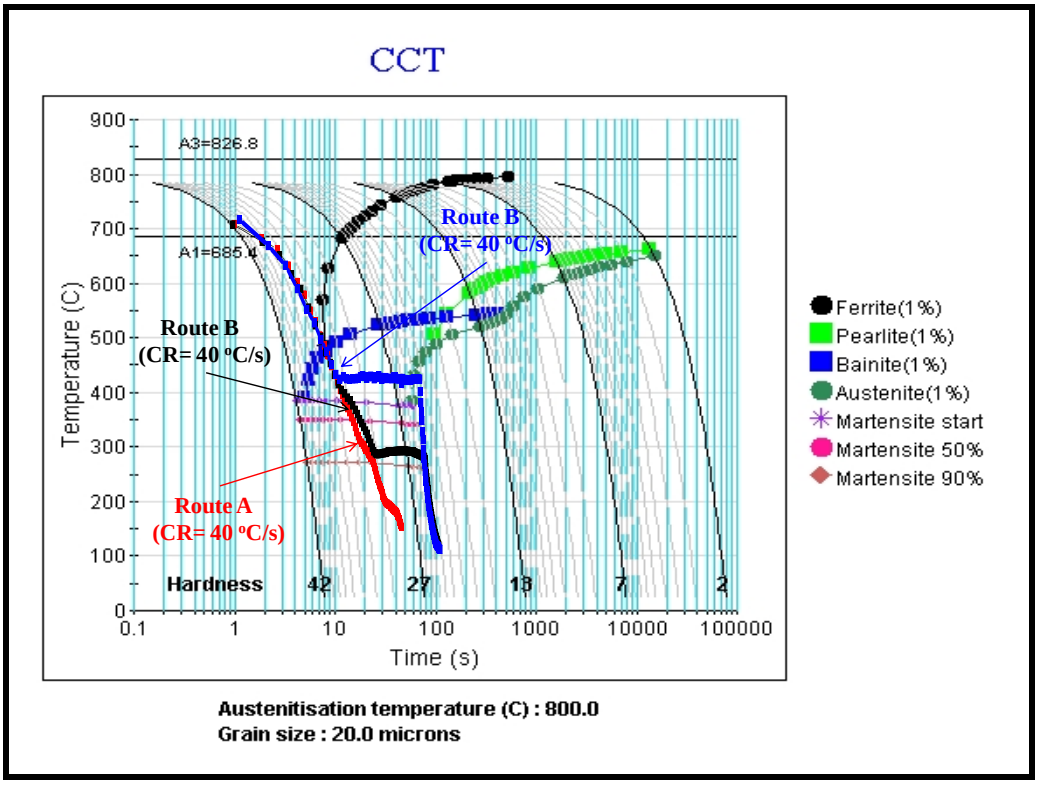

Fig. 4.15: Cooling curves superimposed on CCT diagram at 800 ℃

Next, the samples annealed at 800 ℃ were cooled along the cooling route B. For this, from the austenization temperature of 800 ℃, after 3 min of stipulated soaking, the sample was cooled upto 400 ℃ (bainitic region, identified from the CCT diagram) at a cooling rate of 40 ℃ /s. After holding for 1 min in the bainitic region, the samples were cooled at the cooling rate of 20 ℃ /s to room temperature. On investigating the microstructure of this annealed sample by optical microscopy, a mixture of ferrite, fine bainite, martensite and retained austenite phases was observed as explained in Section 4.6.2.1 and shown in Fig. 4.16b. Thus, annealing at 750 ℃ with cooling route B, multi-phase microstructure was obtained.

Next, the samples annealed at 800 ℃ were cooled along the cooling route C. For this, from the austenization temperature of 800 ℃, after 3 min of stipulated soaking, the sample was cooled upto 280 ℃ (martensitic region, identified from the CCT diagram) at a cooling rate of 40 ℃ /s. After holding for 1 min in the martensitc region, the samples were cooled at a cooling rate 20 ℃ /s to room temperature. On investigating the microstructure of this annealed sample by optical microscopy, a multi-phase microstructure comprising of ferrite, conventional martensite,

tempered martensite, small amount of bainite and retained austenite was observed as explained in Section 4.6.2.1 and shown in Fig. 4.16c.

Thus, annealing at 800 ℃ with cooling route C, produced multi-phase microstructure.

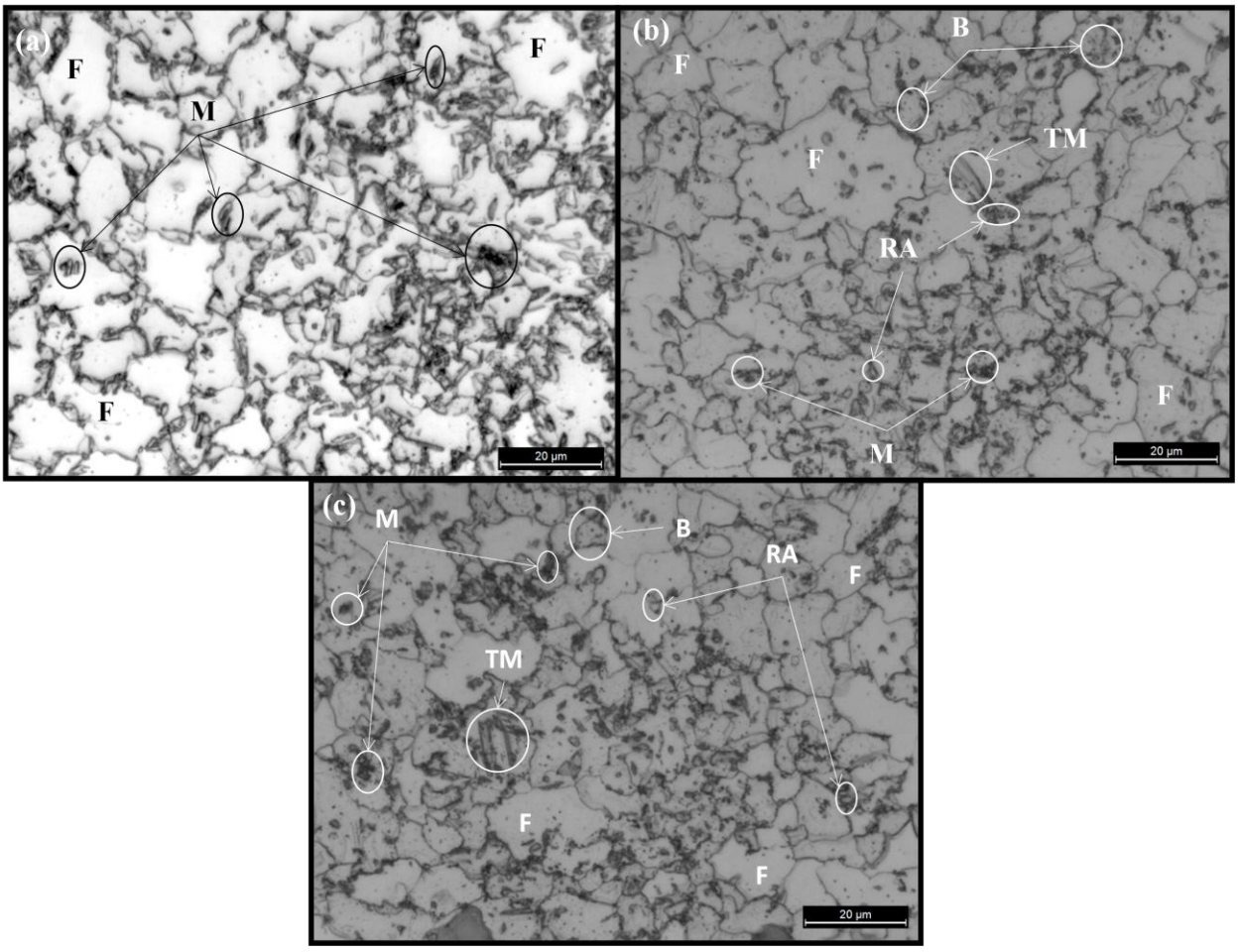

Fig. 4.16: Optical micrographs of samples annealed at 800 ℃ for (a) cooling route A (b) cooling route B (c) cooling rate C. F = Ferrite, B= Bainite, M = Martensite, TM = Tempered Martensite, RA = Retained Austenite

4.5.4.2 Tensile Property Evaluation

After the heat treatment, full tensile tests were conducted for all the three samples (samples formed by routes A, B, and C respectively) annealed at 800 ℃. The results of the tensile tests are presented in Fig. 4.17.

For the sample annealed at 800 ℃ through cooling route A, the yield stress (YS), ultimate tensile strength (UTS), and percent total elongation were calculated as 290 MPa, 610 MPa and 23 % respectively from tensile curve. No yield point elongation was observed in the tensile curve. The

annealed sample showed a low YS/ UTS ratio (0.48 as compared to 0.79 for the as-received steel sample), which is a characteristic of DP steels. Further, it can be noted that the annealed sample (route A) led to improvement in ultimate tensile strength but by losing ductility.

For the sample annealed at 800 ℃ through cooling route B, the yield stress (YS), ultimate tensile strength (UTS), and percent total elongation were calculated as 330 MPa, 570 MPa and 19 % respectively from tensile curve. It can be noted that the annealed sample (route B) led to improvement in ultimate tensile strength but significant decrease in ductility as compared to the as-received sample.

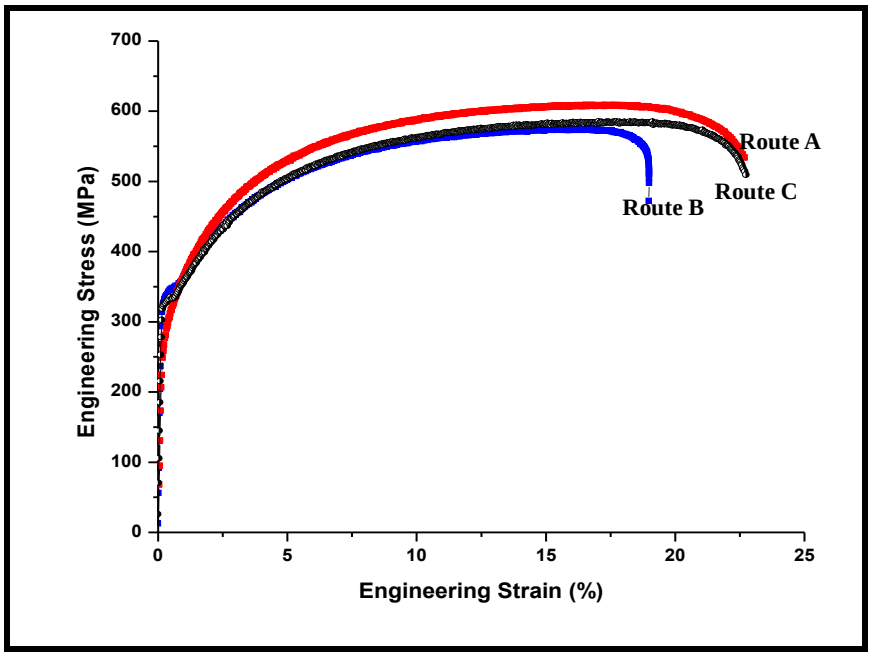

Fig 4.17: Stress-strain curves for steel samples annealed at 800 ℃

For the sample annealed at 800 ℃ through cooling route C, the yield stress (YS), ultimate tensile strength (UTS), and percent total elongation were calculated as 310 MPa, 580 MPa and 23 % respectively from tensile curve. It can be noted that the annealed sample (route C) led to improvement in ultimate tensile strength but decrease in ductility as compared to the as-received sample.

The reasons for change in properties of the annealed samples as compared to as-received sample are the same as discussed in section 4.6.2.2.

4.5.4.3 Comparison of Experimental and Software based Results

This section compares the results regarding martensite fraction observed in the actual microstructure after the annealing experiments with the martensite fraction predicted by the JMat-Pro software. For annealing experiments at 800 ℃, martensite formed during cooling route A (cooling rate: 40 ℃/ s) was 20 % (Image J) in volume fraction. However, JMat-Pro predictions at 40 ℃/ s calculated the martensite fraction to be 65.10 %. %. This amount of martensite (65.10 %) was calculated as follows. For austenization temperature of 800 ℃, the software had calculated [Table 4.1] austenite fraction as 70 % assuming equilibrium heating. For cooling rate of 40 ℃/ s, the software predicted [Table 4.2] that 93% of the available austenite converts to martensite. Therefore, martensite fraction according to software was 93 % of 70 i.e. 65.10 %. The martensite fraction predicted by the software did not match with the actual experimental outcome. This difference was due to the higher heating rates during up-quenching of samples in the annealing simulator.

4.5.5 Heat Treatment of Samples in Simulator at 850 ℃

This section describes the heat treatment of tensile specimens subjected to inter-critical isothermal annealing at a temperature of 850 ℃. The samples were heated to 850 ℃ in the simulator and were soaked there for 3 min. Gas mixture etc. settings for this annealing temperature were adjusted to provide relatively high cooling rates in the range of 20–70 ℃/ s. For annealing of samples with 850 ℃ as the austenization temperature, three different samples following different cooling routes (A, C, and D) were annealed. For austenization temperature of 850 ℃, cooling route B (being used in earlier cases for bainite formation) was not used. This was because for this ICAT (850 ℃), the bainitic region in the CCT diagram had shifted to the left as compared to earlier cases of lower ICATs. Also, the range of temperature for bainitic transformation was very small. Thus, following route B would have demanded for very high initial cooling rate before isothermal holding in the bainite region. With such high cooling rates (and the small bainitic transformation range), it would have been difficult to manage controlled cooling with subsequent holding in the correct transformation temperature range. So, in place of

route B, a new slow cooling route of continuous cooling at a rate of 20 ℃ /s was introduced. The cooling curves for routes A, C, and D respectively were obtained from the data logs of thermocouple of the annealing chamber and were superimposed on the CCT diagram (Figure 4.18) for the steel. The CCT diagram for this austenization temperature (850 ℃) was constructed using JMat-Pro with main inputs as alloy chemistry and annealing temperature.

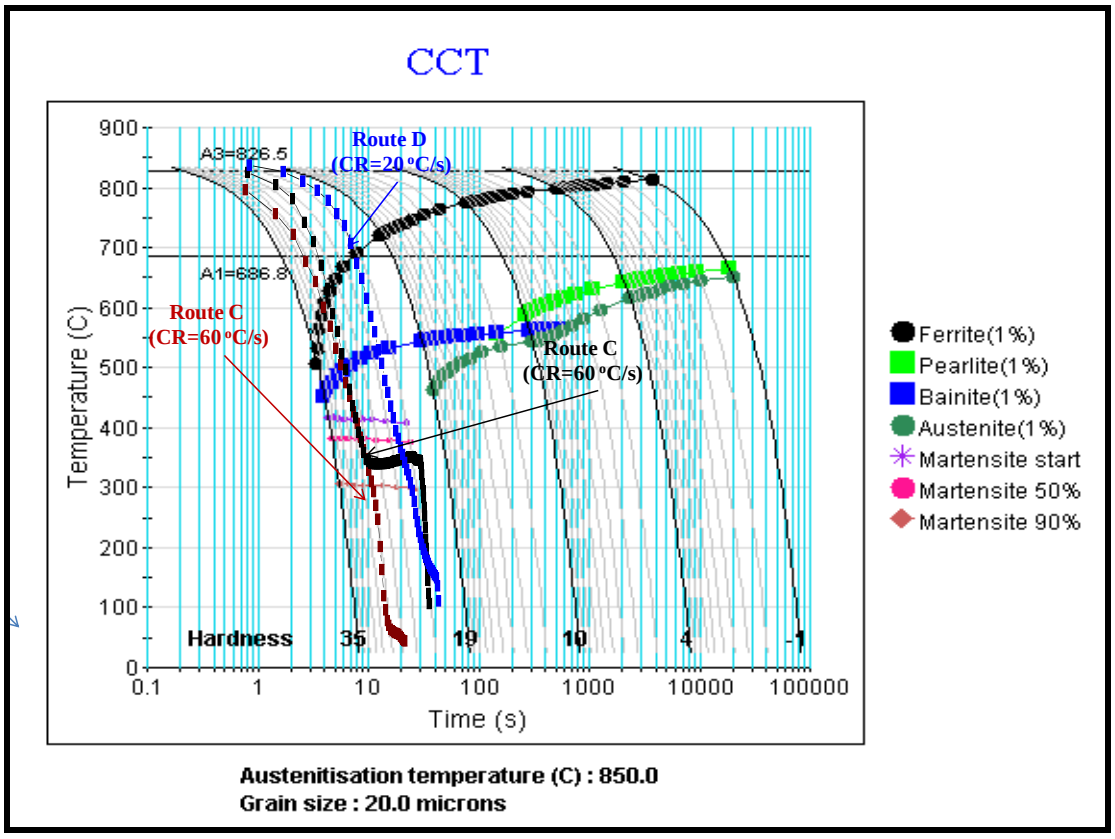

Fig. 4.18 Stress-strain curve of samples annealed at 850 ℃

4.5.5.1 Microstructural Analysis

Samples annealed at 850 ℃ were first cooled along cooling route A. For this, from the austenization temperature of 850 ℃, after 3 min of stipulated soaking, the sample was directly cooled to room temperature at a cooling rate of 60 ℃ /s. On investigating the microstructure of this annealed sample by optical microscopy, ferrite and martensite dual phase structure was observed as shown in Fig. 4.19a. The 'Image J' software detected volume fraction of martensite phase to be 37 %. This showed that during the heating and holding steps of annealing at 850 ℃, pearlite phase mixture converted to austenite. Also, some existing ferrite transformed into fine

grained austenite. During subsequent cooling along route A, the ferrite phase remained unchanged whereas austenite transformed to fine grained martensite. Also, some amount of bainite and ferrite phases may have formed (as is shown by the superimposed cooling curve for route A). Thus, annealing at 850 ℃ with cooling route A obtained a dual phase microstructure due to availability of austenite in a significant amount (37%).

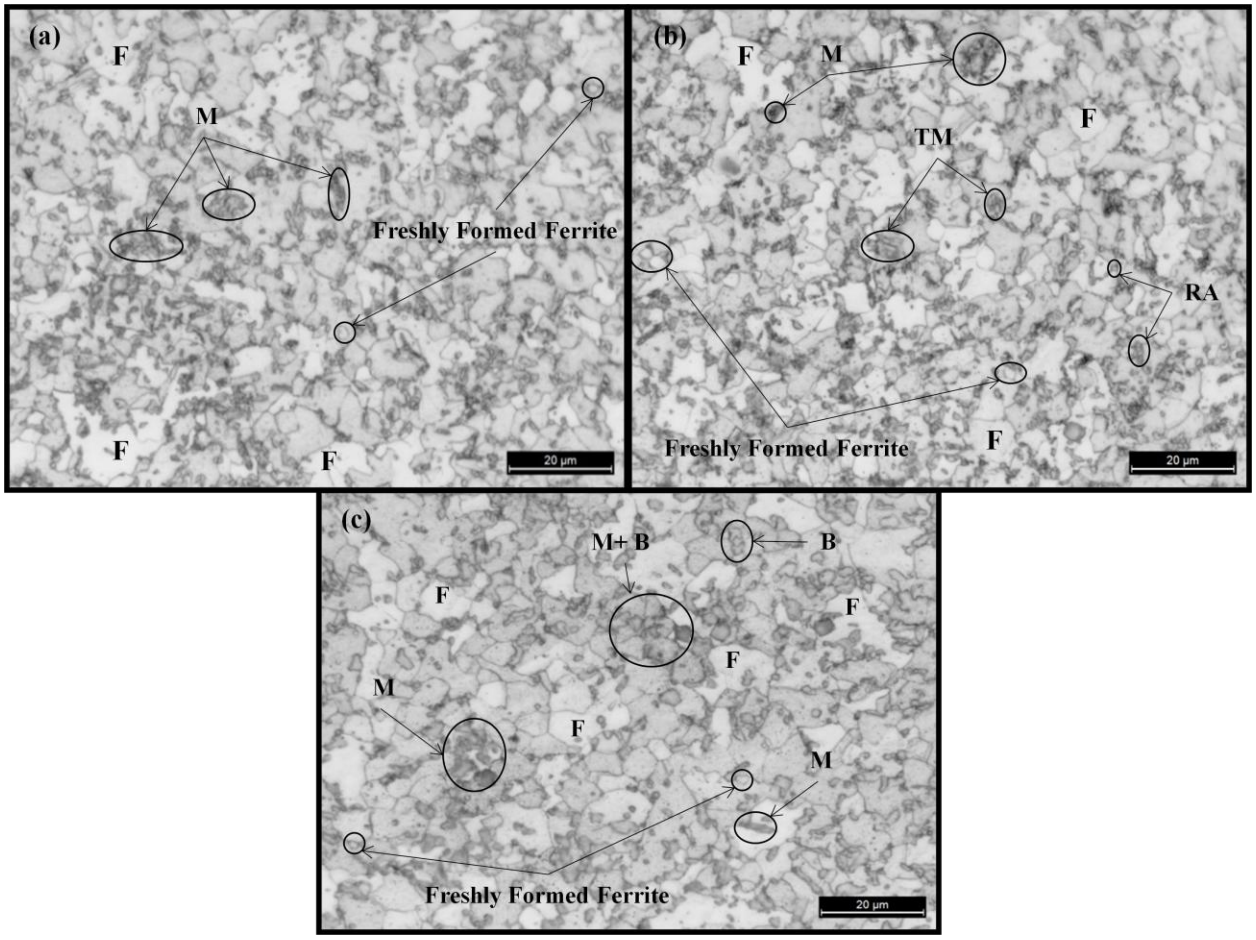

Fig. 4.19: Optical micrographs of samples annealed at 750 ℃ for (a) cooling route A (b) cooling rate C (c) cooling route D. F = Ferrite, B= Bainite, M = Martensite, TM = Tempered Martensite

Next, the samples annealed at 850 ℃ were cooled along the cooling route C. For this, from the austenization temperature of 850 ℃, after 3 min of stipulated soaking, the sample was cooled upto 350 ℃ (martensitic region, identified from the CCT diagram) at a cooling rate of 60 ℃ /s. After holding for 1 min in the martensitc region, the samples were cooled at a cooling rate of 31 ℃ /s to room temperature. On investigating the microstructure of this annealed sample by

optical microscopy, ferrite, fine grained martensite with small amount of retained austenite and bainite was observed as shown in Fig. 4.19b.

During the heating and holding steps of annealing at 850 ℃, pearlite phase mixture converted to austenite. Also, some amount of the existed ferrite was converted into austenite. During cooling and holding in the martensitic region, some amount of carbon from freshly formed martensite diffused to untransformed austenite enriching some portions of austenite. Some fraction of untransformed austenite (low carbon portion of austenite) transformed to supersaturated ferrite (called bainitic ferrite) which ultimately led to formation of bainite phase mixture. The remaining untransformed austenite (high carbon portion of austenite) was stable and was observed as retained austenite in the room temperature microstructure. Carbides did not form, may be due to the high cooling rate (> 30 ℃ /s) followed during second cooling after holding in the martensitic region. Thus, annealing at 850 ℃ with cooling route C produced a multi-phase microstructure.

Next, the samples annealed at 850 ℃ were cooled slowly along the cooling route D. For this, from the austenization temperature of 850 ℃, after 3 min of stipulated soaking, the sample was cooled upto room temperature at a cooling rate of 20 ℃ /s. On investigating the microstructure of this annealed sample by optical microscopy, ferrite (original and freshly formed), fine grained martensite, and bainite phases were observed as shown in Fig. 4.19c. During the heating and holding steps of annealing at 850 ℃, pearlite phase mixture converted to austenite. Also, some amount of the existing ferrite was converted into austenite. During cooling, austenite transformed initially to fine grained ferrite, followed by bainite and finally martensite. Thus, annealing at 850 ℃ with slow cooling produced a multi-phase microstructure.

4.5.5.2 Tensile Property Evaluation

After the heat treatment, full tensile tests were conducted for all the three samples (samples formed by routes A, C and D respectively) annealed at 850 ℃. The results of the tensile tests are presented in Fig. 4.20.

For the sample annealed at 850 ℃ through cooling route A, the yield stress (YS), ultimate tensile strength (UTS), and percent total elongation were calculated as 355 MPa, 705 MPa and 11 % respectively from tensile curve. No yield point elongation was observed in the tensile curve. The annealed sample showed a low YS/ UTS ratio (0.50 as compared to 0.79 for the as-received steel

sample), which is a characteristic of DP steels. Further, it can be noted that the annealed sample (route A) led to improvement in ultimate tensile strength, however by loosing ductility.

For the sample annealed at 850 ℃ through cooling route C, the yield stress (YS), ultimate tensile strength (UTS), and percent total elongation were calculated as 340 MPa, 680 MPa and 19 % respectively from tensile curve. It can be noted that the annealed sample (route C) led to improvement in ultimate tensile strength but decrease in ductility as compared to the as-received sample.

For the sample annealed at 850 ℃ through slow cooling (Route D), the yield stress (YS), ultimate tensile strength (UTS), and percent total elongation were calculated as 320 MPa, 615 MPa and 23 % respectively from tensile curve.

The reasons for change in properties of the annealed samples as compared to as-received sample are the same as discussed in section 4.6.2.2. Amongst the three routes followed for austenization at 850 ℃, route D provided the best ductility because of freshly formed ferrite in the annealed steel.

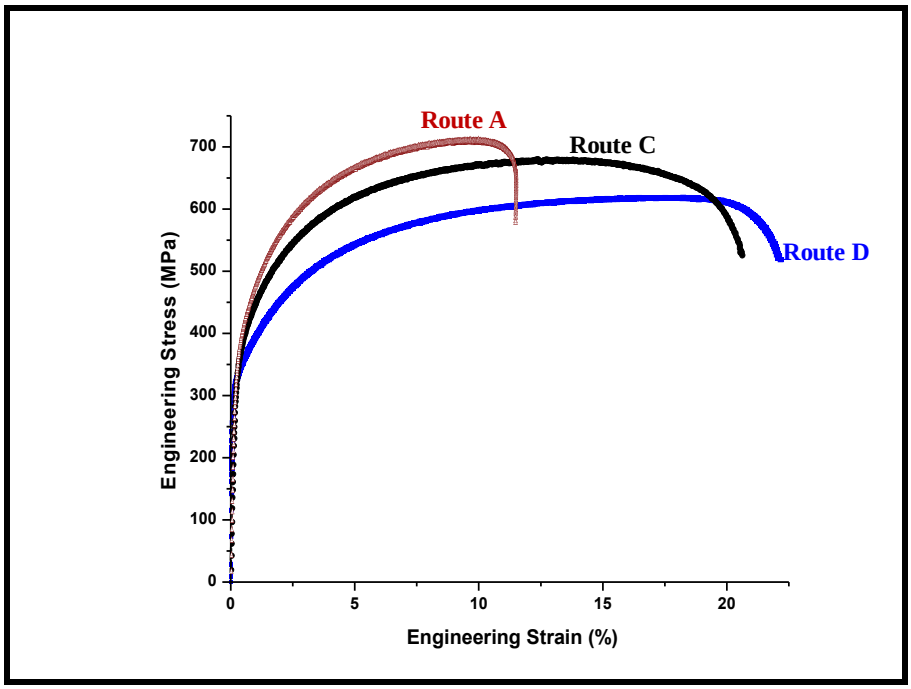

Fig. 4.20: Stress-strain curves for steel samples annealed at 850 ℃

4.5.5.3 Comparison of Experimental and Software based Results

This section compares the results regarding martensite fraction observed in the actual microstructure after the annealing experiments with the martensite fraction predicted by the JMat-Pro software. For annealing experiments at 850 ℃, martensite was formed during cooling route A (cooling rate: 60 ℃/ s) was 37 % (Image J). However, JMat-Pro predictions at 60 ℃/ s calculated the martensite fraction to be 91 % (for austenization temperature of 850 ℃, the software had calculated [Table 4.1] austenite fraction as 100 % assuming equilibrium heating. For cooling rate of 60 ℃/ s, the software predicted [Table 4.2] that 91% of the available austenite converts to martensite. Therefore, martensite fraction according to software was 91 % of 100 = 91 %). The martensite fraction predicted by the software did not match with the actual experimental outcome. This difference was due to the higher heating rates during up-quenching of samples in the annealing simulator.

4.5.6 Hardness Measurements

Micro-hardness measurements (diamond penetration hardness; Vickers 136^{o} pyramid) were made on the Vickers scale (Hv) for the as-received sample and the samples annealed at various annealing temperatures. This was done to predict (through microhardness values) the phases present in the steel under different conditions and thus to validate the observations regarding phase constitution obtained through optical microscopy. These observations were made only for the dual phase microstructures (ferrite and martensite) obtained through cooling route A for different annealing temperatures. This approach was used because martensite particle sizes present in the annealed samples were too small for reliable hardness testing involving individual phases. So, the overall hardness of the samples was calculated.

For this, first the hardness of the as-received sample (containing largely only ferrite phase) was measured which came out to be in the range 100–250 Hv (Table 4.5). So, it was concluded that the hardness of ferrite phase present in the given steel is 151 Hv (average; and in the range 100–250 Hv). For obtaining the hardness of martensite phase in the given steel, a separate sample was prepared.

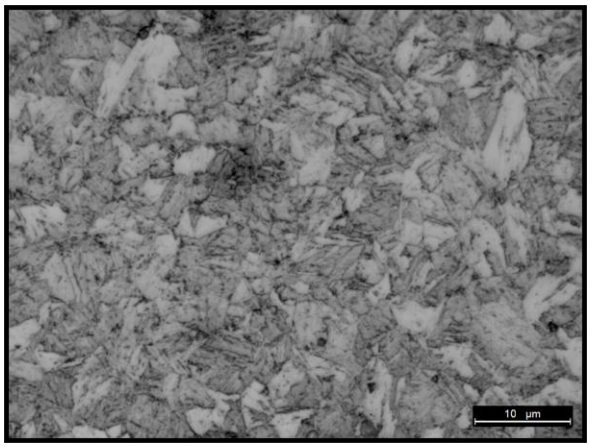

Fig. 4.21: Optical micrograph of fully martensitic structure

This sample was heated to an austenization temperature of 860 ℃, was soaked there for 5 min period, and was finally water quenched to obtain a fully martensitic structure as shown in Fig. 4.21 ('Image J' calculated the martensite fraction as 98%). Microhardness measurements were made which calculated the hardness of martensite phase in the range 425–525 Hv. So, it was concluded that hardness of martensite phase present in the given steel is 464 (average; and in the range 425–525 Hv). The hardness values of the samples as a function of annealing temperature are presented in Fig. 4.22. Phases were verified by comparing the hardness outcomes of samples with calculated values of each phase (ferrite and martensite). Typical values of hardness and scatter range obtained were: T_{700} = 180 (174–187), T_{750} = 207 (188–223), T_{800} = 224 (206–250), T_{850} = 274 (247–321) Hv. Each hardness value represents the average of fifteen values (shown in Appendix III).

Table 4.5: Microhardness of ferrite and martensite phases in the given steel

Phase	Hardness value (Hv)						Average Hardness (Hv)
Ferrite	174	157	136	149	123	220	**151**
Martensite	445	471	449	460	445	512	**464**

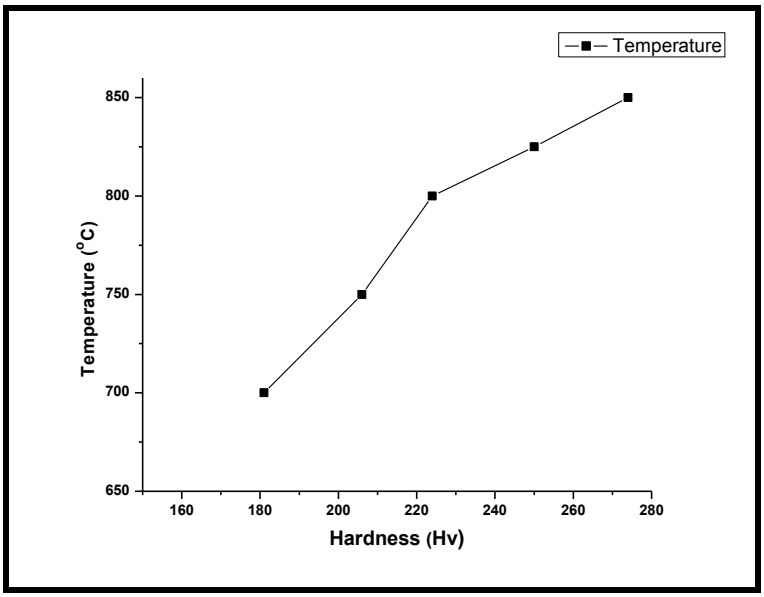

Fig. 4.22: Hardness values as a function of annealing temperature

It is observed from the above figure (Fig. 4.22) that hardness value increased with increase in the annealing temperature. This showed that with increase in annealing temperature, the martensite fraction increased in the annealed sample at the expense of decrease in ferrite phase. The same is concluded from the micrographs also, thus validating the results of optical microscopy. For example, at annealing temperature of 700℃, the average hardness of sample was measured as 181 Hv (which is close to the hardness value (151 Hv) of pure ferrite). Thus, it can be concluded from hardness measurements that the structure is largely ferritic after annealing at 700 ℃. Similarly, at annealing temperature of 850℃, the average hardness of sample was measured as 274 Hv (which is away from the hardness value (151 Hv) of pure ferrite and closer to the hardness value (464 Hv). Thus, it can be concluded from hardness measurements that the structure is containing appreciable quantity of martensite after annealing at 850 ℃ (optical microscopy showed 37% martensite).

4.6 Micro-Mechanical Modeling of Dual Phase Steels

Material characterization is an important tool to describe and enhance the mechanical properties of a material by selecting optimum material chemistries and developing suitable microstructures. The usual approach of achieving these objectives through experimental techniques is generally costly and time consuming. To overcome these constraints of experimental approaches, the

micro-mechanical modeling approach was developed. This modeling technique helps in predicting the material behavior without extensive experimental investigation. It is based on the microstructural characteristics of a given material.

Micro-mechanical model as reported by Alabbasi [2004] has been used in the present work to predict the mechanical properties of DP steels developed in the present work (through route A of annealing process at various temperatures). The tensile properties (of the steel containing DP structure at various annealing temperatures) obtained through actual tensile experiments have been compared with micro-mechanical model predictions to validate the former.

To apply this modeling approach, it was necessary to know the tensile properties of individual phases (i.e. ferrite and martensite) present in the given steel with DP structure. For this, the behavior of each steel phase was determined by tests on the given steel when consisting of a single phase (fully ferritic and fully martensitic structure separately). The single phase structures were obtained in the given steel by subjecting it to conditions as explained in Section 4.5.6. The single-phase steel was then tested in tension to obtain the characteristic tensile behavior of a specific phase. In this manner, the engineering stress-strain curves for ferrite phase and martensite phase were obtained. These engineering stress-stress strain curves were now converted into true stress strain curves for ferrite and martensite. The conversion was done by using the formulae [Callister, 2007]:

$$\text{True Strain} = ln\left(1 + \frac{\varepsilon}{100}\right) \quad 4.1$$

$$\text{True Stress} = \sigma\left(1 + \frac{\varepsilon}{100}\right) \quad 4.2$$

where, ε is engineering strain, σ is engineering stress.

Using Equations 4.1 and 4.2, the values of true strain and true stress were calculated for each phase. These values were used to plot the true stress-strain curve. From this true stress-strain curve, the range of stress-strain values corresponding to the strain hardening region was observed. Now, the obtained values of true stress and true strain were converted to the 'ln' scale using OriginPro 8.0 software. These '*ln* (true stress)' and '*ln* (true strain)' values were now plotted. The tensile curves (*ln-ln* true stress-strain curves) for the single-phase steel containing only ferrite and only martensite are shown in Fig. 4.23a and 4.23b respectively. It may be noted here that the curves are being shown only for the strain hardening region as discussed above.

These curves were now used to determine the strain hardening coefficient (n) for each phase by linear fitting of the curves (Figure 4.23 a–b). The strain hardening value (n) for ferrite and martensite phases was obtained as 0.21 (n_f) and 0.08 (n_m) respectively.

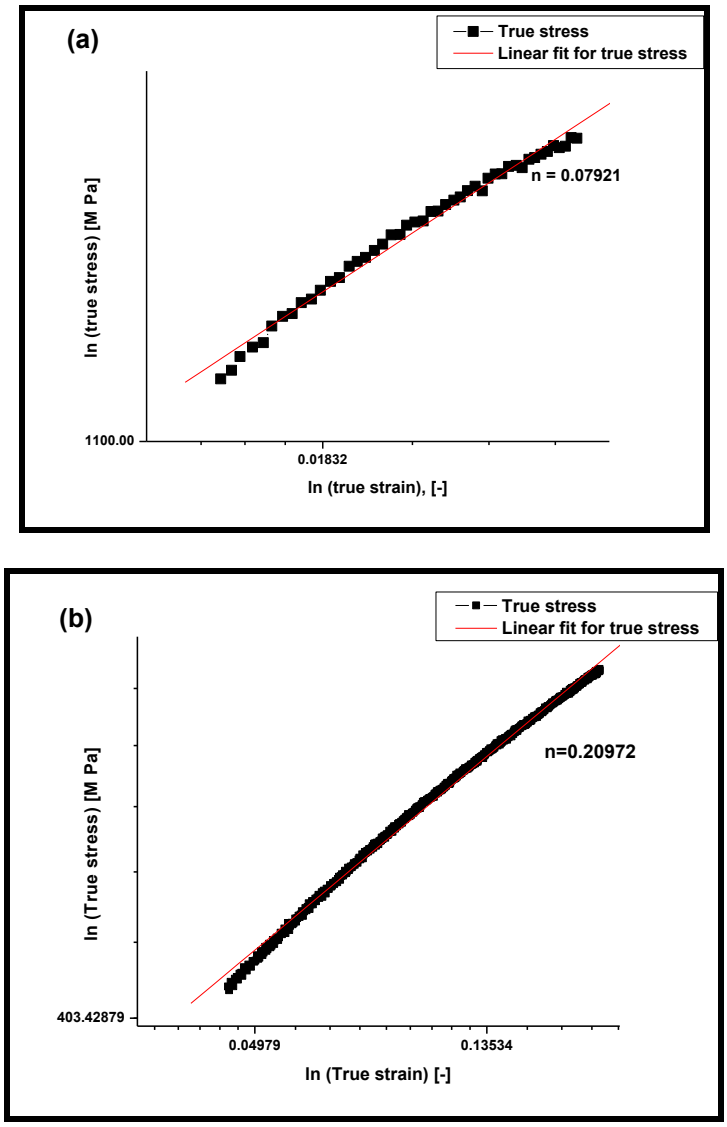

Fig. 4.23: ln-ln true stress-strain curves to obtain strain hardening exponent for (a) martensite and (b) ferrite

These strain hardening coefficient values were fitted to the power law relation as given by [Alabbasi, 2004], and represented as Equations 4.3 and 4.4. These equations were used to obtain the Hollomon strength coefficients (K_f and K_m) as shown below.

$$\sigma_f = K_f \left(\varepsilon_o + \varepsilon_f^p\right)^n_f \qquad 4.3$$

$$\sigma_m = K_m \, (\varepsilon_o + \varepsilon_m^p)^{n_m} \qquad 4.4$$

where, K_m and K_f are the Hollomon strength coefficients for martensite and ferrite respectively. ε_o is the strain corresponding to off-set yield strength and was taken 0.002 in this work. n_m and n_f were taken as 0.08 and 0.21 respectively (as calculated from Fig. 4.23a–b). ε_f^p and ε_m^p are uniform true strains for ferrite and martensite phases respectively (i.e. strains corresponding to ultimate tensile strengths). The values of ε_f^p and ε_m^p were obtained as 0.2517 and 0.039 respectively (according to the tensile experimental results for pure ferritic and pure martensitic structures). The ultimate true tensile stress values for martensite and ferrite phases were calculated as 1188.64 MPa (σ_m) and 595.14 MPa (σ_f) respectively. Using equations 4.3 and 4.4 and the vales of parameters as discussed above, K_m and K_f were calculated as 1530 MPa and 793 MPa respectively.

Finally, the rule of mixtures (Equation 4.5) as reported by Alabbasi (2004) was used to calculate the composite true stress behavior of the DP steel containing known volume fractions of ferrite and martensite phases.

$$\sigma_c = V_m \, K_m \, (\varepsilon_o + \varepsilon_m^p)^{n_m} + (1 - V_m) \, K_m \, (\varepsilon_o + \varepsilon_f^p)^{n_f} \qquad 4.5$$

where, σ_c is the true stress for the composite material (steel containing two phase), V_m is the volume fraction of martensite phase present in the composite material (i.e. the given steel). In this manner, for any given microstructure (with specific martensite fraction) in the DP steel, the true stress values for given strain values were calculated. Thus, the true stress-strain diagram based on micro-mechanical model was generated. This model based true stress-strain diagram was superimposed on the actual (experimental based) true stress-strain diagram for any given annealing condition (i.e. for any microstructure obtained through annealing experiments). Figure 4.24 (a–c) show the model based curves superimposed on the experimental true stress-strain curves for three different microstructures (containing martensite fraction of 15, 20, and 37% respectively) obtained (through route A at annealing temperatures of 750, 800, and 850 ℃ respectively) in the given steel (data logs for MVF= 15% are shown in Appendix IV).

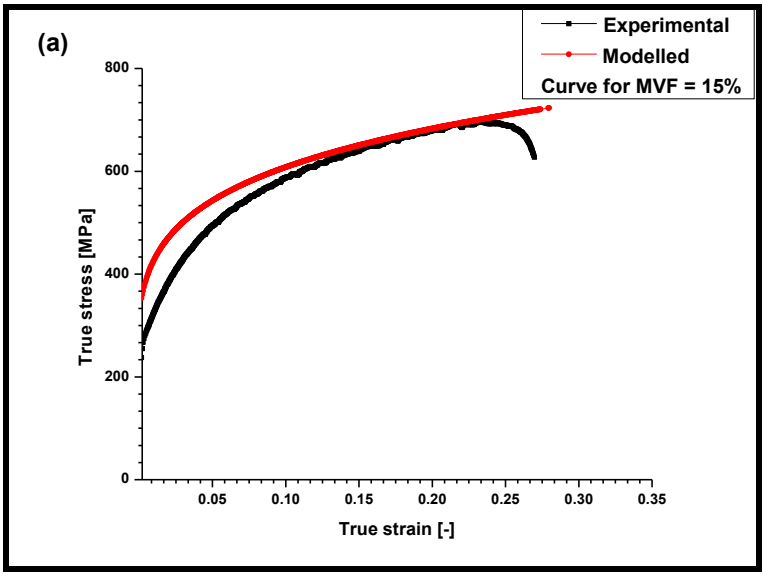
(a)
Experimental
Modelled
Curve for MVF = 15%
True stress [MPa]
True strain [-]
0
200
400
600
800
0.05
0.10
0.15
0.20
0.25
0.30
0.35

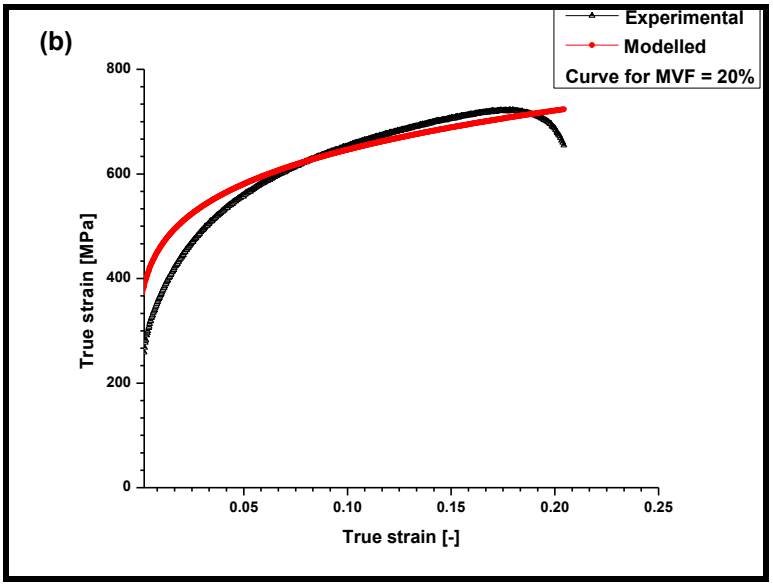
(b)
Experimental
Modelled
Curve for MVF = 20%
True strain [MPa]
True strain [-]
0
200
400
600
800
0.05
0.10
0.15
0.20
0.25

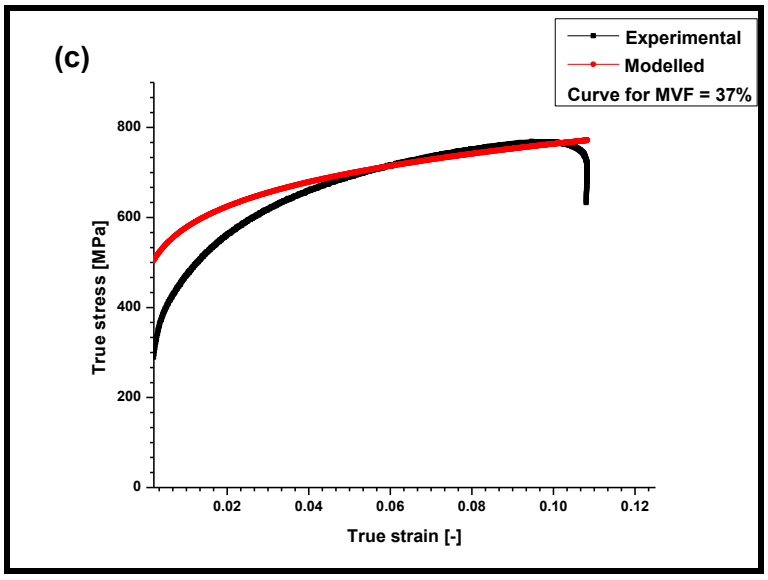

Fig. 4.24: Comparison of experimental and modelled true stress strain curves for different MVF (a) 15% (b) 20% (c) 37%. MVF = Martensite volume fraction

It is observed from Fig. 4.24 that the true stress-strain curves obtained through micro-mechanical modelling match closely to the actual experimental true stress-strain curves for all investigated dual phase microstructures in the given steel. Thus, this modelling technique (micro-mechanical modelling) can be utilized to predict the material behaviour without extensive experimental investigation only on the basis of microstructural characteristics.

Chapter 5

Conclusions

5.1 General

The development of multiphase steels characterized by various combinations of strength and ductility is a subject of significant interest worldwide. Still, there exists curiosity of further augmenting ductility and strength combinations. There have been endless efforts made to develop good ductility and strength combinations. Most of the efforts in the last two decades have been inclined towards the production of these steels by following appropriate heat treatment through water quenching. It can be concluded from the literature survey that very few efforts have been made to produce these steels by using lean chemistry and controlled cooling routes. Keeping in mind these literature gaps, in the present investigation, the dual/ multiphase steel was produced from a lean chemistry through controlled cooling obtaining various combinations of strength and ductility, thus making the steel multifunctional.

5.2 Results and Conclusions

The main results and conclusions from the present experimental work are as follows:

As-received material

- The alloy chemistry of steel permitted various combinations of strengths and ductility to be obtained in it through availability of different microstructures (DP, multiphase) just by varying heat treatment conditions. A diverse range of strength-percent elongation combinations was obtained in the same lean chemistry steel through various heat treatment routes (475 MPa, 33% to 705 MPa, 12%).

Austenite formation in the muffle furnace

- Austenite fraction predicted by the software (i.e. for equilibrium heating conditions) for a given annealing temperature was considerably different from the fraction obtained through actual annealing experiments (i.e. under up-quenching). For the same temperature-time annealing conditions, JMat-Pro predicted higher amount of austenite than actually observed

during annealing. This difference was attributed to the different heating rates under the two conditions.

- With increase in annealing temperature, the percentage difference observed in the austenite fraction under the two cases continuously decreased. This decreased difference at higher temperatures was attributed to the fact that at higher annealing temperatures, the austenization process increases rapidly (thereby actual austenite fraction at higher temperatures got closer to the predicted fraction).
- Higher heating rates followed during actual experimentation led to increase in critical temperatures to higher values (than the equilibrium values of 684 and 834 ℃ respectively).

Heat treatment for producing multiphase steel

- As the annealing temperature increased (700–850 ℃), the fraction of austenite formed during heating and soaking steps also increased (< 5–37%). DP structure was produced through route A only and multiphase was produced through routes B, C, and D.
- As the annealing temperature increased, the cooling rate required to convert the entire available austenite to martensite also increased. Also, the M_S and M_F temperatures increased with increase in the annealing temperature. This was because with increase in annealing temperature, the austenite fraction increases in the given steel, thus, decreasing the carbon concentration in austenite. This austenite of comparatively less carbon concentration has lesser stability and tends to transform to martensite at a relatively higher temperature, hence increasing the M_S and M_F temperatures.
- Carbides were formed during every cooling which followed a holding period (i.e. second cooling of routes B and C). However, this formation was observed only if suitable time was available for carbide formation during the course of cooling (i.e. for slow cooling rates of less than 30 ℃/ s). Carbide formation did not result for annealing temperature of 850 ℃ because the cooling rate during second cooling was 31 ℃ /s. The presences of carbides contributed towards strength but it came at the expense of decrease in ductility.
- The given steel when converted to a DP microstructure showed continuous yielding without a discrete yield point (unlike clear and distinct upper and lower yield points shown in the normalized as-received state). This change in the yielding pattern was attributed to the presence of martensite phase which introduced mobile dislocations leading to continuous

yielding. Also, the presence of hard phases (martensite, and/ or bainite) increased the UTS but deteriorated the ductility and yield strength.

- Presence of bainite in the microstructure reduced the ultimate tensile strength and increased the yield strength as compared to ideal ferritic-martensitic DP steel microstructure. This increased the YS/ UTS ratio, thus deteriorating the key characteristic of low yield to tensile ratio, required in DP steels.
- Hardness values increased with increase in the ICAT during heat treatment along route A. This showed that with increase in annealing temperature, the martensite fraction increased in the annealed sample at the expense of decrease in ferrite phase. The same is concluded from the *mi*crographs also, thus validating the results.

5.3Major Conclusions and Recommendations

- There were variations in the annealing results obtained through annealing experiments and those obtained through software predictions. The variations are attributed to the reason that software predictions are made on the assumption of equilibrium heating which seldom followed during actual industrial heating. Further, the software does not take into account the effect of holding time at the inter-critical annealing temperature. Also, during production of DP steels, cooling rates obtained through water quenching are quite higher than the rates achieved under simulated conditions.
- A diverse range of strength-ductility combinations can be obtained in a steel of lean chemistry by following appropriate cooling routes during the inter-critical annealing process. The alloy chemistry of the investigated steel permitted various combinations of strength and ductility to be obtained in it through availability of different microstructures (DP, multiphase) just by varying the heat treatment conditions.
- In the samples annealed at temperatures 700, 750, and 800 ℃, both UTS and ductility of higher magnitudes were obtained through route A as compared to routes B and C. This was attributed to the formation of carbides during routes B and C. Ductility decreased because of presence of carbides. Strength decreased because these routes (B and C) did not result in formation of martensite fraction as was obtained through route A.

- The true stress-strain curves (of the steel containing DP structure at various annealing temperatures) obtained through actual tensile experiments closely matched with the true stress-strain curves predicted by micro-mechanical modelling. Thus, it is concluded that micro-mechanical modelling technique can be utilized to predict the material behaviour without the need for extensive experimental investigation.

5.4 Scope of Future Work

In the present work, the volume fraction of various phases (obtained under given annealing conditions) was determined through optical micrographs only using Image J software. The volume fractions can be determined more accurately through XRD, EBSD analysis etc. The presence of carbides can also be ensured better by use of SEM and EBSD analysis. In the present study, maximum volume fraction of martensite achieved was 37% at 850 ℃ through route A. Annealing experiments can be extended to even higher temperature ranges to achieve higher austenite and hence higher martensite fraction to evaluate the change in mechanical properties. The study has taken the effect of non-equilibrium heating into account but only qualitatively. Future studies can include the exact effect of heating rates on the microstructure by measuring the heating rate during the process of austenization. In the present study, the TRIP effect was not observed to a significant extent. Further investigations can be conducted for comparatively larger holding times to see the TRIP effect.

References

- Adamczyk, J.; Grajcar, A. (2006) Effect of heat treatment conditions on the structure and mechanical properties of DP-type steel. *Journal of Achievements in Materials and Manufacturing Engineering*, 17: 305–308.
- Ahmad, E.; Manzoor, T.; Hussain, N.; Qazi, N.K. (2008) Effect of thermo-mechanical processing on hardenability and tensile fracture of dual-phase steel. *Materials and Design,* 29: 450–457.
- Alabbasi, F. (2004) Micromechanical Modelling of Dual Phase Steels. Ph.D. Thesis, McGill University, Montreal, Canada.
- Asadi, M.; Polkowski, H. (2011) Investigation on local mechanical properties in multiphase stels for designing local properties of constructional elements. *Metallurgical Science and Technology*, 29(1): 26–31.
- Bhattacharya, D. (2006) Developments in advanced high strength steels', *presented at Advanced High Strength Steel Workshop,* Virginia, USA.
- Bouquerel, J.; Verbeken, K.; De-Cooman B.C. (2006) Microstructure-based model for the static mechanical behaviour of multiphase steels. *Acta Materialia*, 54: 1443–1456.
- Bouquerel. J.; Verbeken, K.; Van Slycken, J.; Verleysen, P.; Houbaert, Y. (2008) Physically based modeling of the mechanical behavior of TRIP steels, *International Journal Material Forming,* Suppl. 1: 57–60.
- Cai, X.; Liu, C.; Liu, Z. (2014) Process design and prediction of mechanical properties of dual phase steels with prepositional ultra fast cooling. *Materials and Design* 53: 998–1004.
- Calcagnotto, M.; Ponge, D.; Rabbe, D. (2010) Effect of grain refinement to 1 μm on strength and toughness of dual-phase steels. *Materials Science and Engineering* A, 527: 7832–7840.
- Callister, W. D. (2007), 'Material Science and Engineering: An Introduction', John Wiley and Sons, Inc., New York.
- Cornet, X.; Herman, J. C. (2003) Method for making a multiphase hot-rolled steel strip. *U.S. Patent 0041933 A1*.
- Davies, R.G. (1978) The deformation behavior of a vanadium-strengthened dual phase steel. *Metallurgical Transactions A*, 9A: 41–52.

- Demir, B.; Erdogan, M. (2008) The hardenability of austenite with different alloy content and dispersion in dual-phase steels. *Journal of Materials Processing technology*, 208: 75–84.
- Dziedzic, M.; Turczyn, S. (2010) Experimental and numerical investigation of strip rolling from dual phase steel. *Archives of Civil and Mechanical Engineering*,10(4): 21–30.
- Erdogan, M.; Tekeli, S. (2002) The effect of martensite particle size on tensile fracture of surface carburised AISI 8620 steel with dual phase core microstructure. *Materials and Design*, 23: 597–604.
- Ganguly, S.; Datta, S.; Chattopadhyay, P.P.; Chakraborti, N. (2009) Designing the multiphase microstructure of steels for optimal TRIP effect: A multi-objective genetic algorithm based approach. *Materials and Manufacturing Processes*, 24(1): 31–37.
- Hao, Q. (2011), Advanced high strength steel through Para-equilibrium carbon partitioning and austenite stabilization, Ph.D. dissertation, Case Western Reserve University, Cleveland, United States.
- Hulka, K. (2005) The Role of Niobium in Multiphase Steel, *presented at METAL 2005*, Germany 20-22 May, 2005.
- Kang, Y. L.; Han, Q. H.; Zhao, X. M.; Cai, M. H. (2013) Influence of nanoparticle reinforcement on the strengthening mechanism of an ultrafine-grained dual phase steels containing titanium. *Materials and Design*, 44: 331–339.
- Korzekwa, D.A.; Lawson, R.D.; Matlock, D.K.; Krauss, G. (1980) A consideration of models describing the strength and ductility of dual-phase steels. *Metallurgica*, 14: 1023–1028.
- Kumar, A.; Singh, S. B.; Ray, K. K. (2008) Influence of bainite/ martensite-content on the tensile properties of low carbon dual-phase steels. *Materials Science and Engineering A, 474*: 270–282.
- Kuziak, R.; Kawalla, R.; Waengler, S. (2008) Advanced high strength steels for automotive industry. *Archives of Civil and Mechanical Engineering*, 8(2): 103–117.
- Kwon, O.; Lee, K.; Kim, G.; Chin, K.G. (2010) New trends in advanced high strength steel developments for automotive applications. *Materials Science Forum*, 638–642: 136–141.
- Li, L.; Zhang, X.; Yang, W.; Sun, Z. (2013) Microstructure and mechanical properties of a low-carbon Mn-Si multiphase steel based on dynamic transformation of under-cooled austenite. *Metallurgical and Materials Transactions A*, 44A: 4337–4345.

- Lorusso, H.; Burgueno, A.; Egidi, D.; Svoboda, H. (2012) Application of dual phase steels in wires for reinforcement of concrete structures. *Procedia Materials Science*, 1: 118 – 125.
- Matlock, D.K.; Speer, J.G. (2010) Processing Opportunities for New Advanced High-Strength Sheet Steels. *Material and Manufacturing Processes*, 25(1): 7-13.
- Matlock, D.K.; Speer, J.G.; Moor, E.D.; Gibbs, P.J. (2012) Recent developments in advanced high strength sheet steels for automotive applications: an overview. *JESTECH*, 15(1): 1–12.
- Meng, Q.; Li, J.; Wang, J.; Zhang, Z.; Zhang, L. (2009) Effect of water quenching process on microstructure and tensile properties of alloy cold rolled dual-phase steel. *Material and Design*, 30: 2379–2385.
- Mohapatra, S.S.; Chakraborty, S.; Pal, S.K. (2012) Experimental studies on different cooling processes to achieve ultra-fast cooling rate for hot steel plate. *Experimental Heat Transfer*, 25: 111–126.
- Mohrbacher, H. (2013) Microstructure optimization for multiphase steels with improved formability and damage resistance, *In Proceedings of ISAS*, Belgium, pp.
- Patel, J.; Klinkenberg, C.; Hulka, K. (2001) Hot rolled HSLA strip steels for automotive and construction applications, International Symposium, Niobium; Science & Technology, 647-674.
- Rajan, T. V.; Sharma, C. P.; Sharma, A. (2011) Heat Treatment principles and techniques. PHI learning private limited, New Delhi.
- Ramazani, A.; Ebrahimi, Z.; Prahl, U. (2014) Study the effect of martensite banding on the failure initiation in dual-phase steel. *Computational Materials Science*, 87: 241–247.
- Reichert, B.; Estrin, Y. (2007) Modular modelling of stress-strain behaviour of ferritic steel grades in strain rate ranges relevant for automotive crash situations. *Steel research international.* 78: 791–797.
- Saleh, M.H.; Priestner, R. (2001) Retained austenite in dual-phase silicon steels and its effect on mechanical properties, Journal of Materials Processing Technology, 113: 587–593.
- Sayed, A. A.; Kheirandish, S. (2012) Affect of tempering temperature on the microstructure and mechanical properties of dual phase steels. *Materials Science and Engineering A*, 532: 21–25.

- Seong, B.S.; Shin, E.J.; Han, Y.S.; Lee, C.H.; Kim, Y.J.; Kim, S.J. (2004) Effect of retained austenite and solute carbon on the mechanical properties in TRIP steels. *Physica B*, 350: e467–e469.
- Sodjit, S.; Uthaisangsuk, V. (2011) High strength dual phase steels and flow curve modeling approach. *Proceedings of The Second TSME International Conference on Mechanical Engineerinng*, Krabi, Thailand, pp.
- Szewczyk, A.F.; Gurland, J. (1982) A study of the deformation and fracture of a dual-phase steel. *Metallurgical Transactions A*, 13A: 1821–1826.
- Tan, W.; Han, B.; Wang, S. H.; Yang, Y.; Zhang, C., Zhang, Y. K. (2012) Effects of TMCP parameters on microstructure and mechanical properties of hot rolled economical dual phase steel in CSP. *Journal of Iron and Steel Research, International*, 19(6): 37–41.
- Thomas, G.A.; Speer, J.G.; Matlock, D.K. (2011) Quenched and Partitioned Microstructure Produced via Gleeble Simulations of Hot-Strip Mill Cooling Practices, *Metallurgical and Materials Transactions A*, 42A: 3652–3659.
- Tong, T.; Shuai, T.; Bingxing, W.; Zhaodong, W.; Guodong, W. (2012) Development and industrial application of ultra-fast cooling technology. *Science China Technological Science*, 55: 1566–1571.
- Wang, J.; Li, G.; Xiao, A. (2011) A Bainite-Ferrite Multi-Phase Steel Strengthened by Ti-Microalloying. *Materials Transactions*, 52: 2027–2031.
- Wu, R.M.; Wang, L.; Jin, X.J. (2013) Thermal Stability of Austenite and Properties of Quenching & Partitioning (Q&P) Treated AHSS. *Physics Procedia*. 50: 8–12.
- Yong, T.; Shuai, T.; Bingxing, W.; Zhaodong, W.; Guodong, W. (2012) Development and industrial application of ultra-fast cooling technology. *Science China Technological Science*, 55: 1566–1571.

Appendix I

Data Logs for determining the Cooling Curve

(Annealing Temperature: 700 ℃; Route A**)**

Time (s)	Temp (℃)	Time (s)	Temp (℃)
0	696.5278	24	215.2778
1	681.9444	25	209.7222
2	651.3889	26	206.25
3	605.5555	27	201.3889
4	565.9722	28	197.9167
5	529.1666	29	195.1389
6	484.0278	30	191.6667
7	453.4722	31	188.8889
8	418.75	32	186.1111
9	388.1944	33	184.0278
10	368.0555	34	181.25
11	345.1389	35	179.1667
12	327.0833	36	177.0833
13	311.8055	37	175.6944
14	295.8333	38	173.6111
15	286.1111	39	172.2222
16	273.6111	40	169.4444
17	264.5833	41	167.3611
18	253.4722	46	159.0278
19	246.5278	47	157.6389
20	238.1944	48	156.9444
21	232.6389	49	154.8611
22	225	50	153.4722
23	220.1389	51	151.3889

Appendix II

Data Logs for determining the Stress-Strain Curve

(Annealing Temperature: 700 ℃; Route A**)**

Strain (%)	Stress (MPa)	Strain (%)	Stress (MPa)	Strain (%)	Stress (MPa)	Strain (%)	Stress (MPa)
0.05633	78.19017	4.59144	463.3867	12.00162	549.7238	19.4936	568.0221
0.06693	105.3888	4.63133	464.3937	12.02756	550.2911	19.54296	568.5587
0.08094	129.869	4.66207	463.1061	12.06908	549.5805	19.57415	569.0193
0.09394	153.9644	4.6882	464.9058	12.1069	550.601	19.60505	569.0818
0.11919	185.9606	4.7147	466.6406	12.12903	549.8831	19.66163	568.4901
1.01944	307.2036	4.74439	465.7046	12.16614	550.9955	19.70102	568.4864
↓	↓	↓	↓	12.21008	551.3704	19.72712	568.3345
↓	↓	↓	↓	12.23977	550.5839	19.7716	568.1593
↓	↓	↓	↓	12.26614	551.0862	↓	↓
1.03915	306.471	5.00789	471.2335	12.30782	552.4093	↓	↓
1.05991	311.516	5.03336	473.0356	12.34785	551.5186	20.28118	569.3133
1.10034	313.3708	5.06615	473.8969	↓	↓	20.33543	569.3501
1.13169	313.8045	5.09968	472.7134	↓	↓	20.35927	569.1749
1.15442	319.1129	5.13341	475.7676	13.07032	554.5753	20.39633	569.404
1.19724	319.9545	5.16111	475.2298	13.10279	554.8093	20.4513	568.9593
1.21303	319.3052	5.18395	474.7569	13.12722	555.1633	↓	↓
1.23948	324.632	5.20954	477.4081	13.16373	555.5664	↓	↓
1.27888	325.8645	5.24558	478.012	13.21043	555.4537	21.00042	569.012
1.30444	325.8044	5.27804	476.4892	13.23748	555.8996	21.03916	568.8772
1.33574	330.281	↓	↓	13.90483	557.7851	21.09523	569.7458
1.37078	331.7952	↓	↓	13.9408	557.861	21.12541	569.8242
1.38989	330.3288	↓	↓	14.00024	557.676	21.15637	568.8919
1.4143	335.7437	6.74629	503.988	14.04735	558.2433	21.21115	568.86
↓	↓	6.78339	503.7271	14.08035	559.0175	↓	↓
↓	↓	6.81357	503.5127	14.10586	558.7468	↓	↓
2.03405	372.1589	6.83753	504.7746	14.14916	558.9783	22.14161	569.295
2.06988	371.7681	6.86217	504.9265	14.19169	558.8435	22.19362	569.0695
2.08713	371.9457	6.8949	505.1997	14.2158	558.7517	22.21759	568.5011
2.11303	376.1233	6.93394	506.4848	14.25498	559.9033	22.25912	569.4873
2.1457	376.5999	6.96811	506.3623	14.29827	559.2797	22.31749	569.306
2.17423	376.9062	6.99009	506.9026	14.32691	559.9731	22.35368	569.5118
2.21024	380.6685	7.0192	506.9357	14.35387	559.8922	↓	↓
2.24301	380.3598	7.04924	508.26	↓	↓	↓	↓
2.26119	380.437	7.08472	507.7785	↓	↓	23.86391	567.755

Strain (%)	Stress (MPa)	Strain (%)	Stress (MPa)	Strain (%)	Stress (MPa)	Strain (%)	Stress (MPa)
2.28894	384.3402	7.12107	508.6435	15.01191	561.6601	23.88656	568.4913
2.31881	384.5252	7.15063	508.9853	15.03529	560.9299	23.9488	568.0747
2.3455	384.2728	7.17592	508.8775	15.07316	561.2019	23.99291	568.5721
2.38055	388.1392	7.20388	509.0343	15.12034	561.3808	24.01599	567.9596
2.4146	388.1172	7.23649	510.1883	15.14591	562.0595	24.07494	568.8245
2.43181	388.8057	7.2718	510.3672	15.17952	561.072	24.12301	568.468
2.46152	392.8118	7.30405	511.6866	15.227	561.3244		
3.00434	412.8864	7.33367	511.1268	15.2618	561.6368	25.63409	566.5911
3.03066	413.5113	↓	↓	↓	↓	25.70291	566.7173
3.06888	416.7896	↓	↓	↓	↓	↓	↓
3.10249	416.8117	↓	↓	↓	↓	↓	↓
3.12627	417.9131	8.33868	523.4685	16.01827	564.2353	26.90685	563.3176
3.20516	420.6647	8.41912	523.3288	16.12136	564.0466	27.04601	563.3397
3.24453	423.3746	8.45399	524.3089	16.16777	563.9376	27.11446	563.8297
3.27401	422.5085	8.49314	524.3898	16.21035	564.272	27.15961	563.5284
3.29334	423.9541	8.52833	524.8063	16.23651	563.7673	↓	↓
3.3293	426.5832	8.55128	524.788	16.27361	563.6276	↓	↓
↓	↓	8.96949	529.7055	16.32163	564.3467	28.88582	555.8469
↓	↓	9.00622	529.5181	16.34993	564.3504	28.91989	554.9992
↓	↓	9.02356	529.4299	↓	↓	28.94679	553.8868
↓	↓	9.05771	530.2862	↓	↓	29.02914	555.1327
4.02377	448.3215	9.09716	530.6648	17.01895	565.7225	29.08585	554.6034
4.05574	447.4603	9.13263	531.7074	17.06212	565.1088	↓	↓
4.0791	448.3791	9.16134	530.8767	17.08368	565.295	↓	↓
4.10627	450.2168	9.18659	531.2786	17.12864	565.8683	30.9088	537.0121
4.12693	449.8872	↓	↓	17.17341	565.3991	30.94622	536.6899
4.15668	451.829	↓	↓	17.20694	566.2273	30.98037	534.9858
4.1977	452.7576	10.99325	544.6445	17.23713	566.3032	31.05252	534.7542
4.22724	451.5975	11.02015	544.2304	17.28543	565.5694	31.13628	533.4385
4.2458	453.7684	11.05155	544.168	17.32268	565.883	31.17457	532.8002
4.27558	454.7313	11.09439	545.458	↓	↓	↓	↓
4.3054	453.8272	11.1222	545.3649	↓	↓	↓	↓
4.33561	456.7331	11.14865	544.4767	18.44661	567.7979	31.93508	515.6327
4.37553	457.6912	11.18915	545.828	18.49644	566.8349	32.00635	514.7384
4.3964	456.8838	11.23409	546.0742	18.53677	567.4573	32.08754	512.8199
4.41965	458.9138	11.2564	545.1823	18.56216	566.9893	32.1318	510.5865
4.45123	459.8228	↓	↓	18.60527	567.8077	32.16037	509.1837
↓	↓	↓	↓	18.65485	568.136	32.23322	506.6906

Appendix III

Microhardness of samples at various Annealing Temperatures

Annealing Temperature (℃)	Microhardness (Hv)	Average Microhardness (Hv)
700	174, 180, 185, 187, 175, 181, 186, 187, 179, 185, 174, 180, 180, 175, 173	180
750	205, 210, 223, 201, 203, 205, 201, 188, 195, 225, 222, 206, 203, 211, 209	207
800	218, 211, 220, 240, 227, 216, 221, 236, 232, 206, 215, 250, 230, 225, 221	224
850	262, 284, 264, 321, 280, 276, 320, 266, 276, 274, 271, 251, 247, 253, 270	274

Appendix IV
Data Logs of Micro-mechanical Modelling for DP Structure
(MVF = 15%)

Engineering Strain (%)	Engineering Stress (MPa)	True Strain (-)	True Stress (MPa)	True Stress MPa
			(Experimental)	(Modelled)
6.31E-04	11.36678	6.31E-06	11.36685	321.9735
0.00218	14.98673	2.18E-05	14.98706	322.3549
0.01252	35.70786	1.25E-04	35.71233	324.8397
0.03305	78.3674	3.30E-04	78.3933	329.4929
0.05897	125.0314	5.90E-04	125.1052	334.9099
1.00798	322.0293	0.01003	325.2753	426.9167
↓	↓	↓	↓	↓
↓	↓	↓	↓	↓
1.03872	323.8693	0.01033	327.2333	428.6149
1.06964	326.0405	0.01064	329.5279	430.3347
1.09803	327.3161	0.01092	330.9101	431.8589
1.1236	328.7083	0.01117	332.4017	433.1971
1.15214	330.8624	0.01146	334.6744	434.7239
2.98	413.738	0.02936	426.0674	499.0801
↓	↓	↓	↓	↓
↓	↓	↓	↓	↓
2.99954	414.8608	0.02955	427.3047	499.5774
3.01831	414.9745	0.02974	427.4997	500.0722
3.03777	415.676	0.02993	428.3032	500.5647
3.0591	417.177	0.03013	429.9389	501.0805
3.08161	417.9114	0.03035	430.7898	501.6449
3.1055	419.0467	0.03058	432.0602	502.2316
4.7162	461.619	0.04608	483.3899	535.6948
↓	↓	↓	↓	↓
↓	↓	↓	↓	↓
4.73998	461.6892	0.04631	483.5732	536.1206
4.76092	462.0617	0.04651	484.0601	536.4895
4.78425	462.9979	0.04673	485.1489	536.8939
4.8086	463.7146	0.04697	486.0128	537.3334
4.83638	464.5716	0.04723	487.0401	537.8076
4.866	465.1066	0.04751	487.7387	538.3159
4.8939	465.3837	0.04778	488.1591	538.8039
4.91814	465.2535	0.04801	488.1354	539.2179
Engineering Strain	**Engineering Stress**	**True Strain**	**True Stress**	**True Stress**

(%)	(MPa)	(-)	(MPa)	MPa
			(Experimental)	(Modelled)
4.94399	466.2171	0.04826	489.2668	539.6661
4.97258	467.4895	0.04853	490.7358	540.1482
5.00339	468.189	0.04882	491.6143	540.6637
5.03413	468.5862	0.04912	492.1754	541.1945
5.06465	468.9066	0.04941	492.6551	541.7051
5.09501	469.3765	0.04969	493.2913	542.196
5.12437	469.6217	0.04997	493.6868	542.6847
6.90855	498.436	0.0668	532.8707	568.762
↓	↓	↓	↓	↓
↓	↓	↓	↓	↓
6.93728	499.2976	0.06707	533.9353	569.136
6.9689	499.6925	0.06737	534.5155	569.5502
7.00076	499.9102	0.06767	534.9077	569.9629
7.0332	500.0439	0.06797	535.2129	570.3741
7.06507	500.505	0.06827	535.866	570.784
↓	↓	↓	↓	↓
↓	↓	↓	↓	↓
8.91978	519.0952	0.08544	565.3973	592.1755
8.94771	519.5911	0.0857	566.0826	592.4722
8.97407	519.6147	0.08594	566.2453	592.7455
9.00146	519.8709	0.08619	566.6668	593.0294
9.02908	520.2497	0.08644	567.2235	593.3128
9.0576	520.4911	0.08671	567.6351	593.6181
9.87537	526.6712	0.09418	578.6819	601.78
10.89036	532.541	0.10337	590.5367	611.145
↓	↓	↓	↓	↓
↓	↓	↓	↓	↓
10.91899	533.5389	0.10363	591.796	611.4001
10.9493	534.0117	0.1039	592.4822	611.6646
10.98216	534.2716	0.1042	592.9462	611.9578
11.01864	535.1088	0.10453	594.0705	612.2795
11.05799	535.3443	0.10488	594.5427	612.6199
11.09896	535.6214	0.10525	595.0699	612.9787
11.92243	538.9658	0.11264	603.2236	619.9441
↓	↓	↓	↓	↓
↓	↓	↓	↓	↓
11.95391	539.5655	0.11292	604.0647	620.2008
11.98559	539.969	0.1132	604.6875	620.457
12.02019	539.6185	0.11351	604.4817	620.74

Engineering Strain (%)	Engineering Stress (MPa)	True Strain (-)	True Stress (MPa)	True Stress MPa
			(Experimental)	(Modelled)
12.1176	540.1289	0.11438	605.5796	621.5311
12.15563	540.769	0.11472	606.5029	621.839
↓	↓	↓	↓	↓
↓	↓	↓	↓	↓
13.90011	546.0725	0.13015	621.9771	635.102
13.92881	546.2956	0.1304	622.3881	635.3064
13.9568	546.0972	0.13065	622.3149	635.5104
13.98386	546.2718	0.13089	622.6616	635.706
14.01097	546.3409	0.13112	622.8886	635.8931
14.03822	546.2122	0.13136	622.8906	636.0881
14.06513	546.7757	0.1316	623.6804	636.2829
15.94391	551.101	0.14794	638.968	648.9206
↓	↓	↓	↓	↓
↓	↓	↓	↓	↓
15.96963	550.7408	0.14816	638.6921	649.083
15.9916	550.9825	0.14835	639.0934	649.2231
16.01778	550.8141	0.14857	639.0423	649.3851
16.03655	549.92	0.14874	638.1082	649.5102
16.05533	550.2606	0.1489	638.6067	649.6278
17.96393	554.0172	0.16521	653.5405	661.12
↓	↓	↓	↓	↓
↓	↓	↓	↓	↓
17.98462	553.2811	0.16538	652.7867	661.2349
18.00716	553.6308	0.16558	653.324	661.37
18.0315	554.191	0.16578	654.1199	661.5049
18.0561	553.6135	0.16599	653.5745	661.6465
18.07497	553.0612	0.16615	653.0268	661.7543
18.09361	552.6957	0.16631	652.6984	661.8619
19.92172	555.7351	0.18167	666.4472	671.8332
↓	↓	↓	↓	↓
↓	↓	↓	↓	↓
19.95032	555.2994	0.18191	666.0834	671.9836
19.9775	555.5046	0.18213	666.4805	672.1213
20.00598	555.7678	0.18237	666.9546	672.2713
20.03525	556.1977	0.18262	667.6333	672.4275
20.06553	555.5337	0.18287	667.0045	672.5835
21.92497	555.8035	0.19824	677.6633	681.861
↓	↓	↓	↓	↓
↓	↓	↓	↓	↓

Engineering Strain (%)	Engineering Stress (MPa)	True Strain (-)	True Stress (MPa)	True Stress MPa
			(Experimental)	(Modelled)
22.00884	555.9121	0.19892	678.2619	682.258
22.03705	555.7508	0.19915	678.2218	682.392
↓	↓	↓	↓	↓
23.9852	557.171	0.21499	690.8095	691.338
24.0547	557.3482	0.21555	691.4166	691.6445
24.12324	557.1016	0.2161	691.4926	691.9449
24.19198	556.6198	0.21666	691.2771	692.2501
24.25832	556.5373	0.21719	691.5439	692.5384
↓	↓	↓	↓	↓
↓	↓	↓	↓	↓
25.92171	551.6235	0.23049	694.6137	699.5951
25.9647	551.6322	0.23083	694.8618	699.7711
26.00795	551.6535	0.23117	695.1273	699.947
26.05607	551.9045	0.23156	695.7091	700.1485
26.10421	551.2386	0.23194	695.1351	700.3445
26.14904	551.0348	0.23229	695.1251	700.5249
↓	↓	↓	↓	↓
27.99091	540.8275	0.24679	692.2101	707.8119
28.03148	540.4087	0.24711	691.8933	707.9688
28.06721	539.7006	0.24739	691.1795	708.1059
28.10194	539.616	0.24766	691.2586	708.2381
↓	↓	↓	↓	↓
↓	↓	↓	↓	↓
29.96522	517.2589	0.2621	672.2567	715.1427
30.00237	516.1762	0.26238	671.0412	715.2736
30.04069	515.3997	0.26268	670.2293	715.4137
30.08061	514.5743	0.26298	669.3613	715.5536
30.11703	513.3725	0.26326	667.985	715.6841
30.15398	512.8196	0.26355	667.4552	715.8191
30.19587	511.7937	0.26387	666.3342	715.968
30.23369	510.3846	0.26416	664.6927	716.1028
30.27187	509.5579	0.26445	663.8105	716.2374
30.78617	488.9423	0.26839	639.4689	718.0554
↓	↓	↓	↓	↓
30.82437	486.2778	0.26869	636.1698	718.1929
30.86799	484.4798	0.26902	634.029	718.3441
30.91354	481.8335	0.26937	630.7853	718.5043

Appendix II

Data Logs for determining the Stress-Strain Curve

(Annealing Temperature: 700 ℃; Route A**)**

Strain (%)	Stress (MPa)	Strain (%)	Stress (MPa)	Strain (%)	Stress (MPa)	Strain (%)	Stress (MPa)
0.05633	78.19017	4.59144	463.3867	12.00162	549.7238	19.4936	568.0221
0.06693	105.3888	4.63133	464.3937	12.02756	550.2911	19.54296	568.5587
0.08094	129.869	4.66207	463.1061	12.06908	549.5805	19.57415	569.0193
0.09394	153.9644	4.6882	464.9058	12.1069	550.601	19.60505	569.0818
0.11919	185.9606	4.7147	466.6406	12.12903	549.8831	19.66163	568.4901
1.01944	307.2036	4.74439	465.7046	12.16614	550.9955	19.70102	568.4864
↓	↓	↓	↓	12.21008	551.3704	19.72712	568.3345
↓	↓	↓	↓	12.23977	550.5839	19.7716	568.1593
↓	↓	↓	↓	12.26614	551.0862	↓	↓
1.03915	306.471	5.00789	471.2335	12.30782	552.4093	↓	↓
1.05991	311.516	5.03336	473.0356	12.34785	551.5186	20.28118	569.3133
1.10034	313.3708	5.06615	473.8969	↓	↓	20.33543	569.3501
1.13169	313.8045	5.09968	472.7134	↓	↓	20.35927	569.1749
1.15442	319.1129	5.13341	475.7676	13.07032	554.5753	20.39633	569.404
1.19724	319.9545	5.16111	475.2298	13.10279	554.8093	20.4513	568.9593
1.21303	319.3052	5.18395	474.7569	13.12722	555.1633	↓	↓
1.23948	324.632	5.20954	477.4081	13.16373	555.5664	↓	↓
1.27888	325.8645	5.24558	478.012	13.21043	555.4537	21.00042	569.012
1.30444	325.8044	5.27804	476.4892	13.23748	555.8996	21.03916	568.8772
1.33574	330.281	↓	↓	13.90483	557.7851	21.09523	569.7458
1.37078	331.7952	↓	↓	13.9408	557.861	21.12541	569.8242
1.38989	330.3288	↓	↓	14.00024	557.676	21.15637	568.8919
1.4143	335.7437	6.74629	503.988	14.04735	558.2433	21.21115	568.86
↓	↓	6.78339	503.7271	14.08035	559.0175	↓	↓
↓	↓	6.81357	503.5127	14.10586	558.7468	↓	↓
2.03405	372.1589	6.83753	504.7746	14.14916	558.9783	22.14161	569.295
2.06988	371.7681	6.86217	504.9265	14.19169	558.8435	22.19362	569.0695
2.08713	371.9457	6.8949	505.1997	14.2158	558.7517	22.21759	568.5011
2.11303	376.1233	6.93394	506.4848	14.25498	559.9033	22.25912	569.4873
2.1457	376.5999	6.96811	506.3623	14.29827	559.2797	22.31749	569.306
2.17423	376.9062	6.99009	506.9026	14.32691	559.9731	22.35368	569.5118
2.21024	380.6685	7.0192	506.9357	14.35387	559.8922	↓	↓
2.24301	380.3598	7.04924	508.26	↓	↓	↓	↓
2.26119	380.437	7.08472	507.7785	↓	↓	23.86391	567.755

Strain (%)	Stress (MPa)	Strain (%)	Stress (MPa)	Strain (%)	Stress (MPa)	Strain (%)	Stress (MPa)
2.28894	384.3402	7.12107	508.6435	15.01191	561.6601	23.88656	568.4913
2.31881	384.5252	7.15063	508.9853	15.03529	560.9299	23.9488	568.0747
2.3455	384.2728	7.17592	508.8775	15.07316	561.2019	23.99291	568.5721
2.38055	388.1392	7.20388	509.0343	15.12034	561.3808	24.01599	567.9596
2.4146	388.1172	7.23649	510.1883	15.14591	562.0595	24.07494	568.8245
2.43181	388.8057	7.2718	510.3672	15.17952	561.072	24.12301	568.468
2.46152	392.8118	7.30405	511.6866	15.227	561.3244		
3.00434	412.8864	7.33367	511.1268	15.2618	561.6368	25.63409	566.5911
3.03066	413.5113	↓	↓	↓	↓	25.70291	566.7173
3.06888	416.7896	↓	↓	↓	↓	↓	↓
3.10249	416.8117	↓	↓	↓	↓	↓	↓
3.12627	417.9131	8.33868	523.4685	16.01827	564.2353	26.90685	563.3176
3.20516	420.6647	8.41912	523.3288	16.12136	564.0466	27.04601	563.3397
3.24453	423.3746	8.45399	524.3089	16.16777	563.9376	27.11446	563.8297
3.27401	422.5085	8.49314	524.3898	16.21035	564.272	27.15961	563.5284
3.29334	423.9541	8.52833	524.8063	16.23651	563.7673	↓	↓
3.3293	426.5832	8.55128	524.788	16.27361	563.6276	↓	↓
↓	↓	8.96949	529.7055	16.32163	564.3467	28.88582	555.8469
↓	↓	9.00622	529.5181	16.34993	564.3504	28.91989	554.9992
↓	↓	9.02356	529.4299	↓	↓	28.94679	553.8868
↓	↓	9.05771	530.2862	↓	↓	29.02914	555.1327
4.02377	448.3215	9.09716	530.6648	17.01895	565.7225	29.08585	554.6034
4.05574	447.4603	9.13263	531.7074	17.06212	565.1088	↓	↓
4.0791	448.3791	9.16134	530.8767	17.08368	565.295	↓	↓
4.10627	450.2168	9.18659	531.2786	17.12864	565.8683	30.9088	537.0121
4.12693	449.8872	↓	↓	17.17341	565.3991	30.94622	536.6899
4.15668	451.829	↓	↓	17.20694	566.2273	30.98037	534.9858
4.1977	452.7576	10.99325	544.6445	17.23713	566.3032	31.05252	534.7542
4.22724	451.5975	11.02015	544.2304	17.28543	565.5694	31.13628	533.4385
4.2458	453.7684	11.05155	544.168	17.32268	565.883	31.17457	532.8002
4.27558	454.7313	11.09439	545.458	↓	↓	↓	↓
4.3054	453.8272	11.1222	545.3649	↓	↓	↓	↓
4.33561	456.7331	11.14865	544.4767	18.44661	567.7979	31.93508	515.6327
4.37553	457.6912	11.18915	545.828	18.49644	566.8349	32.00635	514.7384
4.3964	456.8838	11.23409	546.0742	18.53677	567.4573	32.08754	512.8199
4.41965	458.9138	11.2564	545.1823	18.56216	566.9893	32.1318	510.5865
4.45123	459.8228	↓	↓	18.60527	567.8077	32.16037	509.1837
↓	↓	↓	↓	18.65485	568.136	32.23322	506.6906

Appendix III

Microhardness of samples at various Annealing Temperatures

Annealing Temperature (℃)	Microhardness (Hv)	Average Microhardness (Hv)
700	174, 180, 185, 187, 175, 181, 186, 187, 179, 185, 174, 180, 180, 175, 173	180
750	205, 210, 223, 201, 203, 205, 201, 188, 195, 225, 222, 206, 203, 211, 209	207
800	218, 211, 220, 240, 227, 216, 221, 236, 232, 206, 215, 250, 230, 225, 221	224
850	262, 284, 264, 321, 280, 276, 320, 266, 276, 274, 271, 251, 247, 253, 270	274

Appendix IV
Data Logs of Micro-mechanical Modelling for DP Structure
(MVF = 15%)

Engineering Strain (%)	Engineering Stress (MPa)	True Strain (-)	True Stress (MPa)	True Stress MPa
			(Experimental)	(Modelled)
6.31E-04	11.36678	6.31E-06	11.36685	321.9735
0.00218	14.98673	2.18E-05	14.98706	322.3549
0.01252	35.70786	1.25E-04	35.71233	324.8397
0.03305	78.3674	3.30E-04	78.3933	329.4929
0.05897	125.0314	5.90E-04	125.1052	334.9099
1.00798	322.0293	0.01003	325.2753	426.9167
↓	↓	↓	↓	↓
↓	↓	↓	↓	↓
1.03872	323.8693	0.01033	327.2333	428.6149
1.06964	326.0405	0.01064	329.5279	430.3347
1.09803	327.3161	0.01092	330.9101	431.8589
1.1236	328.7083	0.01117	332.4017	433.1971
1.15214	330.8624	0.01146	334.6744	434.7239
2.98	413.738	0.02936	426.0674	499.0801
↓	↓	↓	↓	↓
↓	↓	↓	↓	↓
2.99954	414.8608	0.02955	427.3047	499.5774
3.01831	414.9745	0.02974	427.4997	500.0722
3.03777	415.676	0.02993	428.3032	500.5647
3.0591	417.177	0.03013	429.9389	501.0805
3.08161	417.9114	0.03035	430.7898	501.6449
3.1055	419.0467	0.03058	432.0602	502.2316
4.7162	461.619	0.04608	483.3899	535.6948
↓	↓	↓	↓	↓
↓	↓	↓	↓	↓
4.73998	461.6892	0.04631	483.5732	536.1206
4.76092	462.0617	0.04651	484.0601	536.4895
4.78425	462.9979	0.04673	485.1489	536.8939
4.8086	463.7146	0.04697	486.0128	537.3334
4.83638	464.5716	0.04723	487.0401	537.8076
4.866	465.1066	0.04751	487.7387	538.3159
4.8939	465.3837	0.04778	488.1591	538.8039
4.91814	465.2535	0.04801	488.1354	539.2179
Engineering Strain	**Engineering Stress**	**True Strain**	**True Stress**	**True Stress**

(%)	(MPa)	(-)	(MPa)	MPa
			(Experimental)	(Modelled)
4.94399	466.2171	0.04826	489.2668	539.6661
4.97258	467.4895	0.04853	490.7358	540.1482
5.00339	468.189	0.04882	491.6143	540.6637
5.03413	468.5862	0.04912	492.1754	541.1945
5.06465	468.9066	0.04941	492.6551	541.7051
5.09501	469.3765	0.04969	493.2913	542.196
5.12437	469.6217	0.04997	493.6868	542.6847
6.90855	498.436	0.0668	532.8707	568.762
↓	↓	↓	↓	↓
↓	↓	↓	↓	↓
6.93728	499.2976	0.06707	533.9353	569.136
6.9689	499.6925	0.06737	534.5155	569.5502
7.00076	499.9102	0.06767	534.9077	569.9629
7.0332	500.0439	0.06797	535.2129	570.3741
7.06507	500.505	0.06827	535.866	570.784
↓	↓	↓	↓	↓
↓	↓	↓	↓	↓
8.91978	519.0952	0.08544	565.3973	592.1755
8.94771	519.5911	0.0857	566.0826	592.4722
8.97407	519.6147	0.08594	566.2453	592.7455
9.00146	519.8709	0.08619	566.6668	593.0294
9.02908	520.2497	0.08644	567.2235	593.3128
9.0576	520.4911	0.08671	567.6351	593.6181
9.87537	526.6712	0.09418	578.6819	601.78
10.89036	532.541	0.10337	590.5367	611.145
↓	↓	↓	↓	↓
↓	↓	↓	↓	↓
10.91899	533.5389	0.10363	591.796	611.4001
10.9493	534.0117	0.1039	592.4822	611.6646
10.98216	534.2716	0.1042	592.9462	611.9578
11.01864	535.1088	0.10453	594.0705	612.2795
11.05799	535.3443	0.10488	594.5427	612.6199
11.09896	535.6214	0.10525	595.0699	612.9787
11.92243	538.9658	0.11264	603.2236	619.9441
↓	↓	↓	↓	↓
↓	↓	↓	↓	↓
11.95391	539.5655	0.11292	604.0647	620.2008
11.98559	539.969	0.1132	604.6875	620.457
12.02019	539.6185	0.11351	604.4817	620.74

Engineering Strain (%)	Engineering Stress (MPa)	True Strain (-)	True Stress (MPa)	True Stress MPa
			(Experimental)	(Modelled)
12.1176	540.1289	0.11438	605.5796	621.5311
12.15563	540.769	0.11472	606.5029	621.839
↓	↓	↓	↓	↓
↓	↓	↓	↓	↓
13.90011	546.0725	0.13015	621.9771	635.102
13.92881	546.2956	0.1304	622.3881	635.3064
13.9568	546.0972	0.13065	622.3149	635.5104
13.98386	546.2718	0.13089	622.6616	635.706
14.01097	546.3409	0.13112	622.8886	635.8931
14.03822	546.2122	0.13136	622.8906	636.0881
14.06513	546.7757	0.1316	623.6804	636.2829
15.94391	551.101	0.14794	638.968	648.9206
↓	↓	↓	↓	↓
↓	↓	↓	↓	↓
15.96963	550.7408	0.14816	638.6921	649.083
15.9916	550.9825	0.14835	639.0934	649.2231
16.01778	550.8141	0.14857	639.0423	649.3851
16.03655	549.92	0.14874	638.1082	649.5102
16.05533	550.2606	0.1489	638.6067	649.6278
17.96393	554.0172	0.16521	653.5405	661.12
↓	↓	↓	↓	↓
↓	↓	↓	↓	↓
17.98462	553.2811	0.16538	652.7867	661.2349
18.00716	553.6308	0.16558	653.324	661.37
18.0315	554.191	0.16578	654.1199	661.5049
18.0561	553.6135	0.16599	653.5745	661.6465
18.07497	553.0612	0.16615	653.0268	661.7543
18.09361	552.6957	0.16631	652.6984	661.8619
19.92172	555.7351	0.18167	666.4472	671.8332
↓	↓	↓	↓	↓
↓	↓	↓	↓	↓
19.95032	555.2994	0.18191	666.0834	671.9836
19.9775	555.5046	0.18213	666.4805	672.1213
20.00598	555.7678	0.18237	666.9546	672.2713
20.03525	556.1977	0.18262	667.6333	672.4275
20.06553	555.5337	0.18287	667.0045	672.5835
21.92497	555.8035	0.19824	677.6633	681.861
↓	↓	↓	↓	↓
↓	↓	↓	↓	↓

Engineering Strain (%)	Engineering Stress (MPa)	True Strain (-)	True Stress (MPa)	True Stress MPa
			(Experimental)	(Modelled)
22.00884	555.9121	0.19892	678.2619	682.258
22.03705	555.7508	0.19915	678.2218	682.392
↓	↓	↓	↓	↓
23.9852	557.171	0.21499	690.8095	691.338
24.0547	557.3482	0.21555	691.4166	691.6445
24.12324	557.1016	0.2161	691.4926	691.9449
24.19198	556.6198	0.21666	691.2771	692.2501
24.25832	556.5373	0.21719	691.5439	692.5384
↓	↓	↓	↓	↓
↓	↓	↓	↓	↓
25.92171	551.6235	0.23049	694.6137	699.5951
25.9647	551.6322	0.23083	694.8618	699.7711
26.00795	551.6535	0.23117	695.1273	699.947
26.05607	551.9045	0.23156	695.7091	700.1485
26.10421	551.2386	0.23194	695.1351	700.3445
26.14904	551.0348	0.23229	695.1251	700.5249
↓	↓	↓	↓	↓
27.99091	540.8275	0.24679	692.2101	707.8119
28.03148	540.4087	0.24711	691.8933	707.9688
28.06721	539.7006	0.24739	691.1795	708.1059
28.10194	539.616	0.24766	691.2586	708.2381
↓	↓	↓	↓	↓
↓	↓	↓	↓	↓
29.96522	517.2589	0.2621	672.2567	715.1427
30.00237	516.1762	0.26238	671.0412	715.2736
30.04069	515.3997	0.26268	670.2293	715.4137
30.08061	514.5743	0.26298	669.3613	715.5536
30.11703	513.3725	0.26326	667.985	715.6841
30.15398	512.8196	0.26355	667.4552	715.8191
30.19587	511.7937	0.26387	666.3342	715.968
30.23369	510.3846	0.26416	664.6927	716.1028
30.27187	509.5579	0.26445	663.8105	716.2374
30.78617	488.9423	0.26839	639.4689	718.0554
↓	↓	↓	↓	↓
30.82437	486.2778	0.26869	636.1698	718.1929
30.86799	484.4798	0.26902	634.029	718.3441